AGGREGATION MANAGEMENT OF THE DISEASE PROTEINS SYNPHILIN-1 AND HUNTINGTIN IN THE YEAST *SACCHAROMYCES CEREVISIAE*

Ju ZHENG

Supervisor:
Prof. J. Winderickx, KU Leuven
Co-supervisor:
Prof. B. Liu, Gothenburg University

Members of the Examination Committee:
Prof. F. Rolland (chair), KU Leuven
Prof. G. Callewaert, KU Leuven
Prof. L. Temmerman, KU Leuven
Dr. V. Franssens, KU Leuven
Prof. T. Nyström, Gothenburg University

Dissertation presented in partial fulfilment of the requirements for the degree of Doctor of Science (PhD): Biology

December 2017

Uitgegeven in eigen beheer, Ju Zheng, Kasteelpark Arenberg 31, 3001 Heverlee, Belgium

Preface

Kasteelpark Arenberg 31, a place full with wonderful memories, where I met so many nice people during my PhD journey, had so many moments that I feel like at home. I always enjoy the Friday beer atmosphere, like family members sitting together, despite the fact that I have very limited alcohol tolerance. As an international student, I can never achieve this final milestone without your help.

First of all, I would like to express my gratitude and appreciation to my promoter Joris, for providing a wonderful chance to start my PhD programme in Lab Functional Biology. From then on, you never stop taking care of me, with continuous efforts in supervising my study and related research, providing trainings and financial support. Your knowledge, patience and trust lead me to final step of this programme.

I would also like to thank my co-promoter Beidong, for offering so many scientific trainings during my study in Sweden, especially in large-scale screenings, which impacts a lot of the main outcomes of this thesis. I wouldn't be able to finish my project in time without your supervision and help. I would like to thank Thomas as well, for sharing your knowledge and the inspiring discussion in lab meetings, and for the constructive advices as a member of Examination Committee.

I want to thank all the members of Examination Committee, Prof. Dr. Fillip Rolland, Prof. Dr. Geert Callewaert, for all your critical evaluations, comments and suggestions. Prof. Dr. Liesbet Temmerman, I appreciate it a lot for you went into every detail to improve the PhD manuscript.

Special thanks to Vanessa, for introducing me into the world of yeast, and providing endless helps from the basic lab work at the beginning to the final revision of reports, publications and thesis, I couldn't thank enough for all you have done.

Tobias - thanks for taking care of me like an elder brother (though you are younger). Gernot, David, Elja, Marie-Anne, Tien-Yang and Joke, I do really enjoy working around with you, life

is much more colorful with your kindness and smile faces, good luck with your projects and wish you much success in your work! Cathy and Luc, thanks a lot for your helpful administrative work. Joelle, Dorien and Cynthia, you are always there in the lab when I need something. All former FBies, Erwin, Ruben, Jeff, Mathias, Tine, Katrien, Catherina and Hanne, thanks for the help and advice.

Guys working/worked at Lundberg, Gothenburg University - Xinxin, Lei, Junsheng, Lihua, Xiuling, Qian, Meng, Deyuan, Sansan, Anna-Maria, Frederik, Ken, Sandra, Lisa, Sarah, Roja, Doryaneh, Katarina, Rebecca A, Per, … Thank you for your help and the fun times I had in Sweden.

My dear mom and dad, my brother, sisters, and my lovely nephew & niece, thank you for your support over the past years, I wish I could have spent more time with you. Even it is thousands of kilometers away, I always feel warm and energetic when I hear your voice over the phone.

Last, I would like to thank China Scholarship Council (CSC) and KU Leuven for providing financial support during my PhD research.

Ju

Summary

Neurodegenerative diseases are associated with deposits of insoluble protein inclusions or aggregates. Evidence shows that different neurodegenerative diseases share some common underlying molecular and cellular mechanisms. However, the exact pathways by which disease-associated proteins form aggregates/inclusions and the steps in this cascade that are linked to pathogenesis, are not fully understood. In the present work, we investigated two known neurodegenerative disease-associated proteins, Synphilin-1 and huntingtin, in yeast models, to explore the aggregation management and translocation of these disease proteins.

Synphilin-1 is a major component of the Lewy body, a hallmark of Parkinson's disease (PD) (Wakabayashi et al., 2000), and a Synphilin-1 yeast model faithfully recapitulates this essential hallmark with Synphilin-1 inclusions formation. However, biological processes and pathways that involved in the inclusion formation are still not known in detail. Given the excellent tool that the yeast model can provide, in this thesis, we use a novel image-based genome-wide high-content microscopy (HCM) screening system, which enables us to validate inclusion body (IB) formation of Synphilin-1 in different genetic background systematically, and identify players controlling inclusion formation of Synphilin-1. In parallel, we study the Huntington's disease (HD) protein huntingtin. PolyQ-expansion of huntingtin exon-1 (Httex1) is responsible for the HD pathogenesis. Although the subcellular localization of polyQ-expanded Httex1 modulates polyQ toxicity in models of HD, the mechanisms involved in the nucleocytoplasmic translocation of polyQ-expanded Httex1 remain to be elucidated. To investigate components and pathways involved in altering the nucleocytoplasmic distribution of polyQ-expanded Httex1-103Q, we performed a dual channel image-based genome-wide HCM screen, which allows us to analyze the subcellular localization of Httex1-103Q.

In the Synphilin-1 study we found that 133 genes are required for the IB formation of Synphilin-1. Functional enrichment and physical interaction network analysis revealed these genes to encode for functions involved in cytoskeleton organization, histone modification, sister chromatid segregation, glycolipid biosynthetic process, DNA repair and replication. We

provide evidence that lower level of Synphilin-1 inclusion formation enhance cytotoxicity of Synphilin-1, supporting the hypothesis that matured inclusions represent an end stage of several events to protect cells from misfolded proteins.

The results of our Huntingtin study show that the ribosome quality control machinery is a key determinant for the nucleocytoplasmic distribution of Httex1-103Q. Defect of the ribosome quality control components, Ltn1 or Rqc1, caused nuclear accumulation of Httex1-103Q through a process that requires the CAT-tail tagging activity of Rqc2 and transport via the nuclear pore complex. We provide evidence that nuclear accumulation of Httex1-103Q enhances its cytotoxicity, suggesting that the ribosome quality control machinery plays an important role in protecting cells against the adverse effects of polyQ expansion proteins.

Samenvatting

Neurodegeneratieve ziekten zijn geassocieerd met afzettingen van onoplosbare proteïne aggregaten. Onderzoek heeft reeds aangetoond dat verschillende neurodegeneratieve ziekten een aantal algemene onderliggende moleculaire en cellulaire mechanismen gemeenschappelijk hebben. De exacte signaalwegen die verantwoordelijk zijn voor de aggregatie van de ziekte-gerelateerde proteïnen zijn echter nog niet volledig gekend. In deze studie maakten we gebruik van gehumaniseerde gistmodellen om het aggregatie-management en de translocatie van de neurodegeneratieve ziekte-gerelateerde proteïnen Synphiline-1 en Huntingtin te bestuderen.

Synphiline-1 is een component van Lewy bodies, een belangrijk kenmerk van de ziekte van Parkinson (Wakabayashi et al., 2000). Een interessante eigenschap van het gehumaniseerde synphiline-1 gistmodel is dat Synphiline-1 in dit model aggregeert net zoals in patiënten met de ziekte van Parkinson. Daarom is dit gistmodel een zeer geschikte *tool* om het aggregatieproces van Synphiline-1 te bestuderen. De biologische processen en signaalwegen die betrokken zijn bij de aggregaatvorming van Synphiline-1 moeten echter nog verder worden opgehelderd. In deze thesis werd het Synphiline-1 gistmodel gebruikt in een genoom-wijd *high-content* microscopie (HCM) screeningssysteem . Dit systeem maakt het mogelijk om de Synphiline-1 aggregaatvorming in verschillende genetische achtergronden te valideren en op deze manier componenten te identificeren die verantwoordelijk zijn voor de Synphiline-1 aggregaatvorming. In parallel met deze studie bestudeerde we het proteïne Huntingtin dat gerelateerd is aan de ziekte van Huntington. Poly-Q expansie van Huntingtin exon-1 (Httex1) is verantwoordelijk voor de pathogenese van de ziekte van Huntington. Alhoewel in modellen voor de ziekte van Huntington reeds werd aangetoond dat de subcellulaire localizatie van verlengde poly-Q varianten van Httex1 verantwoordelijk zijn voor de poly-Q geïnduceerde toxiciteit, zijn de mechanismen die betrokken zijn bij hun nucleocytoplasmatische translocatie nog grotendeels ongekend. Om de componenten en signaalwegen te onderzoeken die deze nucleocytoplasmatische translocatie beïnvloeden, werd

in deze studie een genoom-wijde HCM screening uitgevoerd, gebaseerd op beeldvorming in twee fluorescente kanalen.

De Synphiline-1 studie identificeerde 133 genen die noodzakelijk zijn voor de aggregaatvorming van Synphiline-1. Een analyse van de netwerken voor functionele aanrijking en fysieke interactie toonde aan dat deze genen coderen voor proteïnen betrokken bij cytoskeletorganisatie, histonmodificatie, segregatie van zusterchromatiden, glycolipide biosynthese en DNA herstel en replicatie. Verder toonde we aan dat een verminderde Synphiline-1 aggregaatvorming leidt tot een verhoogde cytotoxiciteit van Synphiline-1, hetgeen de hypothese ondersteunt dat ‘volgroeide’ aggregaten een eindstadium vertegenwoordigen dat de cel beschermt tegen misvouwen proteïnen.

In de Huntingtin studie konden we aantonen dat de machinerie voor ribosomale kwaliteitscontrole een belangrijke factor is voor de nucleocytoplasmatische distributie van Httex1-103Q. Een defect in Ltn1 of Rqc1, die betrokken zijn bij ribosomale kwaliteitscontrole, veroorzaakte een nucleaire accumulatie van Httex1-103Q. Dit proces vereist de zg. *CAT-tail tagging* van Rqc2 en transport via het nucleaire porie complex. Daarnaast toonden we aan dat de nucleaire accumulatie van Httex1-103Q zijn cytotoxiciteit verhoogt, wat aangeeft dat de machinerie voor ribosomale kwaliteitscontrole een belangrijke rol speelt bij het beschermen van cellen tegen de nadelige effecten van proteïnen met een poly-Q expansie.

List of abbreviations

3D-SIM	three-dimensional structured illumination microscopy
AD	Alzheimer’s disease
ATP	adenosine triphosphate
Aβ	amyloid beta
CAT-tails	carboxy-terminal Ala and Thr extension
CCT/TRiC	chaperonin containing TCP-1
CMA	chaperone-mediated autophagy
DAPI	4',6-diamidino-2-phenylindole
DNA	deoxyribonucleic acid
DUbs	deubiquitinating enzymes
ER	endoplasmic reticulum
GFP	green fluorescent protein
GO	gene ontology
GPI	glycosylphosphatidylinositol
GPI-GnT	glycosylphosphatidylinositol-N- acetylglucosaminyltransferase
HCM	high-content microscopy
HD	Huntington’s disease
HPMRS	hyperphosphatasia with mental retardation syndrome
HSP	heat shock protein
HTT	huntingtin gene
Htt	huntingtin protein
Httex1-103QP	mutant Htt that contains the proline-rich region
INQ	intranuclear quality control
IPOD	insoluble protein deposit
JUNQ	juxtanuclear quality control compartment
MoBY	Molecular Barcoded Yeast
mRNA	messenger RNA
N17	first 17 amino acids of huntingtin
NAC	nascent-chain-associated complex
NC	nascent chain
NES	nuclear export sequence
NGD	no-go decay
NLS	nuclear localization signal sequence
NMD	nonsense mediated mRNA decay
NPC	nuclear pore complex
NSD	non-stop decay
NS	non-stop
PBS	phosphate-buffered saline
PD	Parkinson’s disease
polyA	poly-adenine

polyK	poly-lysine
polyQ	poly-glutamine
polyR	poly-arginine
PQC	protein quality control
PRR	proline-rich region
RAC	ribosome-associated complex
RACK1	receptor for activated C kinase 1
RNA	ribonucleic acid
RQC	ribosome quality control
S-AEC	S-(2-Aminoethyl)-L-cysteine hydrochloride
SGA	synthetic genetic array
SG	stress granule
TFIID	transcription factor IID
tRNA	transfer RNA
UPS	ubiquitin proteasome system

Table of Contents

Chapter 1

Literature overview

Section 1.2 and 1.3 in this chapter are adapted from:

Fruhmann G., Seynnaeve D., **Zheng J**., Ven K., Molenberghs S., Wilms T., Liu B., Winderickx J., Franssens V. (2017) Yeast buddies helping to unravel the complexity of neurodegenerative disorders. Mechanisms of Ageing and Development, 161, 288-305

1.1. Protein quality control

To ensure cellular integrity, it is important to strictly control protein synthesis, (re-)folding and degradation. To do this, the cell is equipped with a sophisticated machinery, called the protein quality control (PQC) system. Malfunctioning of this system will lead to accumulation and eventually aggregation of misfolded proteins. Many neurodegenerative diseases, such as PD and HD, are related to the aggregation of amyloidogenic disease proteins such as α-synuclein for PD and Huntingtin (Htt) for HD. Hence, a well-balanced PQC network is essential for maintaining a healthy and functional proteome.

1.1.1. Protein folding and chaperone systems

1.1.1.1. Protein folding

Protein folding is already initiated while the peptide is being translated at the ribosome, and further folding occurs in the ER or the cytosol. The process of protein folding is inherently error-prone, due to the countless possible conformations that a protein can adopt (Balchin et al., 2016). Protein folding is affected by many weak, non-covalent interactions of amino acids within a protein's sequence (Brockwell and Radford, 2007). Furthermore, hydrophobic forces drive the formation of a polar environment by burying the non-polar amino acids within the core of a protein structure in order to form a thermodynamically stable conformation (Bartlett and Radford, 2009; Dinner et al., 2000). An *in vitro* study showed that small proteins refold spontaneously in appropriate folding conditions (Anfinsen, 1973), whereas the folding of larger proteins requires the assistance of chaperones (Fig. 1-1), whose major function is to prevent the aberrant interactions of proteins (Balchin et al., 2016). The major mechanistic paradigms of chaperone function in protein folding include Hsp70, chaperonin and Hsp90 systems.

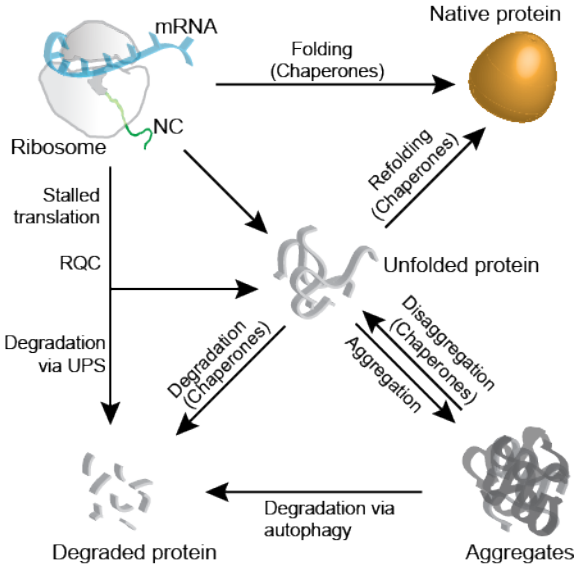

Figure 1-1. The chaperone-dependent network of protein quality control.
Stalled translation or stress-induced unfolded proteins are subject to different pathways. Chaperones play a crucial role in maintaining the native state of the protein, as well as in refolding the unfolded protein to its native state. Chaperones are also required for targeting unfolded proteins for aggregation or degradation. NC, nascent chain; RQC, ribosome quality control; UPS, ubiquitin proteasome system. Figure adapted from (Doyle et al., 2013).

1.1.1.2. Chaperone systems

A molecular chaperone is defined as any protein that interacts with, stabilizes, or helps another protein to acquire its functionally active conformation, without being present in its final structure (Balchin et al., 2016; Hartl, 1996). A large group of chaperones are named heat shock proteins (HSPs) due to their up-regulated role in cellular responses to stress, such as high temperature. Chaperones are evolutionary conserved and typically classified by their molecular mass (i.e. Hsp40, Hsp60, Hsp70, Hsp90, Hsp100, Hsp110 and small Hsp).

Proper protein folding and refolding largely depends on the functional activity of chaperones (Fig. 1-1). Chaperone-assisted protein folding occurs at the ribosome during *de novo* synthesis of proteins. Chaperones delay nascent chain compaction, thereby preventing misfolding and ensuring efficient folding of the protein (Balchin et al., 2016). In eukaryotes, the ribosome-binding chaperones include the ribosome-associated complex (RAC) and the nascent-chain-associated complex (NAC). The RAC, comprising chaperones of the Hsp70

and Hsp40 families, has been shown to play a role in coupling co-translational polypeptide folding during elongation (Chiabudini et al., 2012; Zhang et al., 2014), during which the RAC binds to the nascent polypeptide together with the NAC. When the NAC relocalizes from a ribosome-associated state to a protein aggregate-associated state as a chaperone, it diminishes translational capacity (Kirstein‐Miles et al., 2013). When translation is completed, both the newly synthesized protein and RAC/NAC are released from the ribosome. The folding process is further assisted by Hsp70 and Hsp40, which are required to reach the functional, native state of the protein (Hartl and Hayer-Hartl, 2002). In addition, Hsp70 provides a connection between the protein and the downstream chaperones such as the chaperonins and Hsp90 (Cuéllar et al., 2008; Kirschke et al., 2014).

In eukaryotes, the group II chaperonin CCT (chaperonin containing TCP-1, also named TRiC) facilitates folding of about 10% of the proteome, including many essential proteins such as cytoskeletal components and cell cycle regulators (Lopez et al., 2015). After dissociation of the protein from the ribosome, CCT/TriC-mediated folding of the protein needs a direct interaction between Hsp70 and CCT/TriC (Cuéllar et al., 2008). The ring-shaped CCT/TriC assists in post-translational protein folding by driving the protein substrate through the central cavity of CCT/TriC. This changes the conformation of the protein in order to reach its native state (Spiess et al., 2004).

Pathological conditions including environmental stress (e.g. high temperature), metabolic stress (e.g. oxidative stress), aging and cancer can disrupt the conformational structure of a protein, and enhance the production of misfolded proteins (Chen et al., 2011; Haigis and Yankner, 2010). The PQC system responds to this stress by recruiting the Hsp70 and small HSPs, to initiate protein refolding and to prevent irreversible aggregation (Haslbeck and Vierling, 2015). However, when the generation of misfolded proteins overwhelms the capacity of the PQC machinery, protein aggregates will accumulate.

Under some circumstances, a specialized group of chaperones named disaggregases (such as Hsp104), extract the misfolded protein from the multiprotein aggregate, and make it accessible for refolding or degradation (Glover and Lindquist, 1998; Parsell et al., 1994;

Wendler et al., 2007) (Fig. 1-1). This re-activation of the aggregated protein requires the assistance of Hsp70 and Hsp40 (Glover and Lindquist, 1998).

1.1.2. Protein degradation

1.1.2.1. Ubiquitin proteasome system (UPS)

In eukaryotes, the proteasome is a protein complex located in the nucleus, cytosol and ER (Baumeister et al., 1998; Peters et al., 1994) which functions as an intracellular degradation station for many proteins. Typically, the large 26S proteasome consists of a 20S core and one or two 19S regulatory subunits (Finley, 2009). The UPS plays a very important role in maintaining protein homeostasis as it targets proteins that have already fulfilled their cellular duties, such as proteins functioning during cell cycle, signal transduction, transcription, or decayed proteins from apoptosis or inflammation (Finley, 2009).

Proteins can only be recognized for degradation by the UPS if they are tagged with multiple ubiquitin molecules and this process involves a cascade of enzymes including an E1, E2 and E3 enzyme (Finley, 2009) (Fig. 1-2). The ubiquitination process starts with the activation of a ubiquitin molecule, by the ubiquitin-activating enzyme (E1) (Haas et al., 1982) (Fig. 1-2). The activated ubiquitin is then transferred to a second enzyme, i.e. the ubiquitin-conjugating enzyme E2. Next, the E3 ligase selects the substrate and transfers the ubiquitin from E2 to the substrate (Fig. 1-2). Additional ubiquitin-tagging to the same protein substrate generates a polyubiquitin chain. A minimum of four ubiquitin monomers is required for efficient recognition by the proteasome (Thrower et al., 2000) (Fig. 1-2). In this final step, a variety of E3 ligases are required due to the diversity of proteins targeted by the 26S proteasome (Risseeuw et al., 2003), and due to the fact that different E2s conjugate with different E3 ligases. In yeast, there is only one E1 enzyme, whereas there are 11 E2s, and a large family of E3s with an estimated number ranging from 60 to 100 (Finley et al., 2012).

An ubiquitin-tagged protein is recognized by the 19S lid of the proteasome. Although several ubiquitin receptors (Rpn10, Rpn13, Rad23, Dsk2 and Ddi1) have been reported, it is still not

clear how the number and arrangement of ubiquitin groups on a substrate affect its recognition by the proteasome (Finley, 2009). To become actively degraded by the proteasome, the substrate protein needs to be translocated into the channel of the 20S core of the proteasome. Furthermore, de-ubiquitination of the substrate protein is mandatory before its degradation (Liu et al., 2006), thereby recycling the attached ubiquitin available for recycling. Finally, the disassembled substrate protein is then degraded in the center of the proteasome (Fig. 1-2).

Studies have shown that UPS impairment is partly responsible for neuronal cell death. UPS impairment is induced by neurodegenerative disease-associated protein aggregation, possibly due to fact that aggregate formation inhibits the activity of UPS components, as well as by ageing, which reduces the cellular capacity to degrade misfolded protein degradation (Ciechanover and Kwon, 2015).

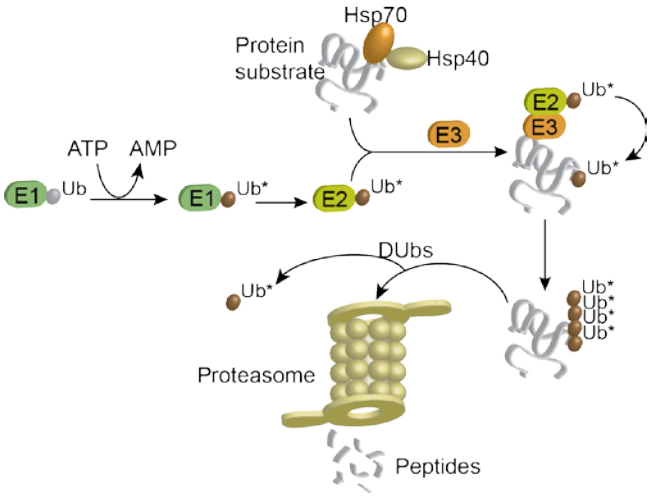

Figure 1-2. Schematic representation of UPS.
Activation of ubiquitin (Ub) by E1 is dependent on ATP hydrolysis. The activated Ub* is transferred to the ubiquitin-conjugating enzyme E2. Next, the E3 ligase recognizes both the E2-Ub* and the chaperone associated protein substrate and Ub* is transferredto the protein substrate. Finally, recognition of the poly-ubiquitinated protein substrate by the proteasome triggers removal of the ubiquitin molecules by deubiquitinating enzymes (DUbs), resulting in translocation of the protein substrate into the 20S core where the protein substrate is eventually degraded.

1.1.2.2. Autophagy and lysosomal degradation

Autophagy is a process that degrades misfolded proteins and damaged organelles in the lysosome (vacuole in yeast) (Mizushima et al., 2008). In this way, cellular components including small peptides and free amino acids are recycled (Chen and Klionsky, 2011; Kobayashi, 2015; Mizushima and Komatsu, 2011). There are several different types of autophagy including macroautophagy, microautophagy and chaperone-mediated autophagy (CMA) (Mizushima et al., 2008). During macroautophagy, cytoplasmic constituents or even entire damaged organelles are engulfed by a double-membrane vesicle, which is known as an autophagosome. These autophagosomes are transported to and fused with the lysosome where the contents of the autophagosome are degraded and recycled (Mizushima et al., 2011; Nakatogawa et al., 2009; Xie and Klionsky, 2007). Microautophagy refers to the sequestration of cytosolic components by lysosomes, through invaginations of their limiting membrane. Both macro- and microautophagy have the capacity to engulf large structures. Conversely, CMA degrades only soluble proteins and involves direct translocation of unfolded substrate proteins across the lysosome membrane with the assistance of chaperones (Mizushima et al., 2008). It has been reported that both macroautophagy and CMA are important for removing aggregated proteins (Cuervo and Wong, 2014; Iwata et al., 2005). Furthermore, it has been suggested that the autophagic system and the UPS system complement each other, thereby playing a crucial role in the cellular protein quality control.

Several studies also show that autophagic degradation is linked to neurodegeneration. More specifically, the degradation of disease-related misfolded proteins such as mutant Htt and α-synuclein is dependent on autophagy (Iwata et al., 2005; Rubinsztein, 2006; Rubinsztein et al., 2005). These findings suggest that the autophagic machinery is important for the cell’s defense against neurodegeneration.

1.1.3. Spatial distribution/sequestration of proteins

1.1.3.1. Protein aggregation

Protein aggregation and accumulation in neurons is a common hallmark of many neurodegenerative disorders, including PD and HD. Neurodegenerative disease-associated protein aggregation represents an end-stage of molecular cascades, which might be linked to the pathogenesis of these diseases. Deciphering the machinery of protein aggregation will provide clues to minimize the toxicity of misfolded protein.

Protein aggregation occurs when cells experience cellular stress which overwhelms the capacity of the PQC system (Wolfe and Cyr, 2011). Protein aggregation is dependent on hydrophobic forces, as well as on substrate concentration (Balchin et al., 2016; Chiti and Dobson, 2006). Most aggregates are amorphous/disordered, however, a subset of non-native protein aggregates seems to associate and fold into structural stable amyloid fibrils, which are forming cross-β structures (Balchin et al., 2016; Chiti and Dobson, 2006; Wolfe and Cyr, 2011). Moreover, these fibril structures are often generated by the accumulation of oligomeric aggregates, which are thought to be toxic species (Arrasate et al., 2004; Balchin et al., 2016; Choe et al., 2016).

Under certain circumstances, protein aggregates are also found in subcellular compartment, which are capable of sequestering, folding, refolding, and/or degrading aberrant proteins (Wolff et al., 2014). The first described subcellular compartment harboring protein aggregates was called aggresome (Kopito, 2000), which is a cytoplasmic microtubule-dependent inclusion. Protein aggregates are delivered to the aggresome via a microtubule-based transport (Johnston et al., 1998). More recently, also other subcellular compartments sequestering aggregates have been identified including IPOD, JUNQ/INQ, Q-bodies and it has been shown that the transport of protein aggregates to these compartments involves the actin cytoskeleton. (Liu et al., 2010; Ogrodnik et al., 2014; Song et al., 2014; Specht et al., 2011; Zhao et al., 2016).

1.1.3.2. IPOD and JUNQ/INQ

In 2008, Kaganovich and his colleagues reported the localization of protein aggregates in two spatial compartments i.e. the juxtanuclear quality control compartment (JUNQ) and the insoluble protein deposit (IPOD) (Kaganovich et al., 2008). JUNQ is positioned in close proximity of the nucleus and contains soluble ubiquitinated misfolded proteins. Moreover, components of the 26S proteasome and chaperones were also found in this compartment, which is thought to facilitate both degradation and refolding of misfolded proteins (Kaganovich et al., 2008). The other cytosolic compartment IPOD, is more stable, and preferentially harbors insoluble amyloidogenic misfolded proteins at the surface of the vacuolar membrane (Kaganovich et al., 2008; Spokoini et al., 2012). However, a recent study questioned the localization of the JUNQ compartment by showing that JUNQ resides inside the nucleus, and therefore re-defined this compartment as intranuclear quality control (INQ). Furthermore, they also demonstrated that ubiquitination of the substrate protein is not required for targeting both nuclear and cytosolic misfolded proteins to this compartment (Miller et al., 2015). This is also in contrast with the earlier findings of Kaganovich et al. (2008), showing that ubiquitin serves as an important signal to sort misfolded proteins to JUNQ (Kaganovich et al., 2008).

1.1.3.3. Asymmetric inheritance of damaged proteins

Spatial asymmetric distribution of proteins occurs between mother and daughter during cell division. Investigations in yeast have shown that damage proteins tend to accumulate in the mother cells, whereas daughter cells are free from damage proteins to this compartment (Aguilaniu et al., 2003; Erjavec et al., 2007; Liu et al., 2010). Similar asymmetric inheritance phenotype are observed in bacteria and mammalian cells as well (Lindner et al., 2008; Rujano et al., 2006). To ensure that daughter cells are born with a full replicative potential, cells have developed a conserved machinery for retrograde transport of heat-induced aggregates (Liu et al., 2010) and dysfunctional mitochondria (Higuchi et al., 2013). This retrograde transport of damaged cellular constituents depends on actin cables and Sir2. Asymmetric inheritance of

aggregated proteins is also regulated by vacuolar functions (Hill et al., 2016) and vacuolar acidity, in turn, impacts on cellular fitness and longevity (Hughes and Gottschling, 2012; Wilms et al., 2017).

1.1.4. Protein quality control at the ribosome

The normal translation of a protein is regulated by a variety of proteins. The messenger RNA (mRNA) template dependent translation guarantees that the accurate information is passed from the gene to its encoded protein. However, translational errors that occur at the ribosome can be the result of defective mRNAs, or mutation/insufficiency of tRNA that cause the ribosome to stall during translation and produce aberrant nascent chains (NCs). Cells have developed an evolutionary conserved quality control machinery to distinguish and clear the aberrant mRNA and NCs, hence preventing cells from consuming the limited available energy and substrates to synthesize defective products.

In eukaryotes, three types of defective mRNAs have been described that trigger the mRNA surveillance system: (1) The absence of a stop codon causes rapid degradation of the mRNA through the non-stop decay (NSD) pathway (Frischmeyer et al., 2002; van Hoof et al., 2002); (2) mRNA bearing a nonsense mutation leads to the generation of premature termination codons, which subjects the mRNA to the nonsense mediated mRNA decay (NMD) pathway (Kervestin and Jacobson, 2012; Losson and Lacroute, 1979; Maquat et al., 1981); (3) Hairpin RNA structures, rare codons and polylysine-codons cause ribosomes to stall and activate the no-go decay (NGD) pathway to eliminate the damaged mRNAs (Chen et al., 2010; Doma and Parker, 2006b; Tsuboi et al., 2012; van den Elzen et al., 2010).

The aberrant NCs from the ribosomal stall, however, will be recognized by the ribosome-associated quality control system and targeted for degradation (Bengtson and Joazeiro, 2010; Brandman et al., 2012; Choe et al., 2016). Recently, several breakthroughs have increased our understanding of this ribosome-associated quality control system. Here, we will highlight the discovery and the current insights of this quality control system.

1.1.4.1. The discovery of the RQC complex

For a long time, the fate of a nascent polypeptide generated from abnormal translation was largely unknown. However, in 2010 Bengtson and Joazeiro reported that the ribosome-associated E3 ubiquitin ligase Ltn1 labels nascent non-stop (NS) proteins with ubiquitin to direct them to the proteasome for degradation (Bengtson and Joazeiro, 2010). Next, a study by Brandman *et al*., which aimed to identify factors that modulate the activity of the heat-shock response factor (Hsf1), reported that deficiency of a group of proteins in a conserved ribosome-bound complex induces Hsf1 activity. This complex was called the ribosome quality control (RQC) complex, and comprises Ltn1, Rqc1, Rqc2 (named Tae2 at the time), Cdc48 and its cofactors Ufd1 and Npl4 (Brandman et al., 2012). This RQC complex was later confirmed by Defenouillere and his colleagues using a different approach. They showed that Cdc48, together with Ltn1, Rqc1 and Rqc2, is required for efficient degradation of NS-proteins (Defenouillère et al., 2013). At the same time, an independent research group under the supervision of Deshaies et al. demonstrated that Cdc48, Ufd1-Npl4 and Ltn1 are involved in mediating the clearance of ubiquitinated, tRNA-linked nascent peptides (Verma et al., 2013). Overall, these studies show that the RQC complex plays an important role in the clearance of aberrant protein from ribosome-stall during translation.

1.1.4.2. The RQC machinery

The key event for triggering the RQC pathway is ribosome stalling and translation arrest. Ribosome stalling is induced by multiple errors, including defective mRNA and tRNA.

Current insights in the RQC machinery are mainly obtained from studies using non-stop mRNAs (NS-mRNA) as substrate (Bengtson and Joazeiro, 2010; Choe et al., 2016; Defenouillère et al., 2013). In case the mRNA lacks a stop codon, the ribosome will read into the polyA tail of the mRNA during translation (Fig. 1-3) and consequently generates a poly-lysine (polyK) in the NCs. It has been shown that these polyKs are critical for ribosome stalling (Ito-Harashima et al., 2007). A similar stalling effect is observed when a polyK or

poly-arginine (polyR) tract was introduced into the amino acid sequence of a NC, and this may be identical to the effect of a NS mRNA (Dimitrova et al., 2009). Thus, the presence of a polybasic residue (polyK/R) in the NC seems to be sufficient to trigger ribosome stalling and translation arrest (Brandman et al., 2012; Choe et al., 2016; Dimitrova et al., 2009) (Fig. 1-3).

Other situations such as truncated mRNA (Shao et al., 2013; Tsuboi et al., 2012) and stem-loop structure mRNA (Doma and Parker, 2006b), which are directed to the no-go degradation (Fig. 1-3), also trigger ribosome stalling during translation and the stalled NCs are subjected to the RQC pathway. Interestingly, the rare codon CGA repeat strongly affects the translation efficiency and results in ribosome stalling (Letzring et al., 2010; Letzring et al., 2013) (Fig. 1-3). Moreover, mutation of a central-nervous-system-specific tRNA was found to cause ribosome stalling (Ishimura et al., 2014) (Fig. 1-3). Together, these findings suggest that the RQC mechanism is likely to be a vital part of the general machinery that recognizes aberrant NCs from the stalled ribosome during translation.

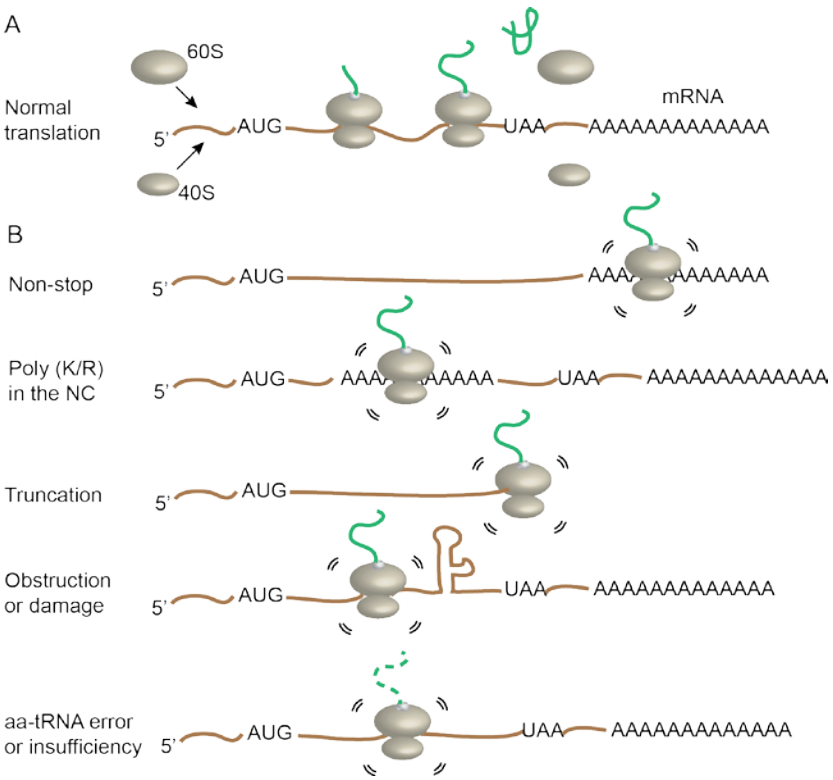

Figure 1-3. Different causes of ribosome stalling during translation.
(**A**) Normal mRNA template translation involves initiation (ribosome assembly), elongation, and termination (release of polypeptide and ribosome disassembly).

(**B**) Overview of aberrant translation in five different situations that cause ribosome stalling and translation arrest. The generated defective mRNAs and NCs are recognized and cleared by the mRNA decay pathway and the RQC pathway respectively. NC: nascent chain. Figure adapted from (Brandman and Hegde, 2016; Rodrigo-Brenni and Hegde, 2012).

So far, little is known about ribosome stalling and how translation arrest occurs exactly. It has been reported that the receptor for the activated C kinase 1 (RACK1) (yeast homolog Asc1) participates in the translation arrest of polyR nascent peptides (Kuroha et al., 2010). In addition, it was found that the RING-domain-containing E3 ligase Hel2 is involved in mediating the stalling of translation, although by an unknown mechanism (Brandman et al., 2012). However, it has been recently shown that Asc1, Hel2 and Slh1 are not required for the efficient translation arrest induced by a stalling reporter. Instead, these factors are essential for the RQC-mediated modification of NCs (Sitron et al., 2017). Thus, factors that are directly responsible for the ribosome stalling still remain to be elucidated.

Furthermore, stalled translation is required for the recruitment of the RQC complex (Brandman et al., 2012). Here, we focus on the events downstream of ribosome stalling, including the 80S ribosome disassembly, the RQC complex recruitment and the NCs ubiquitination and extraction (Fig. 1-4). First of all, dissociation of the 80S ribosome requires the presence of Hbs1, Dom34 and Rli1 (Becker et al., 2012; Pisareva et al., 2011; Shoemaker and Green, 2011). An *in vitro* study that recapitulates the ubiquitination of stalled NCs reveals that the stalled 80S ribosome splits into the 60S and 40S subunit (Shao et al., 2013) (Fig. 1-4). Removal of the 40S subunit exposes the inter-subunit interface of the 60S subunit that contains the NCs (Brandman and Hegde, 2016). While the short NCs drop off the 60S-NCs complex (Pisareva et al., 2011; Shoemaker et al., 2010), the longer NCs together with 60S recruit Rqc2 and Ltn1 (Lyumkis et al., 2014; Shao et al., 2015) (Fig. 1-4). Structural analysis of the RQC complex provides evidence that the Rqc2/Tae2 (mammalian nuclear export mediator factor, NEMF) binds to the 60S-NCs prior to Ltn1, and this binding facilitates the recruitment of Ltn1's N-terminal domain to the complex (Lyumkis et al., 2014; Shao et al., 2015). By performing a cryo-electron microscopy structure study, Shen et al. were able to conclude that Rqc2 and Ltn1 bind to the exposed sites of the 60S subunit after 40S

dissociation (Shen et al., 2015). Furthermore, ribosome stalling induces NC ubiquitination which is highly dependent on Ltn1 (Bengtson and Joazeiro, 2010; Brandman et al., 2012), and results in the recruitment of Cdc48 in a Rqc2- and Rqc1-dependent manner (Brandman et al., 2012; Defenouillère et al., 2013; Verma et al., 2013) (Fig. 1-4). In a next step, Cdc48 mediates extraction of NCs from the 60S-NCs complex in cooperation with its cofactors Ufd1 and Npl4. Finally, the ubiquitinated NCs are targeted to the proteasome for degradation (Bengtson and Joazeiro, 2010; Brandman et al., 2012; Verma et al., 2013) (Fig. 1-4).

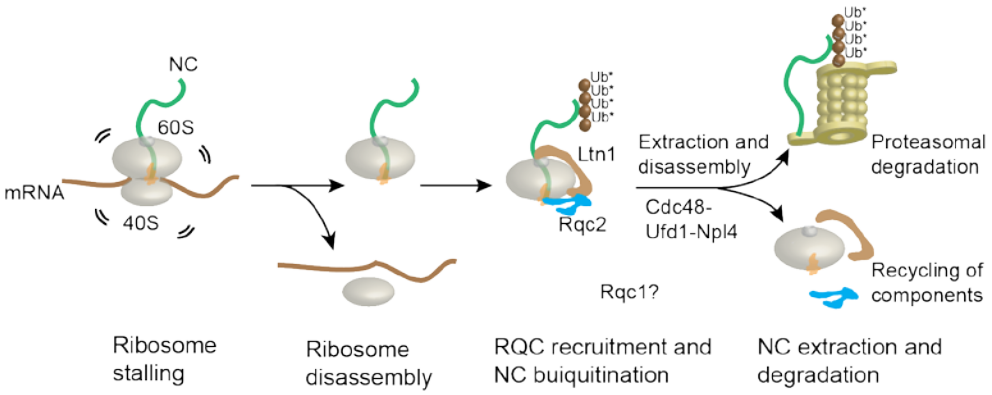

Figure 1-4. Primary steps and events of the RQC machinery.
Ribosome stalling and translation arrest triggers the disassembly of 80S ribosome into the 60S and 40S subunit. Removal of the 40S subunit exposes the 60S-NCs, which recruits the Rqc2 and Ltn1. Ltn1-mediated ubiquitination of NCs subsequently results in the recruitment of Cdc48 and its cofactors Ufd1 and Npl4. Rqc1 also appears to be required for Cdc48 recruitment, but its role in the RQC pathway is poorly known. Next, the Cdc48-mediated extraction of NCs takes place. Finally, free ubiquitinated NCs are targeted to the proteasome for degradation, whereas the 60S subunit, Ltn1 and Rqc2 are thought to be recycled. The mechanistic details via which the 60S-NCs-RQC complex disassembles remain largely elusive. Figure adapted from (Brandman and Hegde, 2016).

Both Ltn1 and Rqc2 are key players of the RQC machinery. While Ltn1 recognizes and ubiquitinates stalled NCs for degradation, Rqc2 fulfills a more diverse set of functions in the RQC machinery. First, Rqc2 monitors translation stress and signals to Hsf1 (Brandman et al., 2012), or signals for misfolded protein aggregation (Yang et al., 2016). More recently, it was reported that stalled NCs at the 60S ribosome elongate in an mRNA-independent manner, in which Rqc2 recruits and attaches carboxy-terminal Ala and Thr extensions (CAT-tails) to the stalled NCs (Shen et al., 2015). These CAT-tails species range from 5 to 19 residues and it has

been hypothesized that the CAT-tails promote Hsf1 activation (Shen et al., 2015). Follow-up studies show that the CAT-tails mediate NCs aggregation (Choe et al., 2016; Yonashiro et al., 2016), possibly as defense against aberrant translational stress at the ribosome. In addition, CAT-tails serve as a back-up mechanism that enables the degradation of RQC substrates that failed to be recognized by Ltn1 (Kostova et al., 2017). The exact role of these CAT-tails in NCs aggregation remains unclear, and other characteristics of the CAT-tails still need to be further explored.

1.1.4.3. Defective RQC and neurodegenerative diseases

It has been shown that the RQC machinery is highly conserved from yeast to mammals. As translation is under surveillance of the RQC system to guarantee the quality of the translational products, it is not surprising that malfunctioning of the RQC system has been implicated to play a crucial role in various protein misfolding diseases (Choe et al., 2016).

Indeed, it was shown that mutation of Listerin (mammalian orthologue of *LTN1*) causes neurodegeneration in a mouse model by an unclear mechanism (Chu et al., 2009). Mutation of tRNA synthetase, which results in low levels of mischarged tRNA, very likely triggers aberrant translation and can lead to an intracellular accumulation of misfolded proteins in neurons (Lee et al., 2006). Interestingly, mutation of a tRNA gene that is specifically expressed in the central nervous system under the GTPBP2-deficient background, causes ribosome stalling and widespread neurodegeneration in mice (Ishimura et al., 2014). A study aimed to identify players involved in IB formation of mutant Htt (mHtt103QP) in a yeast model, revealed the involvement of the RQC-Hsf1 system to direct compartmentalization of mHtt103QP (Yang et al., 2016). Thus, these studies provide evidence that there exists a connection between the RQC surveillance system and neurodegeneration. However, mechanisms underlying the defective-RQC instigated neurodegeneration are still largely unknown.

1.2. PD and the humanized Synphilin-1 yeast model

1.2.1. Introduction to PD

PD is, after Alzheimer's disease (AD), the second most common neurodegenerative disease. Moreover, it is the most prevalent movement disorder in elderly people. The disease is characterized by a decline in normal movement and daily functions. PD patients suffer from resting tremor, balance impairment, stiffness and bradykinesia. Furthermore, non-motor manifestations, including autonomic and cognitive dysfunction, have been associated with PD (Bostantjopoulou et al., 2013; Tolosa et al., 2006). In affected brains, there is a continuous and specific loss of dopaminergic neurons in the substantia nigra pars compacta, a brain section important in motor control. Another typical characteristic feature of PD is the presence of proteinaceous inclusion deposits, termed Lewy bodies, in the surviving neurons (Schneider and Obeso, 2014).

Different factors have been identified to increase the risk for developing PD. First, the prospect of sporadic PD increases with age and above the age of 60, the risk can rise up to 4%. Furthermore, the risk for PD onset can increase by certain environmental factors (De Lau and Breteler, 2006) or it can have a genetic cause. In fact, there are 21 loci and genes that are associated with familial forms of PD (Kalinderi et al., 2016).

The first gene discovered was the autosomal dominant gene, SCNA, which encodes α-synuclein, a 140 amino acid presynaptic protein (Polymeropoulos et al., 1997). Five missense mutations in α-synuclein (i.e. A30P (Krüger et al., 1998), E46K (Zarranz et al., 2004), H50Q (Porcari et al., 2015), G51D (Lesage et al., 2013), A53E (Pasanen et al., 2014) and A53T (Puschmann et al., 2009)), a duplication and a triplication of the gene are found in certain familial forms of PD (Chartier-Harlin et al., 2011; Singleton et al., 2003). Furthermore, this protein is the major component of the PD-typical Lewy bodies (Spillantini et al., 1997). Although the exact cellular function of α-synuclein remains unclear, several roles have been suggested, such as regulation of dopamine neurotransmission, synaptic vesicular recycling (Tofaris and Spillantini, 2007) and a role in the lipid metabolism (Golovko et al., 2009).

Overall, the discovery of PD risk genes made it possible to use modified cellular and animal models, carrying the mutant gene, to explore its effect on PD pathogenesis. Here we will focus on the use of *Saccharomyces cerevisiae* as a tool to study the role of Synphilin-1, an interaction partner of α-synuclein in PD.

1.2.2. Yeast model to study the role of Synphilin-1 in PD

In 2010 Büttner et al. established a yeast model to investigate the role of Synphilin-1 in PD (Büttner et al., 2010; Swinnen et al., 2011). Synphilin-1 is a α-synuclein interaction partner, which is found in Lewy bodies, together with α-synuclein. So far, the exact function of Synphilin-1 remains unclear. However, since it binds to presynaptic vesicles in the presynaptic terminal, a role in dopamine release, similar to α-synuclein, has been suggested (Szargel et al., 2009), in addition to a role as adaptor protein (Engelender et al., 1999). Studies in yeast models revealed that overexpression of Synphilin-1 induced a moderate growth defect on the cells during the exponential phase. However, Synphilin-1 gained toxicity in aged yeast cells and this appeared to be dependent on the sirtuin Sir2. Localization studies showed that Synphilin-1 initially spreads throughout the cytoplasm and forms inclusions in about one third of the yeast cells. Upon entering the diauxic shift, these small inclusions merge into one or a few large inclusions, often located at the poles of the cell (Büttner et al., 2010). Further investigation of these large Synphilin-1 inclusions suggested that they have a cytoprotective character and that both microtubules and the actin cytoskeleton are involved in the transport of the small Synphilin-1 inclusions into large aggregates (Büttner et al., 2010; Zhao et al., 2016). The fact that this model recapitulates an important hallmark of PD, i.e. the aggregation of disease proteins, makes it a useful tool to further investigate the mechanisms underlying aggregation management.

1.3. HD and the humanized Htt yeast model

1.3.1. Characteristics of HD and toxicity mechanisms

1.3.1.1. HD

HD is a neurodegenerative disorder characterized by uncontrolled movements, loss of cognition and behavioural changes. First symptoms arise around an age of 40 years and progress to death within 10-20 years after the disease onset. HD has a prevalence of 5-10 persons per 100,000 in the western world and many others carry a risk of developing the disease.

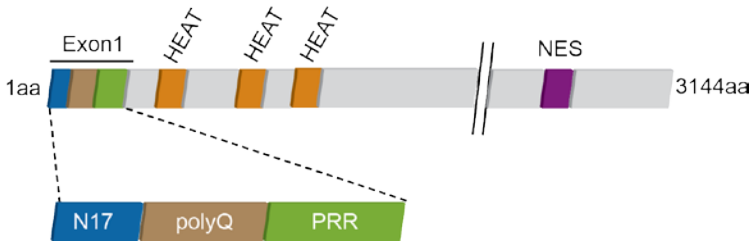

Figure 1-5. Schematic representation of the sequence and interaction domains of the Htt protein. Studies highlight the protein domains within the Htt, HEAT repeats and a nuclear export sequence (NES). Exon1 includes the first 17 amino acids of Htt (N17), the polyQ repeat domain, and the proline-rich region (PRR) and has shown to be critical for determining the toxicity of Htt. In our research, we use a construct containing N17 and 103Q repeats, which are widely used to study the HD pathogenesis. Figure adapted from (Truant et al., 2007).

A genetic defect in the gene named huntingtin (*HTT*) is directly responsible for HD. The *HTT* gene was first identified in 1993 and is located at chromosome 4p16.3 (MacDonald et al., 1993). An expanded CAG trinucleotide repeat in this gene was found in disease families compared to unaffected individuals. The expansion of the CAG triplet repeat encodes a polyglutamine (polyQ) domain in the N-terminus of the Htt protein (Fig. 1-5). Researchers have confirmed that the CAG repeat is unstable, and that individuals with more than 35 CAG repeats in *HTT* are under high risk of developing HD (MacDonald et al., 1993). However, mechanisms underlying the polyQ-induced toxicity or neuronal selective death remain

elusive.

1.3.1.2. Expanded polyQ in mutant Htt-induced cytotoxicity

Extensive effort has been made to understand the role of polyQ in HD. Deletion of *HTT* in mice resulted in the decease of homozygotes during embryonic development, indicating that normal Htt protein plays an important role in maintaining a healthy individual (Cattaneo et al., 2005; Duyao et al., 1995; Nasir et al., 1995; Walker, 2007). This suggest that mutant *HTT* is linked to a loss-of-function (Cattaneo et al., 2001). Nevertheless, increasing evidence supports the idea that the polyQ expansion results in a toxic gain-of-function. First, a single copy of the mutant *HTT* is sufficient to cause the neurological HD phenotype (Mangiarini et al., 1996), and the polyQ expansion does not block the expression of the *HTT* gene in mice (Schilling et al., 1995). Secondly, expression of mutant *HTT* in transgenic mice causes behavioral abnormalities, even in the presence of endogenous *HTT* with a normal expression level (Schilling et al., 1999). Finally, expression of the N-terminal part of mutant *HTT* exon 1 with 103Q is toxic to yeast cell (Meriin et al., 2002).

The accumulation of neuronal inclusions in neurons is a hallmark of HD pathology. However, whether the inclusion formation of mutant Htt is toxic or cytoprotective remains controversial. The observation of inclusions and the onset of neurological dysfunction of HD during the early phase of inclusion formation leads to the assumption that inclusions may be a causative species of HD (Morton et al., 2000). However, there is also evidence against a link between inclusions and HD pathology since behavioural changes, motor dysfunction and striatal neuronal loss can also be observed months before the detection of Htt inclusions (Slow et al., 2003; Van Raamsdonk et al., 2005). Furthermore, many neurons die without forming IB s, and the amount of diffuse intracellular Htt predicts whether and when IB formation or death will occur, thereby leading to the conclusion that IB formation reduces the levels of mutant Htt and the risk of neuronal death (Arrasate et al., 2004).

1.3.1.3. Localization and toxicity of mutant Htt

Studies investigating the Htt localization in neuronal cells, mammalian cell lines and transgenic mice reveal that both full-length and truncated N-terminal fragments of Htt are found in the nucleus and cytoplasm (Davies et al., 1997; De Rooij et al., 1996; DiFiglia et al., 1997; Saudou et al., 1998). These observations point towards a possible role for the nuclear localization of polyQ in HD pathology. Introducing a polyQ expanded Htt with a nuclear localization signal sequence (NLS) into transgenic mice enabled the majority of the mutant Htt to localize to the nucleus. In addition, the accumulation of the mutant Htt in the nucleus caused sufficient toxicity to elicit behavioral abnormalities. The results suggests that disruption of the nuclear processes may be a dominant mechanism causing toxicity in mouse models of HD (Schilling et al., 2004). Later studies also found that transcription factors co-localize with mutant Htt in nuclear inclusions, which provides evidences that polyQ protein causes cellular toxicity by sequestering essential proteins in the nucleus (Choi et al., 2012; Jiang et al., 2006; Schaffar et al., 2004). Moreover, a study in a striatal neurons cellular model reveals that nuclear localization of Htt induced neurodegeneration by an apoptotic mechanism (Saudou et al., 1998). Another study in a yeast model revealed that polyQ protein interferes with the degradation of other misfolded protein by sequestrating Sis1, an essential chaperone of Hsp40 family (Park et al., 2013). Nevertheless, it is still not clear how the mutant Htt is transported between the nucleus and the cytoplasm.

1.3.2. Budding yeast models for the investigation of mutant Htt-induced toxicity

By expressing different versions of human Htt protein, yeast models to investigate polyQ expanded Htt have been established successfully (Krobitsch and Lindquist, 2000; Meriin et al., 2002; Willingham et al., 2003). In these models, mutant Htt-induced toxicity behaves in a polyQ length-dependent manner. Overexpression of mutant Htt with 72 or 103 glutamines suppressed the growth of the yeast cells and induced the formation of misfolded protein aggregates, similar to those formed in human neuron (Krobitsch and Lindquist, 2000; Meriin

et al., 2001). This suggests that yeast models can faithfully recapitulate HD pathologic phenotypes, and the key steps in pathologic pathways might be shared in both human neuron and yeast. Indeed, several important findings in yeast have been successfully validated in mammalian models, or even patients. For example, kynurenine 3-monooxygenase was identified as a target to inhibit mutant Htt toxicity, which was confirm later in mammalian models (Mason and Giorgini, 2011; Winderickx et al., 2008).

Furthermore, insights in the mechanisms of mutant Htt-induced toxicity were obtained from yeast models. Many factors determining the mutant Htt-induced toxicity have been identified, including the sequence flanking the Htt polyQ domain, chaperone system, prion status, autophagy and cytoskeleton.

1.3.2.1. The flanking sequence of polyQ region affects mutant Htt toxicity

The proline-rich region (PRR) is a flanking sequence that belongs to the full length Htt, right behind the polyQ sequence in human cell. It has been shown that a toxic Htt polyQ construct without this PRR formed small, multiple and amorphous aggregates in yeast, which are considered to be the toxic species (Duennwald et al., 2006b; Meriin et al., 2002). In contrast, the Htt polyQ construct including the PRR formed big, tight inclusions, which were later described as “aggresome” (Wang et al., 2009), These “aggresomes” did not produce clear cytotoxicity effects in yeast (Dehay and Bertolotti, 2006; Duennwald et al., 2006b; Wang et al., 2009), supporting the notion that sequestration of misfolded protein into a tight, narrow compartment has a protective role in yeast. Interestingly, the cytotoxicity of 103Q was greatly reduced when co-expressed with a 25Q tract containing a PRR (25QP) (Duennwald et al., 2006a), suggesting that the PRR plays a critical role in antagonize the polyQ toxicity in yeast. By comparing the structure of the polyQ region in the presence and in the absence of the PRR, Lakhani et al were able to show that the PRR forms polyproline type II helices and decreases the probability of the polyQ region to form a β-rich state. This β-rich state formation is positive correlated to polyQ expansion length (Lakhani et al., 2010), These findings indicate that the PRR antagonizes the polyQ toxicity by interfering with the Htt polyQ domain folding

state.

1.3.2.2. Chaperones and prion status determine mutant Htt toxicity

The importance of the chaperone system and prion status in mutant Htt-induced toxicity has been reported intensively in yeast model systems. Investigation of the polyQ expanded Htt shows that polyQ protein aggregation depends on Hsp104, Sis1, Ssa1/2 and Rnq1. Moreover, it has been shown that the aggregation of the polyQ expanded protein is directly correlated to its cytotoxicity (Krobitsch and Lindquist, 2000; Meriin et al., 2002). Interestingly, overexpression of Hsp104, Sis1 or Ssa1 reduces the aggregation of mutant Htt in yeast (Krobitsch and Lindquist, 2000), and overexpression of Hsp104 in a mammalian cell model or mouse model reduced the aggregation and toxicity of the polyQ expanded protein (Bao et al., 2002; Carmichael et al., 2000; Vacher et al., 2005), even in the absence of a Hsp104 ortholog in the animal genome. Taken together, these findings suggest that a proper dosage of chaperone Hsp104 is required to maintain aggregation and cytotoxicity of polyQ expanded Htt. This is probably due to the essential role of Hsp104 in propagation of endogenous yeast prions, including *[PSI$^+$]* and *[PIN$^+$]* (Chernoff et al., 1995; Derkatch et al., 1997), which are thought to promote polyQ expanded Htt aggregation and toxicity (Gokhale et al., 2005). Thus, deletion of HSP104 will decrease prion formation, which results in the absence of clear mutant Htt induced toxicity. On the other hand, overexpression of Hsp104 cures yeast *[PSI$^+$]* by promoting dissolution of the prion seeds (Park et al., 2014), which also explains the detoxification effect of Hsp104 overexpression.

1.3.3. Yeast genome-wide screens to understand mutant Htt toxicity mechanism and to identify toxicity modifiers

The well-studied genomic sequence of *Saccharomyces cerevisiae*, easy DNA transformation and highly specific genetic modification through DNA recombination, make it possible to construct several yeast libraries such as the single deletion mutant collection (Tong et al., 2001) and the yeast GFP clone collection (Huh et al., 2003), These collections allow

automated high-throughput genetic modification through synthetic genetic array (SGA) analysis (Tong et al., 2001). Taking advantage of these techniques, researchers have performed several genome-wide screens in yeast model, and illustrate numerous fundamental molecular and biological processes of the mutant Htt, many of which can be recapitulated in multicellular organisms.

1.3.3.1. Genetic screens to identify toxicity modifiers of mutant Htt

In 2003 Willingham et al pioneered on using the yeast single deletion library to identify genes that influence the mutant Htt toxicity (Willingham et al., 2003), In this screen they identified 52 loss-of-function nonessential genes that enhance mutant Htt toxicity. These genes were clustered in proteins related to stress response, chaperones responsible for protein folding and UPS. A similar screen was performed for the PD associated protein α-synuclein. This screen identified different non-overlapping categories of loss-of-function genes that enhance α-synuclein toxicity, indicating that distinct pathogenic mechanisms underlie HD and PD. Following study, which performed the screen in a yeast deletion library, focused on loss-of-function genes that suppress mutant Htt toxicity (Fig. 1-6). Among the 28 genes that suppressed the toxicity of mutant Htt was Bna4 (kynurenine 3-monogenase), an enzyme in the kynurenine pathway of tryptophan degradation. These findings suggest a role for the kynurenine pathway in modulating mutant Htt toxicity (Giorgini et al., 2005), and thereby providing novel potential therapeutic targets for HD.

Three screens, which were performed almost simultaneously, introduced mutant Htt into a genome-wide overexpression collection (Fig. 1-6), to examine proteins that suppress polyQ expanded Htt toxicity. The screen overexpressing Htt103Q and an ORF library using two high-copy plasmids that both carried a galactose-inducible promoter, and identified two main suppressors of mutant Htt toxicity i.e.*GPX1* and *HYR1*. In addition, overexpression of *GPX1* in mammalian cells and *Drosophila*, also reported to ameliorate HD-relevant metrics (Mason et al., 2013). However, two other conceptually similar screens show no overlap with the identified mutant Htt toxicity modifiers of this screen, and provide evidence that the role of

GPX1 in suppressing Htt103Q toxicity is controversial. On the other hand, the two other screens identified proteins with prion-like domains to be key suppressors of mutant Htt toxicity (Kayatekin et al., 2014; Wolfe et al., 2014). Replacing asparagines with glutamines potently suppressed Htt103Q toxicity, while replacing glutamines with asparagines failed to suppress Htt103Q toxicity, suggests that the prion-like sequences of these proteins were themselves potent suppressors of polyQ expanded Htt toxicity (Kayatekin et al., 2014). A screen to identify modifiers of mutant Htt toxicity with a distinct strategy, in which yeast genomic DNA library (with endogenous promoter of each gene) was transformed into cells containing 103Q-GFP construct with galactose-inducible promoter. By validating transformants which were able to grow on induction of 103Q-GFP, Ripaud et al identified six suppressors of Htt103Q, three of which are glutamine-rich prion-like proteins (Ripaud et al., 2014). These findings suggest a critical role for glutamine-rich prion-like proteins in suppressing mutant Htt toxicity.

1.3.3.2. Chemical compound based screens

Apart from yeast genetic screens, libraries of chemical components and natural product extracts have been used to identify compounds that eliminate polyQ protein aggregation and toxicity. By expressing Htt103Q in a library of 16,000 small chemical compounds, Zhang et al. identified nine compounds that increased the growth of the yeast cells in the presence of Htt103Q (Zhang et al., 2005). Overexpression of Htt103Q in cell cultures with natural product extracts, led to the discovery of actinomycin D as a strong inhibitor of mutant Htt aggregation and toxicity (Walter et al., 2014).

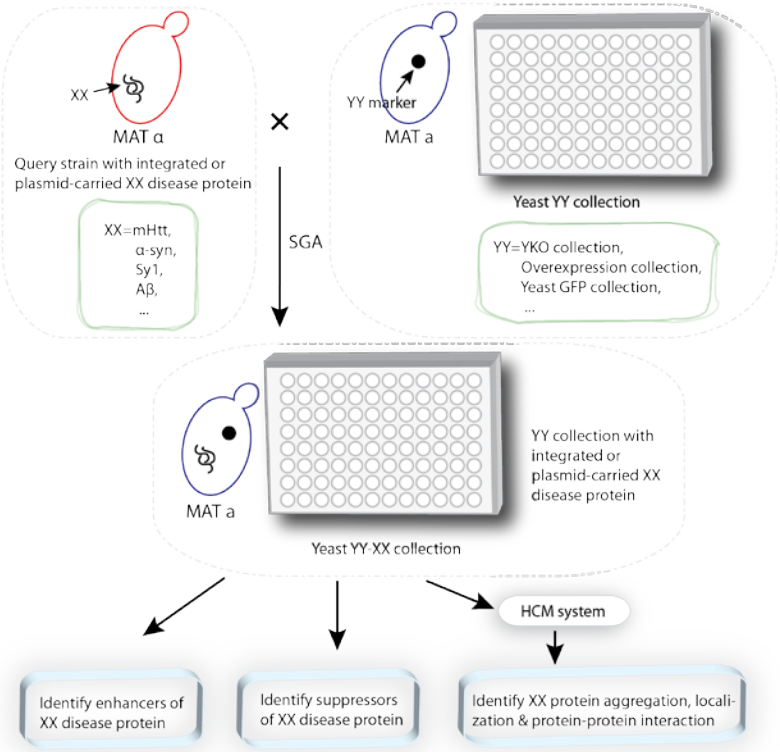

Figure 1-6. Key strategies of yeast based genome-wide screens.
Disease proteins (XX) with a specific selection marker can be introduced into the query strain, by integration in yeast genomic DNA or by expression from a plasmid. Examples of disease proteins for which such screens have been established are mutant Huntingtin (mHtt), α-synuclein (α-syn), Synphilin-1 (Sy1) and Amyloid beta (Aβ). A yeast collection (YY) with a different selection marker than the XX disease protein can be used as a starting collection. This YY collection can be a Yeast Knock-Out (YKO) collection, a yeast essential gene temperature sensitive (TS) alleles collection or a yeast overexpression collection, or a yeast GFP collection. Taking advantage of the SGA methodology, a new YY collection containing the XX disease protein (YY-XX) can be generated, by crossing the query strain (containing XX) with the YY collection. Further analysis of the YY-XX collection, such as growth analysis, can be used to identify enhancers or suppressors of XX disease protein. By combining the YY-XX collection with a recently developed HCM system, systematically analysis of factors affecting XX disease protein aggregation, localization can be identified, or by analyzing proteins co-localize with XX disease protein, proteins interact with XX disease protein can also be identified. Figure adapted from (Fruhmann et al., 2016).

1.3.3.3. Image-based HCM screen

Recently, a technique combining automated yeast genetics, SGA and HCM has been applied to study protein localization, protein-protein interaction and aggregate morphology in yeast (Chong et al., 2015; Vizeacoumar et al., 2010; Yang et al., 2016). This image-based screening

system, greatly relies on the SGA technique, either plasmid-borne fluorescence protein, or endogenous fluorescence proteins are tagged. This can be achieved by an elaborated design of the strain construction using the SGA technique (Fig. 1-6). Compared to the traditional SGA analysis which usually monitors growth, the HCM screening system allows more detailed analysis, including protein aggregation, protein localization, or protein interaction (Fig. 1-6).

Based on this unique high-throughput approach, a screen that focuses on stress granule (SG) formation has been performed. In this study, Yang et al. introduced a RFP-labeled Pab1 (a marker of SGs, which enables the visualization of SG *in vivo*) to a yeast single deletion collection, induced of SG formation and obtained images by the HCM system. This approach identified numerous genes involve in SG formation, providing valuable insights for understanding the mechanism involved in SG formation (Yang et al., 2014). A similar strategy was used in a later screen, in which an IB marker was introduced into the yeast GFP clone collection. By analyzing proteins that co-localize with IBs, the researchers found two proteins that exhibited strong interactions with lipid droplets, revealing an essential role for lipid droplets in cytosolic IBs clearance (Moldavski et al., 2015). More recently, Yang et al introduced the inclusion-forming mutant Htt (mHtt103QP) into the yeast collection, and induced the expression of mHtt103QP. The samples were applied to the HCM system, which allows automated image acquisition and analysis. They focused on the IB formation under different genetic backgrounds and were able to demonstrate the involvement of the RQC-Hsf1 system in directing compartmentalization of mHtt103QP (Yang et al., 2016).

Thus, we can expect more breakthroughs by using this versatile HCM system in investigating HD and other neurodegenerative diseases in yeast.

Aim of this thesis

Lewy body formation is a hallmark of PD, and Synphilin-1 was found as one of the major components of the Lewy body (Wakabayashi et al., 2000). However, the mechanisms involved in aggregation of these proteins are poorly understood.

The polyQ expansion of Htt is responsible for polyQ aggregation, and this is intimately linked with the polyQ-induced cytotoxicity that is typically associated with HD (Mangiarini et al., 1996). Fragments of polyQ-expanded Htt have been reported to localize both in the cytoplasm and nucleus (Davies et al., 1997; DiFiglia et al., 1997; Saudou et al., 1998), and alter the Htt-mediated cytotoxicity, suggests a potential role for the nuclear localization of polyQ proteins in HD pathology. However, the mechanisms involved in the translocation of polyQ-expanded Htt between the cytoplasm and the nucleus remain to be elucidated.

The main objectives of this thesis were:

1. To identify genes required for the inclusion formation of Synphilin-1 systematically. To this end, we performed an image-based genome-wide HCM screen, crossing the dsRed-Synphilin-1 to the yeast single knockout collection and the essential temperature sensitive allele collection. And to elucidate links and differences among hits involved in Synphilin-1 inclusion management, by analyzing enrichment of Gene Ontology (GO) categories, and classified them into several functional groups.

2. To identify players that alters the nucleocytoplasmic distribution of polyQ-expanded Httex1. Towards this aim, we performed a dual channel image-based genome-wide HCM screen, which allowed us to inspect the Httex1-103Q and nucleus simultaneously in different genetic background. And to decipher the roles of the components identified from HCM genome-wide screen in regulating the nucleocytoplasmic transport of Httex1-103Q.

Chapter 2

Establishment of genome-wide screening systems in yeast model

2.1. Introduction

A SGA analysis is a technique that makes the systematic construction of double mutants possible. In a typical SGA analysis a yeast query strain is crossed to an ordered array of ~5000 viable deletion mutants. The versatile SGA analysis allows genetic elements, which are marked by selectable markers, to cross to the ordered array of strains (Yan Tong and Boone, 2006). These genetic elements include specific alleles of genes, point mutants and temperature-sensitive alleles, or plasmids. This makes it possible to construct yeast strains systematically and investigate synthetic genetic interactions in a large scale (Tong et al., 2001; Tong et al., 2004). These advantages allowed researchers to perform genome-wide screens in yeast (Liu et al., 2010; Tong et al., 2001).

In this thesis we took advantage of the SGA methodology to address two important questions. The first question concerns the formation of Synphilin-1 inclusions. In 2010, Büttner et al. developed a yeast model to study the PD associated protein Synphilin-1. They were able to show that Synphilin-1 forms inclusions in yeast, which are often located at the poles of the cell (Büttner et al., 2010). However, the players involved in the inclusion formation of Synphilin-1 remain largely unknown. The second question involves another disease related protein Huntingtin. Similar as for Synphilin-1, a yeast model to study polyQ length-dependent toxicity of mutant Htt was established. The subcellular distribution of mutant Htt was shown to be important for determining its cytotoxicity, however, the exact mechanisms by which mutant polyQ-expanded Htt causes cytotoxicity and neuropathology remain unclear, and nuclear translocation of mutant Htt is poorly understood. To study both research questions in detail we designed several SGA screens. In this chapter, we give a detailed description of the strategies used for the different screens, the different steps of the SGA analysis and the SGA-based HCM screening systems. The results of these screens will be discussed in the following chapters.

2.2. Materials and methods

2.2.1. Construction of the Synphilin-1 SGA collection

Since the Synphilin-1 yeast model faithfully recapitulates one of the essential hallmarks of PD development i.e. the aggregation of Synphilin-1 in inclusions, this model is an excellent tool to search for players involved in the formation of Synphilin-1 inclusions (Büttner et al., 2010; Engelender et al., 1999). In this study, we used the same Synphilin-1 construct as described previously (Büttner et al., 2010). The construct has a pYX212 backbone and carries the dsRed-Sy1 under the control of the constitutive TPI1 promoter (pYX212-dsRed Sy1) (Fig. 2-1). The pYX212-dsRed construct served as a control. The Synphilin-1 SGA collection is used in the study described in chapter 3.

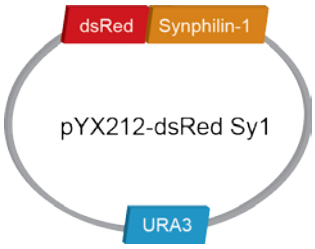

Figure 2-1. Schematic representation of the Synphilin-1 construct used in this study.
dsRed and Synphilin-1 were cloned and inserted into the pYX212 backbone plasmid, which carries an *URA3* selective marker (Büttner et al., 2010). Sy1 represents Synphilin-1.

To start the screen, we introduced the pYX212-dsRed Sy1 plasmid into a yeast genome-wide single deletion array (SGA-V2) (Tong et al., 2001) and a yeast temperature-sensitive conditional mutant array (ts-V5) (Li et al., 2011), all mutants are derived from BY4741.

2.2.1.1. Query strain

To cross the pYX212-dsRed Sy1 plasmid with the (SGA-V2) and (ts-V5) collection, we first introduced the pYX212-dsRed Sy1 plasmid into the starting query strain Y7092 (Tong and Boone, 2007). This Y7092 strain harbors reporters and markers necessary for SGA haploid

strain selection following meiotic recombination. In the *MATα* Y7092 strain, the *CAN1* is replaced by the SGA reporter *STE2pr-Sp_his5*, and the *STE2pr* represents the *MATa*-specific *STE2* promoter, driving the *Schizosaccharomyces pombe his5* (*Sp_his5*) gene, which complements *S. cerevisiae HIS3* (Baryshnikova et al., 2010). In addition, the pYX212-dsRed Sy1 carries a selective marker *URA3* (Fig. 2-1). The obtained query strain Y7092 pYX212-dsRed Sy1 was used for the Synphilin-1 SGA strain construction.

2.2.1.2. Mating, sporulation and selections

Haploid yeast cells have mating type a (*MATa)* or α (*MATα)*. The query strain Y7092 pYX212-dsRed Sy1 is a *MATα* strain and carries selective markers including *URA3*, *can1*Δ::*STE2pr-Sp_his5* and *lyp1*Δ. This query strain is crossed to the (SGA-V2) and (ts-V5) array, which are *MATa* strains carrying a gene deletion mutation or temperature sensitive allele linked to a *kanMX* marker that confers resistance to the antibiotic geneticin (G418). The contact of *MATa* and *MATα* cells makes it possible to generate the zygotes (diploid cells) (Fig. 2-2). The zygotes are then transferred to the minimal medium with limited carbon and nitrogen to induce the sporulation. The spores together with the zygotes are transferred to the medium lacking histidine, thereby allowing the selection of cells carrying the *STE2pr-Sp_his5* reporter (Fig. 2-2). Since the *STE2* promoter is *MATa*-specific, only *MATa* meiotic progeny are able to proliferate. Furthermore, the administration of canavanine and thialysine (S-AEC, (S-(2-Aminoethyl)-L-cysteine hydrochloride)), kill the unwanted diploid cells and spores with the *CAN1* and *LYP1* gene (Grenson et al., 1966; ZWOLSHEN and Bhattacharjee, 1981). Therefore, the haploid selection medium (SD-His/Arg/Lys/Ura + canavanine & S-AEC) selects the haploid *MATa* cells with the marker *can1*Δ::*STE2pr-Sp_his5* and *lyp1*Δ (Fig. 2-2). Cells are then transferred to the KanR selection medium with G418, which selects the cells with a KanR marker (Fig. 2-2). All mediums are lacking uracil to maintain the pYX212-dsRed Sy1 plasmid in the cells throughout the construction. The medium protocol for the construction of the Synphilin-1 SGA collection is described in Appendix.

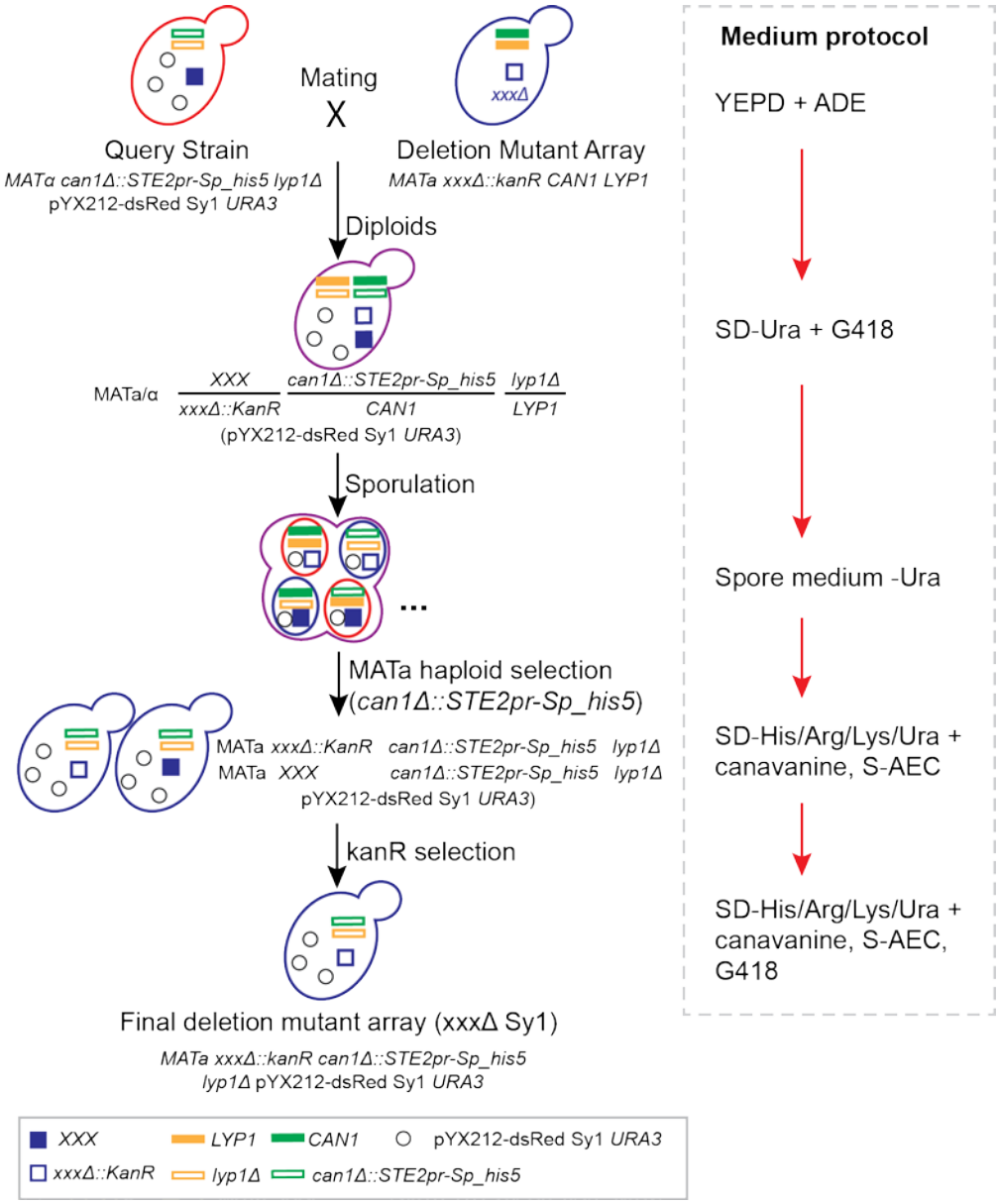

Figure 2-2. SGA methodology to cross the pYX212-dsRed Sy1 plasmid into the SGA-V2 or (ts-V5) collection (Figure adapted from (Baryshnikova et al., 2010; Tong and Boone, 2007))**.** The *MATα* strain, carries the selective markers *can1*Δ::*STE2pr-Sp_his5*, *lyp1*Δ and pYX212-dsRed Sy1 *URA3* and is crossed into the (SGA-V2) and (ts-V5) array. These arrays are ordered with *MATa* strains each carrying a gene deletion mutation or temperature sensitive allele linked to a *kanMX* marker that confers resistance to the antibiotic geneticin (G418). Contact of *MATa* and *MATα* cells generates the diploid cells. Following, the diploid cells are incubated in minimal medium with limited carbon and nitrogen to induce the sporulation. Next, the spores and the remaining diploid cells are transferred to medium lacking histidine, which allows the selection of *MATa* cells carrying the *STE2pr-Sp_his5* reporter. The *can1*Δ and *lyp1*Δ strains confered resistance to canavanine and S-AEC respectively. While addition of canavanine and S-AEC to the selection medium kills *CAN1* and *LYP1* cells. Finally, the cells are transferred to the KanR selection medium with G418, which selects the cells with the KanR marker.

2.2.2. Construction of the Httex1-103Q SGA collection

The Exon-1 of *HTT* contains a polyQ tract and it has been demonstrated that expansion of this polyQ tract is responsible for the development of HD (MacDonald et al., 1993). In this study, we used a construct that contains the N17 sequence of the *HTT* gene, as well as an expansion region with 103 glutamines (103Q) under the control of the *GAL1* galactose-inducible promoter and a FLAG tag at the N-terminus of the construct (Fig. 2-3). In addition the pYES2 backbone contains the selective marker *URA3* and a C-terminal GFP tag enabling *in vivo* visualization of the 103Q protein (Meriin et al., 2002) (Fig. 2-3). Expression of this construct has shown to induce toxicity in yeast cells (Meriin et al., 2002).

To construct the Httex1-103Q SGA collection we used the same strategy as described for the construction of the Synphilin-1 SGA collection in 2.2.1, i.e. we crossed the pYES2-Httex1-103Q-GFP plasmid to the (SGA-V2) and (ts-V5) collection. The Httex1-103Q SGA collection is used in the study described in chapter 4.

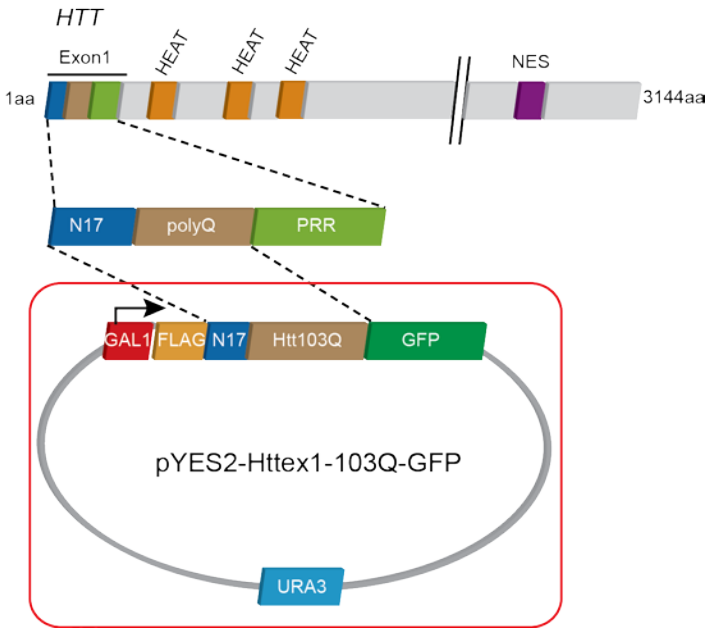

Figure 2-3. Schematic representation of the mutant Htt construct used in this study.
The sequence and domains of the Htt protein are described in Figure 1-5. The construct used in this study is a gift from Dr. Sherman (Meriin et al., 2002). The N17 and polyQ repeat region of Htt were replicated, together with a N-terminal tagged FLAG, and a C-terminal tagged GFP. These segments were inserted in the high copy pYES2 plasmid with the galactose-inducible GAL1 promoter and a selective *URA3* marker in the backbone.

2.2.2.1. Query strain

The query strain used is the Y7092 strain containing the pYES2-Httex1-103Q-GFP plasmid. The genetic background of the Y7092 strain is described in 2.2.1.1.

2.2.2.2. Mating, sporulation and selections

The different steps to construct the Httex1-103Q SGA collection including mating, sporulation and selections are identical to the steps that are described in 2.2.1.2 for the construction of the Synphilin-1 SGA collection. Details of the genetic modification processes are described in Fig. 2-4, and the medium protocol for the construction of the Httex1-103Q SGA collection is described in Appendix.

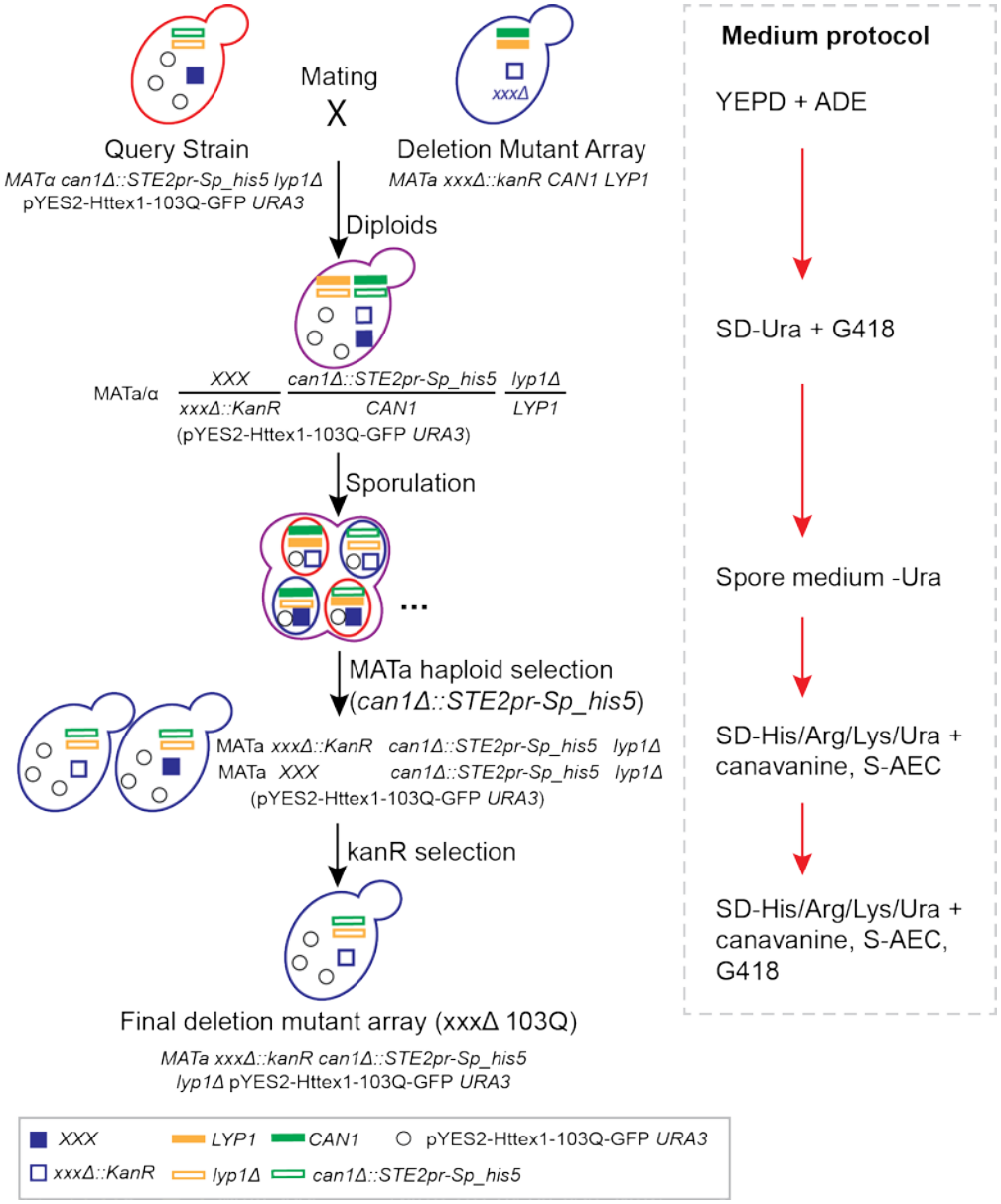

Figure 2-4. SGA methodology to cross the pYES2-Httex1-103Q-GFP plasmid into the SGA-V2 or (ts-V5) collection (Figure adapted from (Baryshnikova et al., 2010; Tong and Boone, 2007))**.** The *MATα* strain, carries the selective markers *can1*Δ::*STE2pr-Sp_his5*, *lyp1*Δ and pYES2-Httex1-103Q-GFP *URA3* and is crossed into the (SGA-V2) and (ts-V5) array. These arrays are ordered with *MATa* strains each carrying a gene deletion mutation or temperature sensitive allele linked to a *kanMX* marker that confers resistance to the antibiotic geneticin (G418). Contact of *MATa* and *MATα* cells generates the diploid cells. Following, the diploid cells are incubated in minimal medium with limited carbon and nitrogen to induce the sporulation. Next, the spores and the remaining diploid cells are transferred to medium lacking histidine, which allows the selection of *MATa* cells carrying the *STE2pr-Sp_his5* reporter. The *can1*Δ and *lyp1*Δ strains confered resistance to canavanine and S-AEC respectively. While addition of canavanine and S-AEC in the selection medium kills *CAN1* and *LYP1* cells. Finally, the cells are transferred to the KanR selection medium with G418, which selects the cells with the KanR marker.

2.2.3. Construction of the *ltn1*Δ Httex1-103Q SGA collection

The construction of the *ltn1*Δ Httex1-103Q SGA collection is similar to the construction of the Httex1-103Q SGA collection described in section 2.2.2.

2.2.3.1. Query strain

The query strain Y7092 *ltn1*Δ pYES2-Httex1-103Q-GFP was used for the construction of the *ltn1*Δ Httex1-103Q SGA collection. To obtain this query strain, an insertion of the nourseothricin-resistance *natR* cassette into the *LTN1* loci (*ltn1*Δ::*natR*) was made in the query strain Y7092 pYES2-Httex1-103Q-GFP (2.2.2.1) .

2.2.3.2. Mating, sporulation and selections

The different steps to construct the Httex1-103Q SGA collection including mating, sporulation and selections are similar to the steps described in 2.2.1.2 for the construction of the Synphilin-1 SGA collection. Additional clonNAT is added to select cells carrying the natR cassette. Details of the genetic modification processes are described in Fig. 2-5. The medium protocol for the construction of the *ltn1*Δ Httex1-103Q SGA collection is described in Appendix.

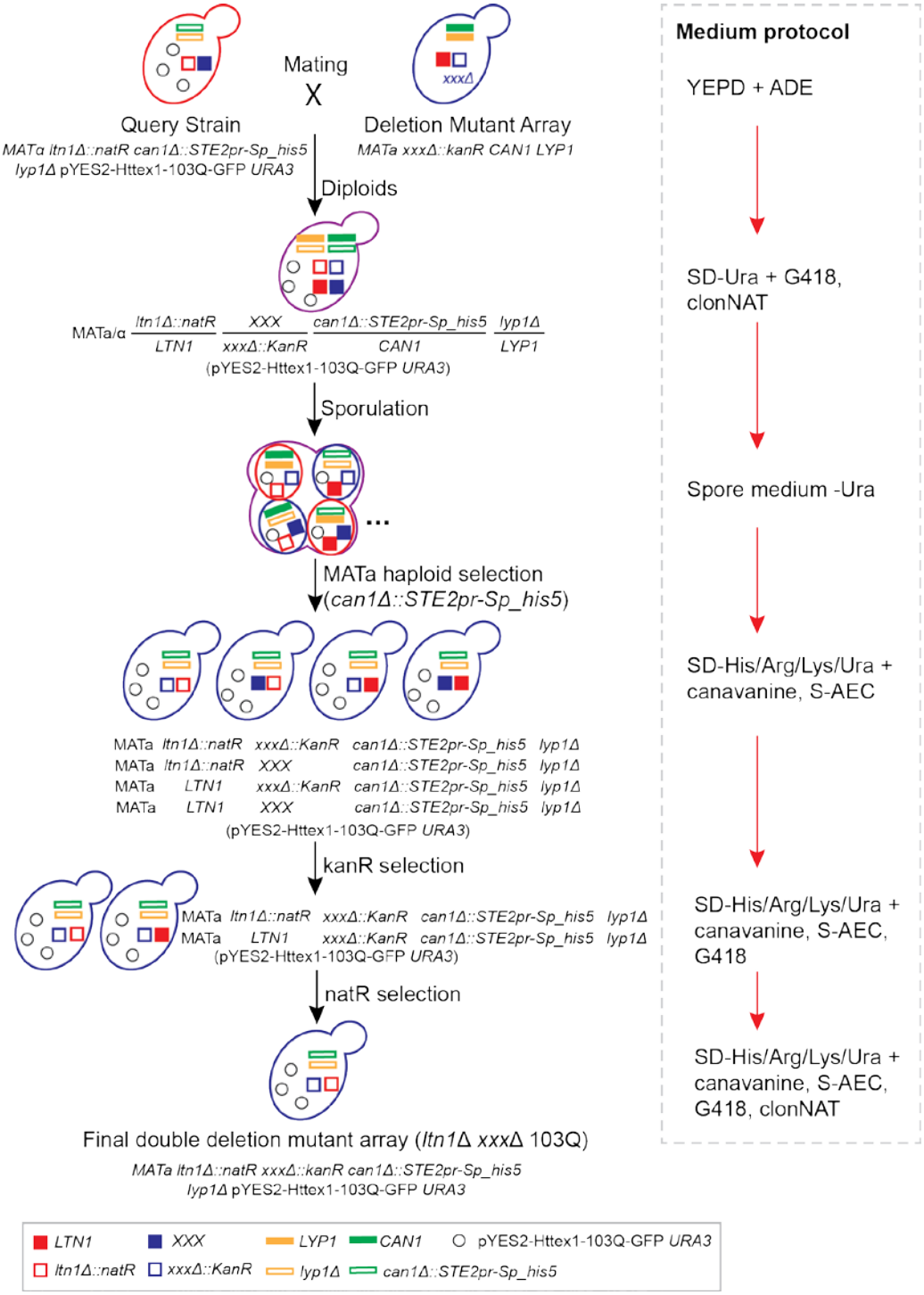

Figure 2-5. SGA methodology to cross the *LTN1* deletion and pYES2-Httex1-103Q-GFP plasmid into the SGA-V2 or (ts-V5) collection (Figure adapted from (Baryshnikova et al., 2010; Tong and Boone, 2007))**.** The query strain, which is *MATα*, carries the selective markers *can1*Δ::*STE2pr-Sp_his5*, *lyp1*Δ and pYES2-Httex1-103Q-GFP *URA3* in the *ltn1*Δ background and is crossed into the (SGA-V2) and (ts-V5) array. These arrays are ordered with *MATa* strains each carrying a gene deletion mutation or temperature sensitive allele linked to a *kanMX* marker that confers resistance to the antibiotic geneticin (G418). Contact of *MATa* and *MATα* cells generates the diploid cells. Following, the diploid cells are incubated in minimal medium with limited carbon and nitrogen to induce the sporulation. Next, the spores and the remaining

diploid cells are transferred to medium lacking histidine, which allows the selection of *MATa* cells carrying the *STE2pr-Sp_his5* reporter. The *can1*Δ and *lyp1*Δ strains confered resistance to canavanine and S-AEC respectively. While addition of canavanine and S-AEC in the selection medium kills *CAN1* and *LYP1* cells. The cells are then transferred to the KanR selection medium with G418, which selects the cells with a KanR marker. This is followed by natR selection by adding additional clonNAT to the selective medium.

2.2.3.3. Validation of Httex1-103Q toxicity suppressors in *ltn1*Δ background

We replicated the *ltn1*Δ Httex1-103Q SGA collection to an agar plate with medium containing SD-His/Arg/Lys/Ura + canavanine, S-AEC, G418 & clonNAT and galactose as the sole carbon source of the medium. The cells were kept at 30 ^{o}C for 3 days, and the growth was recorded by imaging the colonies on the plates. We assessed the Httex1-103Q cytotoxicity of the different double mutants by scoring the size of the colonies (Wagih and Parts, 2014).

2.2.4. Construction of the Httex1-103Q-mRFP Yeast GFP Clone Collection

To investigate proteins that interact with Httex1-103Q *in vivo*, we performed an image-based screen to visualize both endogenous GFP-tagged proteins and Httex1-103Q. To achieve this goal, we first constructed a Yeast GFP Clone Collection (Huh et al., 2003) containing the Httex1-103Q-mRFP reporter (Wang et al., 2007).

2.2.4.1. Query strain

To cross the pYES2-Httex1-103Q-mRFP plasmid (Wang et al., 2007) to the Yeast GFP Clone Collection, we first introduced the pYES2-Httex1-103Q-mRFP plasmid into the starting strain Y7039 (Tong and Boone, 2007). The Y7039 strain harbors the reporters and markers necessary for the SGA haploid strain selection following meiotic recombination. In the *MATα* Y7039 strain, the *CAN1* is replaced by the SGA reporter *STE2pr-Sp_LEU2*. The query strain Y7039 pYES2-Httex1-103Q-mRFP is used for the construction of the Httex1-103Q-mRFP Yeast GFP Clone Collection.

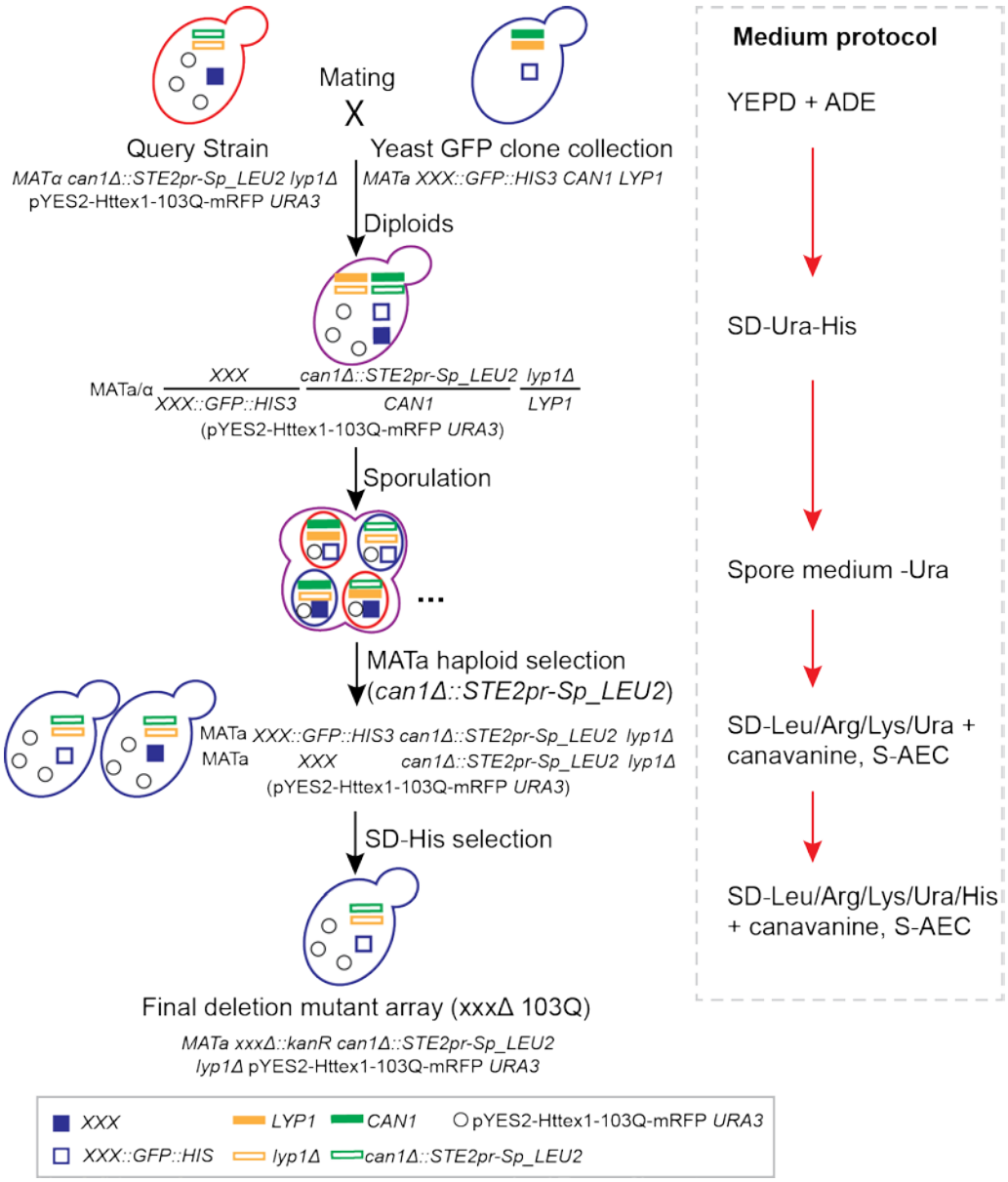

Figure 2-6. SGA methodology to cross the pYES2-Httex1-103Q-mRFP plasmid into the Yeast GFP Clone Collection (Figure adapted from (Baryshnikova et al., 2010; Tong and Boone, 2007))**.** The query strain, which is *MATα*, carries the selective markers *can1*Δ::*STE2pr-Sp_LEU2*, *lyp1*Δ and pYES2-Httex1-103Q-mRFP *URA3* and is crossed to the Yeast GFP Clone Collection. This collection is ordered with *MATa* strains each carrying a gene that is follow by a GFP cassette and *HIS3* cassette. Contact of *MATa* and *MATα* cells generates the diploid cells. Following, the diploid cells are incubated in minimal medium with limited carbon and nitrogen to induce the sporulation. Next, the spores and the remaining diploid cells are transferred to medium lacking leucine, which allows the selection of *MATa* cells carrying the *STE2pr-Sp_LEU2* reporter. The *can1*Δ and *lyp1*Δ strains confered resistance to canavanine and S-AEC respectively. While addition of canavanine and S-AEC in the selection medium kills *CAN1* and *LYP1* cells. Finally, the cells are transferred to the SD-His medium that lacks histidine, which selects the cells with the *HIS3* cassette.

2.2.4.2. Mating, sporulation and selections

The query strain Y7039 pYES2-Httex1-103Q-mRFP is a *MATα* strain and carries selective markers including *URA3*, *can1*Δ::*STE2pr-Sp_LEU2* and *lyp1*Δ. This strain is crossed to the Yeast GFP Clone Collection, which is ordered with *MATa* strains each carrying a gene that is followed by a GFP cassette and *HIS3* marker. Details of the genetic modification processes are described in Fig. 2-6. The medium protocol for the construction of the Httex1-103Q-mRFP Yeast GFP Clone Collection is described in Appendix.

2.2.5. Image-based HCM screening systems

2.2.5.1. HCM to investigate Synphilin-1 inclusion formation

The collection obtained from section 2.2.1 was applied to the HCM system. We used the Singer ROTOR HDA robot (SINGER INSTRUMENTS, Somerset) to pin cells to 96-well plate with 200μl minimal selective SC-Ura liquid medium with antibiotics at 30°C（22°C for ts mutants）for 3 days without shaking. Subsequently, each pre-culture was diluted to a starting OD_{600nm} around 0.1 in a 200μl culture in SC-Ura medium, by using the Automated Liquid Handling robot (HAMILTON, Reno NV). After 12h (16h for ts mutants) growing with shaking at 30°C (for both single and ts mutants), cells were fixed by adding 20 μl 37% formaldehyde to a final concentration of 3.7% for 30min at room temperature. Then cells were washed twice with 1xPBS (4,000 rpm for 3min). Finally, the cells were re-suspended in 200μl 1xPBS and stored at 4°C overnight. For imaging, 9μl re-suspended cells were transferred to new 96-well glass bottom plates (Matri-plate) with 200μl 1×PBS in each well. The OD_{600nm} values were adjusted to 0.06-0.08, which corresponds to about $6\text{-}8\times10^4$ cells. The cells in the 96-well plate were spun down at 400rpm for 45s, and kept in dark for 30 min before imaging (Texas Red channel, Exposure time: 400ms) with the automated cellular imaging system ImageXpress MICRO, Molecular Devices Corporation (MDC).

The key procedures of this screen are described in Fig. 2-7.

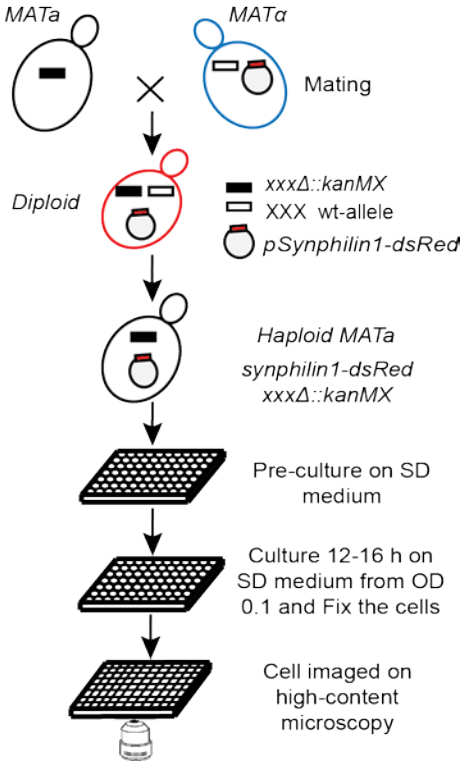

Figure 2-7. Schematic representation of the HCM screening system to investigate Synphilin-1 inclusion formation. Cells generated as described in the section 2.2.1 were pre-cultured in selective medium, until cells reached saturation. The cells were diluted to OD_{600nm} ~0.1 in selective medium for 12h or 16h (ts). Next, the cells were collected and fixed with 3.7% formaldehyde. Finally, the cells were applied to the HCM imaging microscope. Images were obtained in Texas Red channel.

2.2.5.2. HCM to investigate the subcellular localization of Httex1-103Q

We used the Singer ROTOR HDA robot (SINGER INSTRUMENTS, Somerset) to pin cells from the Httex1-103Q SGA (section 2.2.2) collection to the agar plate (SD-His/Arg/Lys/Ura + canavanine, S-AEC & G418). The strains were laid out in 12-by-8 arrays, and incubated at 30^{o}C for 2 days. Subsequently, cells were inoculated in the 96-well plates with liquid medium (SD-His/Arg/Lys/Ura + canavanine, S-AEC & G418) and incubated at 30^{o}C for 2 days. We used the Automated Liquid Handling robot (HAMILTON, Reno NV) to transfer 10µl cells from the SGA 96-well liquid plate to the pre-culture plate, containing 190µl liquid medium (SD-His/Arg/Lys/Ura + canavanine, S-AEC & G418) with 2% raffinose and incubated the cells at 30^{o}C without shaking for 2 days.

The OD_{600nm} for each sample was measured by using the Plate Reader (POLARstar Omega, BMG LABTECH). The pre-cultured cells were diluted in fresh liquid medium with 2% raffinose (SD-His/Arg/Lys/Ura + canavanine, S-AEC & G418) to an OD_{600nm} of 0.1 in a final volume of 180µl. Then the cells were incubated overnight at 30^{o}C while shaking, until most of the cells reached OD_{600nm} ~0.5. Next, 20µl 20% galactose was added to each well and incubated again at 30^{o}C for 3 hours while shaking. After this 22µl 37% formaldehyde was added to each well and mixed thoroughly by pipetting. The samples were kept at room temperature for 30 minutes, and centrifuged at 4000 rpm for 3 min. The supernatant was removed and washed with 1xPBS twice.

Subsequently, a proper volume of the cells was transferred to 96-well clean bottom optical imaging microplates (Brooks, MGB096-1-2-LG-L) and the OD_{600nm} of the samples was adjusted to ~0.15 with 1xPBS. Then 20µl 1µg/ml 4',6-diamidino-2-phenylindole (DAPI) was added to each well to obtain a total volume 200µl. The samples were kept in the dark at room temperature for 30min and spun down to the bottom of the imaging microplates at 400rpm for 30s.

Finally, the cells were imaged by using the high-content imaging microscope (ImageXpress MICRO) in both GFP and DAPI channels with an exposure time of 400 ms for GFP and 100 ms for DAPI.

The key procedures of this screen are described in Fig. 2-8.

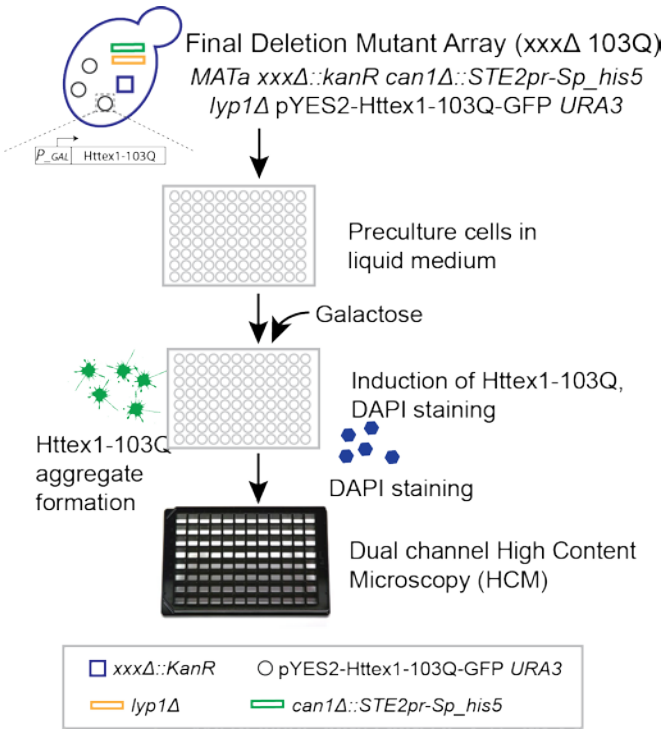

Figure 2-8. Schematic representation of the HCM screening system to investigate subcellular localization of Httex1-103Q. Cells generated as described in section 2.2.2 were incubated in selective medium (containing 2% glucose), until the cells reached saturation and subsequently diluted cells to OD_{600nm} ~0.1 in selective medium with 2% raffinose. When the OD_{600nm} reached ~0.5, galactose (final concentration 2%) was added directly to the medium to start the induction of Httex1-103Q-GFP expression. The cells were stained with DAPI to visualize the nucleus. Images were obtained under GFP and DAPI channels.

2.2.5.3. HCM to identify proteins that co-localized with Httex1-103Q

Induction of Httex1-103Q-mRFP for this HCM screen was similarly as described in 2.2.5.2, and the SD-Leu/Arg/Lys/Ura/His medium with canavanine and S-AEC was used. Samples were prepared without the DAPI staining procedure (Fig. 2-9).

The cells were imaged by using the high-content imaging microscope (ImageXpress MICRO) in both GFP and Texas Red channels, with an exposure time of 3000 ms for GFP and 400 ms Texas Red.

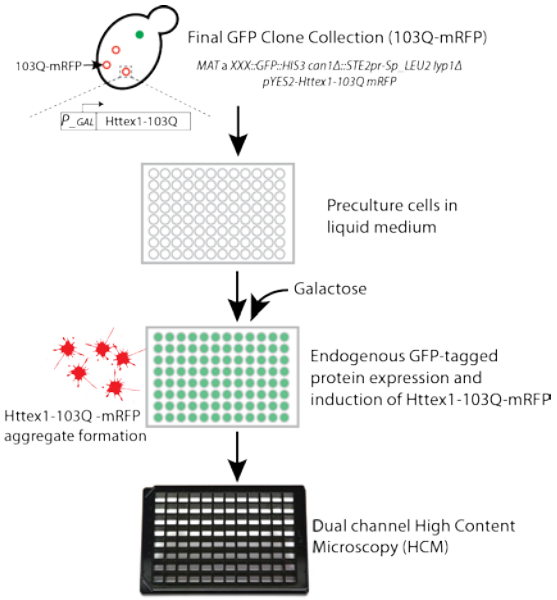

Figure 2-9. Schematic representation of the HCM screening system to identify proteins that interacted with Httex1-103Q. Cells generated as described in the section 2.2.4 were incubated in selective medium (containing 2% glucose), until the cells reached saturation. Then the cells were diluted to an OD_{600nm} ~0.1 in selective medium with 2% raffinose. When the OD_{600nm} reached ~0.5 galactose (final concentration 2%) was added directly to the medium to start the induction of Httex1-103Q-mRFP expression. Images were obtained under GFP and Texas Red channels. Red circle represent the pYES2-Httex1-103Q-mRFP plasmid and green dots represent endogenous GFP-tagged protein.

2.2.5.3. Super-resolution three-dimensional structured illumination microscopy (3D-SIM)

For super-resolution 3D-SIM, we used the same setting as previously described (Song et al., 2014). Excitation light wavelengths of 561nm (mRFP), and 488nm (GFP) were used respectively. Image acquisition, super-resolution processing and calculation were performed by ZEN black 2-1SP1 (Carl Zeiss, Jena, Germany).

2.3. Results

2.3.1. Yeast strains obtained in this study

In this study, by using the SGA methodology, we systematically generated four yeast genome-wide collections: (1) the Synphilin-1 SGA collection, which contains the pYX212-dsRed Sy1 plasmid; (2) the Httex1-103Q SGA collection, which contains the pYES2-Httex1-103Q-GFP plasmid; (3) the *ltn1*Δ Httex1-103Q SGA collection, in which all cells have a *LTN1* deletion background and contain the pYES2-Httex1-103Q-GFP plasmid; (4) the Httex1-103Q-mRFP Yeast GFP Clone Collection, in which the pYES2-Httex1-103Q-mRFP plasmid is crossed into the Yeast GFP Clone Collection.

2.3.2. Genes involved in Synphilin-1 inclusion formation

The Synphilin-1 SGA collection (section 2.2.1) was used in the HCM screen to identify genes required for the Synphilin-1 inclusion formation in yeast (section 2.2.5.1). The results are presented and discussed in Chapter 3.

2.3.3. Genes affect subcellular distribution of Httex1-103Q

The Httex1-103Q SGA collection (section 2.2.1) was used in the HCM screen to identify genes that alter the subcellular distribution of the polyQ protein Httex1-103Q in yeast (section 2.2.5.2). The results are presented and discussed in Chapter 4.

2.3.4. Loss-of-function genes suppress toxicity of Httex1-103Q in *ltn1*Δ background

To identify the factors that contribute to the Httex1-103Q-induced cytotoxicity in the *ltn1*Δ cells, we assessed the suppressors of Httex1-103Q in the *ltn1*Δ background (section 2.2.3). The results are presented and discussed in Chapter 4.

2.3.5. Proteins that co-localized with Httex1-103Q

Expression of Httex1-103Q in yeast perturbs the fitness of the cells and the cytotoxicity of Httex1-103Q is at least in part regulated by Q-rich and prion-like proteins (Duennwald et al., 2006a; Kayatekin et al., 2014). Proteins that physically interact with Httex1-103Q will provide valuable insights in elucidating aggregation formation of Httex1-103Q and Httex1-103Q-induced cytotoxicity. To achieve this goal, we designed a novel approach for studying protein-protein interactions, by identifying GFP-tagged proteins that co-aggregate with the Httex1-103Q-mRFP aggregates. We performed a HCM screen using the Yeast GFP Clone Collection in which we introduced the pYES2-Htt103Q-mRFP plasmid by means of the SGA methodology (section 2.2.4 and 2.2.5.3).

Using this approach, we were able to simultaneously visualize both the mRFP-tagged Httex1-103Q protein and the endogenous GFP-tagged proteins. We manually inspected the images obtained from the HCM system and obtained confirmation by conventional fluorescence microscopy. This revealed that several proteins co-localized with Httex1-103Q. Consistent with earlier studies showing that Q-rich and prion-like proteins sequester polyQ proteins (Duennwald et al., 2006a; Kayatekin et al., 2014), the obtained hits included Sup35, Pan1 and Rnq1 (Fig. 2-10A) (Kayatekin et al., 2014). We further analyzed the spatial distribution of Sup35 and Httex1-103Q by 3D-SIM analysis and this confirmed that the majority of the Sup35 was tightly sequestered by Httex1-103Q (Fig. 2-10B). Sup35 is a translation termination factor that contains N-terminal QN-rich prion domains. These QN-rich domains of Sup35 interact with polyQ protein (Gong et al., 2012) (Fig. 2-10B) and therefore might play a role in polyQ protein aggregation. The translation termination role of Sup35 might be interrupted by protein aggregation of polyQ protein and Sup35.

Previously it was reported that Ltn1-EGFP co-localized with the proline-rich containing reporter Httex1-103QP-mRFP (Yang et al., 2016). As Ltn1-EGFP is not included in the Yeast GFP Clone Collection, we manually introduced the pYES2-Htt103Q-mRFP plasmid into the Ltn1-EGFP strain, and validated the localization of Ltn1-EGFP and Httex1-103Q-mRFP by

3D-SIM analysis. This clearly shows that Ltn1 was recruited to the Httex1-103Q aggregates (Fig. 2-10B), which indicates that the RQC machinery may be involved in detoxification and translocation of Httex1-103Q.

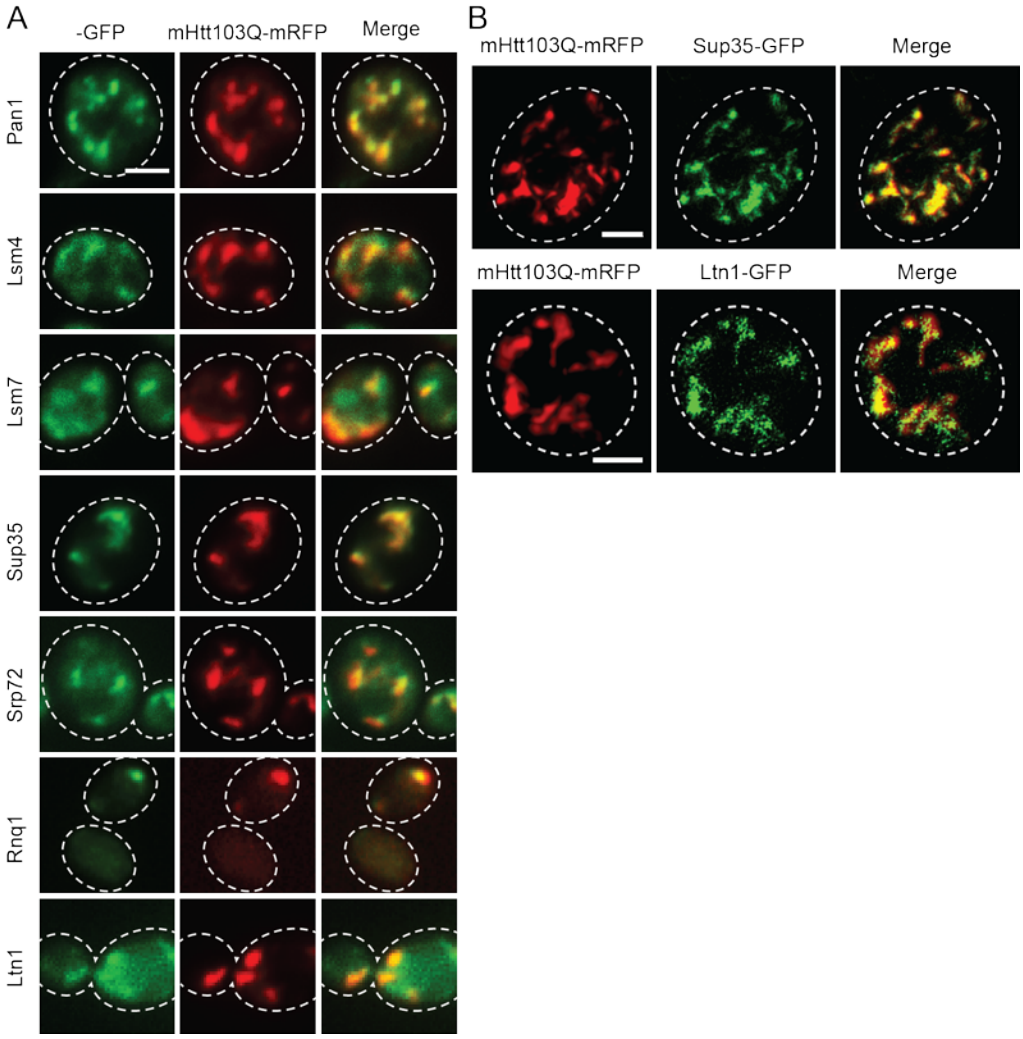

Figure 2-10. Genome-wide screen to identify proteins that co-localize with Httex1-103Q aggregates.
(A) Fluorescence microscopy images that shows proteins which co-localize with Httex1-103Q aggregates. These proteins include the Q-rich proteins Pan1, Sup35 and Rnq1 and the RQC component Ltn1. Yellow spots in the merge channel indicate the overlap of Httex1-103Q and the proteins. Scale represents 2 μm.
(B) Super-resolution fluorescence microscopy images of Httex1-103Q and Sup35/Ltn1 in WT cells. Yellow spots in the merge channel indicate the overlap of Httex1-103Q and Sup35/Ltn1. Scale represents 1 μm.

2.4. Summary

In this chapter, we described the establishment of different screening systems in a yeast model,

including the purposes, strategies, systematic genetic modification of yeast strains and HCM screening systems. We generated four yeast collections, and performed unbiased screens by combining the collection with the HCM screening system. The results from the screens have contributed to the identification of genes that are involved in the Synphilin-1 inclusion formation (Chapter 3) and the discovery of the ribosome quality control machinery in regulating the subcellular distribution of polyQ proteins (Chapter 4) and will be further discussed in the following chapters.

Furthermore, we found that Q-rich and prion-like proteins interact with the polyQ protein, which is in line with earlier studies (Duennwald et al., 2006a; Kayatekin et al., 2014), Moreover, we demonstrated that a key component of the RQC complex, Ltn1, as well as the translational termination factor Sup35 interact with the polyQ protein. These results indicate that the RQC pathway is somehow connected with the polyQ protein, consistent with later studies in Chapter 4. The role of RQC in detoxification and translocation of polyQ protein is further discussed in Chapter 4.

Chapter 3

A genome-wide imaging-based screening to identify genes involved in Synphilin-1 inclusion formation in *Saccharomyces cerevisiae*

This chapter is published as:

Zhao, L., Yang, Q., **Zheng, J.**, Zhu, X., Hao, X., Song, J., Lebacq, T., Franssens, V., Winderickx, J., Nystrom, T., and Liu, B. (2016) A genome-wide imaging-based screening to identify genes involved in Synphilin-1 inclusion formation in *Saccharomyces cerevisiae*. Scientific Reports 6.

Author Contributions:

B.L., T.N. and J.W. conceived and designed experiments. L.Z., J.Z., X.H., J.S., and T.L. performed experiments. B.L. L.Z., J.W, V.F., X.Z., and Q.Y analyzed the data and B.L., L.Z., J.W., V.F., and X.Z. wrote the manuscript.

Abstract

Synphilin-1 is a major component of PD IB implicated in PD pathogenesis. However, the machinery controlling Synphilin-1 inclusion formation remains unclear. Here, we investigated Synphilin-1 inclusion formation using a systematic genome-wide HCM in the yeast *Saccharomyces cerevisiae*. By combining this with a secondary screening for mutants showing significant changes in fluorescence signal intensity, we filtered out hits that significantly decreased the expression level of Synphilin-1. We found 133 yeast genes that didn't affect Synphilin-1 expression but that were required for the formation of Synphilin-1 inclusions. Functional enrichment and physical interaction network analysis revealed these genes to encode for functions involved in cytoskeleton organization, histone modification, sister chromatid segregation, glycolipid biosynthetic process, DNA repair and replication. In addition, all hits were confirmed by conventional microscopy. Complementation assays were performed with a selected group of mutants. The results indicated that the observed phenotypic changes in Synphilin-1 inclusion formation were directly caused by the loss of corresponding genes of the deletion mutants. Further growth assays of these mutants showed a significant synthetic sick effect upon Synphilin-1 expression, which supports the hypothesis that matured inclusions represent an end stage of several events meant to protect cells against the Synphilin-1 cytotoxicity.

3.1. Introduction

Increasing evidence shows that neurodegenerative diseases such as PD, AD, and HD share common underlying molecular and cellular mechanisms and that protein IB formation is a typical hallmark for these diseases. PD affects about 2% of the population over 65 years old, is an age-associated neurodegenerative disease that is characterized by degeneration of dopaminergic neurons and the formation of intracellular protein inclusions called Lewy bodies. It has been shown that the protein alpha-synuclein is the major component in these Lewy bodies (Baba et al., 1998). In addition to alpha-synuclein, the presynaptic protein Synphilin-1 was also found as one of the constituents of Lewy bodies (Wakabayashi et al.,

2000). Synphilin-1 not only interacts with alpha-synuclein (Engelender et al., 1999) but also with other proteins involved in the pathogenesis of PD, such as parkin and LRRK2 (Chung et al., 2001; Ito et al., 2003). This suggests that it may link several PD related gene products to a common pathogenic mechanism based on protein aggregation. Hence, a systematic analysis of mechanisms governing Synphilin-1 inclusion formation will increase our understanding of the pathogenesis of PD.

Synphilin-1, encoded by the gene SNCAIP, contains 919 amino acids and 3 characterized domains: two protein-protein interaction domains (ankyrin-like repeats and coiled coil domain) and a predicted ATP/GTP-binding motif (Ribeiro et al., 2002). However, the physiological functions of Synphilin-1 are still not fully understood. When expressed in yeast Synphilin-1 forms aggregates, similar as in mammalian systems (Büttner et al., 2010). To further investigate the mechanisms involved in Synphilin-1 IB formation, we performed a genome-wide imaging-based screening to isolate yeast deletion mutants that altered the formation of Synphilin-1 inclusions. To this end, we applied the yeast SGA methodology (Costanzo et al., 2010; Tong et al., 2001; Tong et al., 2004) and further developed a yeast HCM approach to monitor the Synphilin-1 inclusion phenotype. Several groups are currently applying yeast HCM screening approaches to investigate a wide range of biological questions. The pioneer proof-of-principle studies from Vizeacoumar and colleagues (Vizeacoumar et al., 2010) applied their high-content screening system to examine mitotic spindle morphogenesis. Recent results from the same group provided a proteome scale evaluation of protein abundance and localization in the cell (Chong et al., 2015). Studies using the HCM approach have been performed in other research groups as well. Yang and colleagues investigated the machinery for the formation of SGs as well as IB by the misfolded Von Hippel–Lindau tumor suppressor protein (Moldavski et al., 2015; Yang et al., 2014). Combined, these results demonstrate that the yeast HCM approach is a powerful tool for investigating mechanisms underlying different cellular processes.

The results of our current study led us to identify the interaction networks and components involved in the formation of Synphilin-1 inclusions. The synthetic sick effect, observed from

the identified mutants by expressing Synphilin-1, supports the hypothesis that Synphilin-1 inclusion formation has a cytoprotective effect to the cell. These results provide a molecular basis for understanding potential roles of Synphilin-1 in the pathogenesis of PD.

3.2. Materials and methods

3.2.1. Screening design

3.2.1.1. Yeast strains

The strain Y7092 was used as the SGA starting strain for query strain constructions. The plasmid pYX212-dsRed-Sy1 was described previously (Büttner et al., 2010) and used for expressing N-terminally tagged dsRed-Sy1 in the query strain. The yeast single gene knock-out collection (SGA-V2) and the essential gene temperature sensitive allele collection (ts-V5) (Li et al., 2011) are kind gifts from Prof. Charlie Boone. Detailed information regarding the strains used in this study is listed in the Supplementary Table 3-1. Plasmids p4339, pSG32, pYM28 were used to amplify the natMX4, hphMX4 and EGFP cassettes, respectively. A full list of plasmids used in this study is shown in the Supplementary Table 3-2.

3.2.1.2. Construction of a genome-wide collection of *S. cerevisiae* single deletion mutants expressing Synphilin-1-dsRed

Query strains were constructed by transferring the pYX212-dsRed-Sy1 (sample) into the yeast Y7092 query background. Further, the query strain with Synphilin-1-dsRed marker was combined with the SGA-V2 single gene knock-out collection and the ts-V5 array by an automatic SGA method (Costanzo et al., 2010; Tong et al., 2001; Tong et al., 2004). A control set of the same collection was constructed by introducing the plasmid pYX212-dsRed (control) into both collections. A Singer RoToR HDA robot (Singer Instrument) was used for all the pinning steps for collection handling.

3.2.1.3. Genome-wide high content screening with Synphilin-1 inclusions

The collections obtained from the previous steps were stored at -80°C in 96-well plates. Cells (both single and the ts mutants) were pre-cultured in 200 µl minimal selective SC-Ura liquid medium with antibiotics at 30°C（22°C for ts mutants）for 3 days without shaking. Subsequently, each pre-culture was diluted to a starting OD_{600nm} around 0.1 in 200 µl liquid SC-Ura medium. After 12h (16h for ts mutants) growing with shaking at 30°C (for both single and ts mutants), cells were fixed by adding 20 µl 37% formaldehyde to a final concentration of 3.7% for 30 min at room temperature. Then cells were washed twice with 1xPBS (4,000 rpm for 3 min). Finally, the cells were re-suspended in 200 µl 1xPBS and stored at 4°C overnight. For imaging, 9µl re-suspended cells were transferred to new 96-well glass bottom plates (Matri-plate) with 200µl 1×PBS in each well. The OD_{600nm} values were adjusted to 0.06-0.08, which corresponds to about $4\text{-}8\times10^4$ cells. The cells in the 96-well plate were spun down at 400 rpm for 45 s, and kept in dark for 30 min before imaging (Texas Red channel, Exposure time: 400 ms) with the automated cellular imaging system ImageXpress MICRO, Molecular Devices Corporation (MDC).

3.2.1.4. Phenotypes

Based on the dsRed-labelled Synphilin-1 fluorescence signal, cells expressing Synphilin-1 have two distinct phenotypes i.e. a diffused or an aggregated phenotype. The percentage of cells with Synphilin-1 inclusion was defined as the amount of cells with Synphilin-1 inclusions among all cells showing Synphilin-1-dsRed fluorescent signal. The percentage of cells with Synphilin-1 inclusions was recorded as the phenotypic readout from the screening. To automatically quantify the Synphilin-1 aggregation phenotype, a customized sub-program of the software MetaXpress (MDC) was applied on the obtained images for quantification of percentage of cells carrying Synphilin-1 inclusions and to measure the average fluorescence intensity within the cells. Parameters used for the software quantification are set as follows: the signal intensity threshold for cell isolation: ⩾300 grayscale units difference between cellular regions and the background of the image, which allow the MDC software recognize

specific area as a “cell”; the threshold for Synphilin-1 inclusion isolation: ⩾400 grayscale units difference between inclusion regions and cellular regions, which allow the MDC software recognize specific area within a cell as a “inclusion”.

3.2.1.5. Verification of mutants and complementation assay

All mutants that showed statistically significant differences from the wild type were re-streaked and tested manually in triplicates to confirm the phenotypic differences observed in the screening. Statistical analysis was conducted using the Student’s *t*- test, and $p<0.05$ was used as the cutoff for selecting significant hits. At least 300 cells were counted in the manual confirmation for each mutant. For manual confirmation, cells were grown from starting OD_{600nm} of 0.1 in in a 3 ml liquid SC-Ura medium for 20 h (22 h for TS mutants), subsequently fixed and washed in 1xPBS as described above. All potential hits generated from our high content screening were manually verified by using conventional microscopy. The aggregation phenotype of any high content screening hit, which cannot be repeated in our manual conformation, will be excluded from the final confirmed hits list. To handle the difference between our high content screening and the manual confirmation results, we used the actual values from the manual confirmation as the final results showed in supplementary tables. Complementation assays were performed with a selected group of mutants using the corresponding MoBY plasmids and the empty vector control (Ho et al., 2009).

3.2.1.6. Functional enrichment and interaction network analysis

The functional enrichment analysis was based on the results from Gene Ontology Term Finder. P-values were calculated using a hypergeometric distribution with multiple hypothesis correction as described in Boyle *et al* (Boyle et al., 2004). Manually confirmed hits (Supplementary Table 3-3) were analyzed for enrichment of GO biological processes, cellular components and molecular functions by comparison to a background set list of SGA-V2 (4368 genes) plus ts-V5 array (787 ts alleles, covering 497 essential genes) with a P-value cut-off $p<0.05$.

The Synphilin-1 interaction network diagrams were extracted from the interaction analysis by using Osprey 1.2.0(Breitkreutz et al., 2003) and the physical interactions between confirmed hits were added according to the BioGRID interaction database (Breitkreutz et al., 2008). Osprey extracts all experimental interaction data (including large-scale survey and classical genetics) from the BioGRID interaction database, and represents genes as nodes and interactions as edges between nodes. A filter was set for excluding any genetic interactions between the hits, and only presented physical interactions in the diagrams.

3.2.2. Fluorescence microscopy

Cell images were obtained by using a Zeiss Axio Observer.Z1 inverted microscope with 100x oil objectives (NA1.4). Filter sets used were GFP, dsRed, Texas Red and DAPI.

3.2.3. Western blot analysis

Protein extractions and Western blot analysis were performed as previously described(Büttner et al., 2010). The primary antibodies used were specific for Synphilin-1 (Sigma Aldrich, St. Louis, MO, USA) and Adh2 (Merck-Millipore, Overijse, Belgium)

3.2.4. Synphilin-1 cytotoxicity assay

The Synphilin-1 cytotoxicity assays were performed by micro-cultivation experiments in triplicate at 30°C using the Bioscreen C system (Labsystems Oy, Helsinki, Finland). The optical density was measured every 30 min for 72 h. The significant test was performed and p-values were calculated as described previously (Liu et al., 2010).

3.2.5. Statement on data and reagent availability

Strains are available upon request. File Supplementary Table 3-1 contains genotypes for each individual strain used. File Supplementary Table 3-2 contains plasmids used in this study. Full lists of confirmed hits involved in Synphilin-1 inclusion formation and their functional enrichment analysis results are listed in File Supplementary Table 3-3, 3-4, 3-6 and 3-7. File

Supplementary Table 3-5 contains the homologues of yeast genes with function enriched. Mutants showing a decrease in both the percentage of cells with Synphilin-1 inclusion and fluorescence intensity are listed in Supplementary Table 3-8.

3.3. Results

It was previously demonstrated that expression of the N-terminal fusion protein dsRed-Sy1 leads to inclusion/aggregate formation in yeast cells, similarly to expression of WT-Synphilin-1. This indicates that Synphilin-1 is being processed in a similar way in yeast and mammalian cells (Büttner et al., 2010; Swinnen et al., 2011). To identify components regulating Synphilin-1 inclusion formation *in vivo*, we performed a yeast genome-wide high-throughput imaging screening. The plasmid pYX212 carrying dsRed-Sy1 under the control of constitutive *TPI1* promoter was introduced into yeast Y7092 query strains. The morphology of the Synphilin-1 inclusions was tested manually as shown in Fig. 3-1a.

The setup of the robotic screening system is shown in Fig. 3-1b. This high content imaging screening system was designed to explore inclusion phenotypes through assessing fluorescent labeled protein markers in the yeast single deletion collection (SGA-V2) and the essential gene temperature sensitive (ts) allele collection (ts-V5) that contains yeast mutants harboring ts alleles of the essential genes. To incorporate the control plasmid expressing only dsRed or the plasmid for dsRed-Sy1 into the collections, we applied the yeast SGA methodology (Costanzo et al., 2010; Tong et al., 2001; Tong et al., 2004). In this robotic procedure, standard mating and meiotic recombination is used to select the haploid cells that combine a specific deletion or ts-mutant allele with the presence of the desired plasmid (Fig. 3-1b). We also designed a scoring program to automatically process the large amount of acquired images. It has the ability to automatically query and identify the cells on the images, extract the number of cells carrying IBs and export the measurements as a separate output (Fig. 3-1c). The phenotype scored in this screening is the percentage of cells carrying inclusions formed by dsRed-Sy1.

There is a possibility that certain mutants would show an altered inclusion formation

phenotype because of changes in the Synphilin-1 expression level. To address this possibility, we also monitored steady-state levels of Synphilin-1 by measuring the dsRed-Sy1 fluorescence intensity on the acquired images. Mutants with no significant difference ($p>0.05$, Student's *t*-test) in their fluorescence level compared to the wild-type cells are more likely to represent strains affected in the cellular machinery that supports inclusion formation and aggregation.

The criteria to include a particular mutant strain as a potential hit is based on the following: 1) the difference in the number of cells with Synphilin-1 inclusions between wild type and mutant cells is statistically significant ($p<0.05$, Student's *t*-test), 2) the absolute difference of the percentage of wild type and mutant cells carrying Synphilin-1 inclusions must be at least 25% and 3) no significant ($p>0.05$, Student's *t*-test) fluorescence intensity changes can be observed between wild type and mutant cells. Potential hits acquired from the screening were confirmed for their aggregation phenotype by using a manual microscopy approach. Based on these criteria and our manual confirmation, a total of 148 confirmed hits were obtained from the screening of the SGA collection and the ts collection (totally 5155 yeast mutants, including 4368 single deletion mutants and 787 ts alleles). Of these, 15 mutants showed an increase of cells carrying Synphilin-1 inclusions, but most of them also display a significantly increased Synphilin-1 expression level as measured by fluorescence intensity. The remaining 133 mutants showed a decrease in the percentage of cells carrying Synphilin-1 inclusions without significant changes in the signal intensity of Synphilin-1 (Supplementary Tables 3-3 & 3-6). Among these, 100 were non-essential gene deletion mutants and 33 were essential gene ts alleles. For the mutants with a decrease in Synphilin-1 inclusion formation, the confirmation rate obtained by this manual microscopic inspection was 92.9% when using a cutoff of 25% difference between the wild type and the mutants for the number of cells with Synphilin-1 inclusions.

Mutants showing significant decrease ($p<0.05$, Student's *t*-test) in both the percentage of cells with Synphilin-1 inclusions and the fluorescence intensity are listed in Supplementary Table 3-8. For these mutants, there is a possibility that the observed decreased inclusion formation

phenotype is caused by the low expression level of the Synphilin-1 protein.

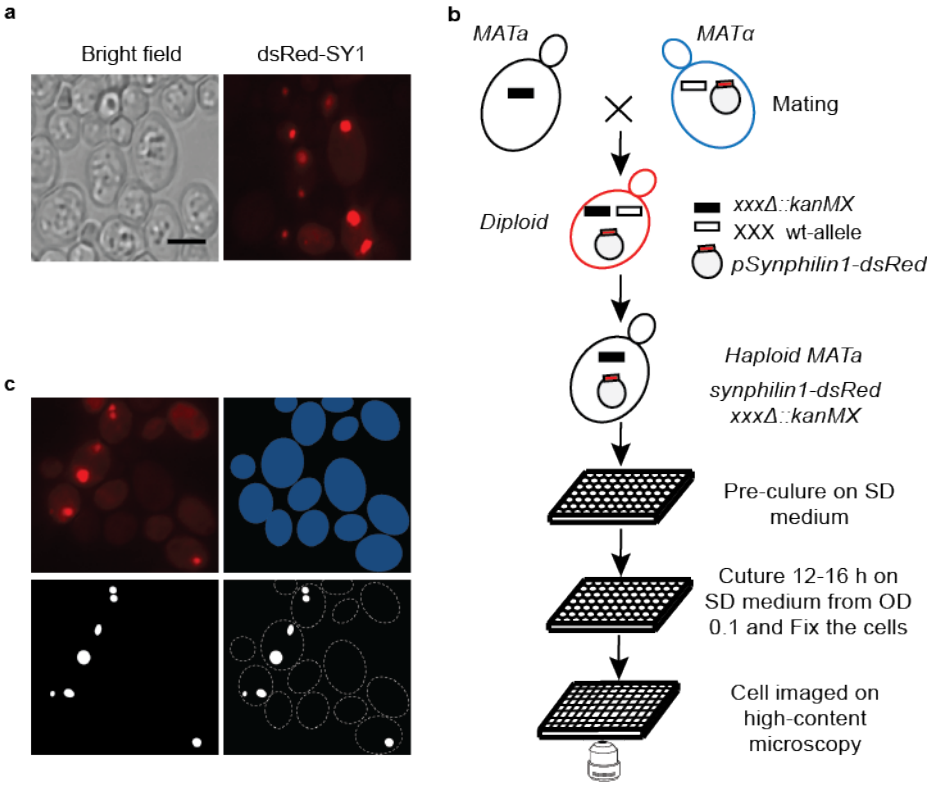

Figure 3-1. Genome-wide HCM approach to identify components involved in Synphilin-1 inclusion formation. a) Phenotype of WT cells harboring Synphilin-1 inclusions. Right panel: dsRed-tagged Synphilin-1 (SY1); Left panel: Bright field. Scale bar, 5 μm. **b**) Workflow of the HCM to identify mutants altering the Synphilin-1 inclusion formation. **c**) Software approach for Synphilin-1 inclusion identification and quantification. Image pre-processing with shade correction and background subtraction (Top left); Cells (Top right) and IBs (Bottom left) were isolate from their background based on the signal intensity differences. Then the percentage of cells with inclusions were extracted (Bottom right) by combining the two (cells and IBs) masks.

3.3.1. Mutants displaying a decreased capacity to form Synphilin-1 inclusions

Representative images of some top hits with high significant differences on decreased inclusion formation by dsRed-Sy1 are shown in Fig. 3-2a, and their quantitative differences as compared to the wild type strain are presented in Fig. 3-2b. Next, the mutants were analyzed for the enrichment of Gene Ontology (GO) categories, which classified them into different functional groups, including cytoskeleton organization, histone modification, sister chromatid

segregation, glycolipid biosynthetic process, DNA repair, and DNA replication (Fig. 3-3a, Supplementary Table 3-4). Within these functional groups several protein complexes were identified such as the dynein complex, dynactin, prefoldin complex, the Ctf18 RFC-like complex, the RNA polymerase complex and the Cdc73/Paf1 complex (Fig. 3-3b). Overall, this analysis revealed the complexity of the machinery involved in the formation of dsRed-Sy1 inclusions. Furthermore, we identified the human homologues of these enriched hits using YeastMine web-based software (a multifaceted search and retrieval system) (Balakrishnan et al., 2012). The results are shown in Supplementary Table 3-5.

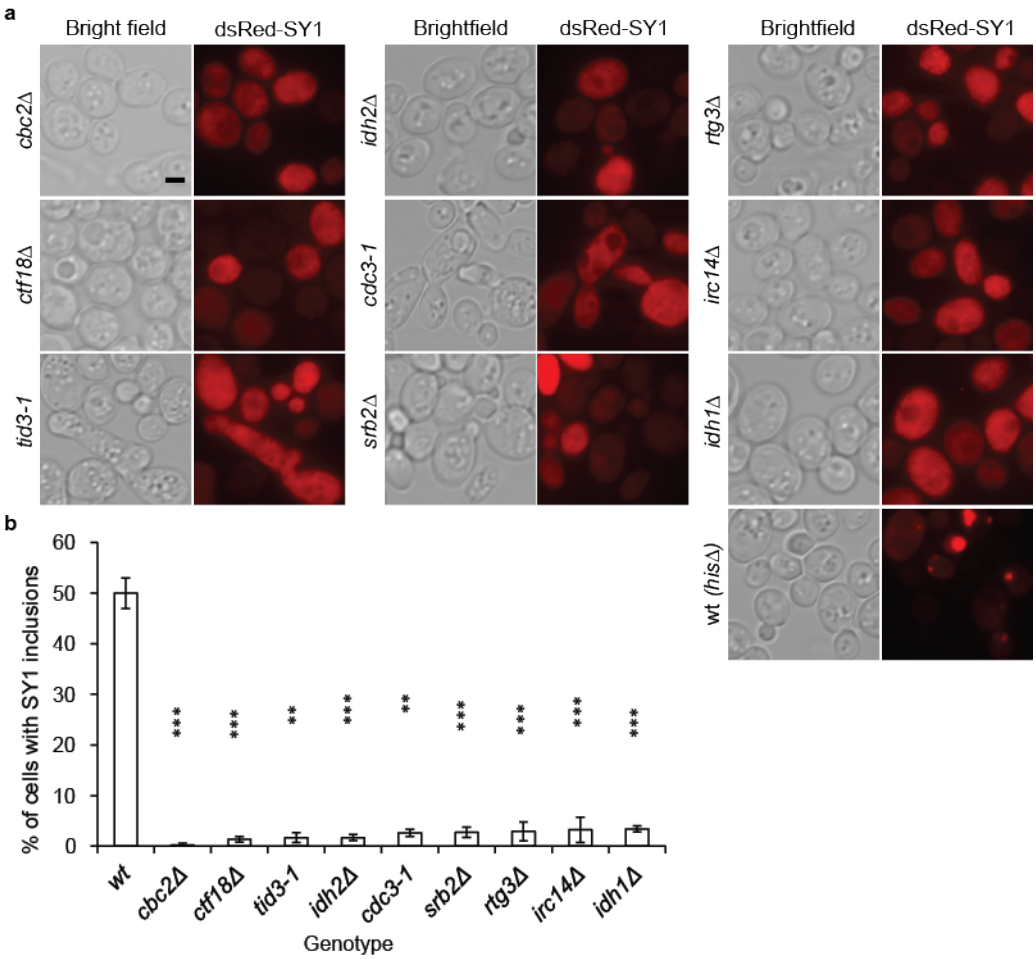

Figure 3-2. Top hits showing a decreased percentage of cells with Synphilin-1 inclusions obtained from the HCM screening. a) Images of mutants displaying less Synphilin-1 inclusions than WT (*his3*Δ) cells. Left panel: bright field, right panel: dsRed-Sy1. Scale bar, 2 μm. **b**) Quantification of the percentage of cells with inclusions in WT and mutant strains. Statistical analysis was performed using Student's *t*-test. Error bars represent standard deviation from triplicates of about 200 cells each. Asterisks denote significant differences between WT and mutants: *P, 0.05; **P, 0.01; ***P, 0.001.

3.3.2. Genes involved in cytoskeleton organization, dynein, dynactin and prefoldin complex

It has previously been reported that the actin cytoskeleton is involved in Synphilin-1, Htt and heat induced protein inclusion/aggregate management (Büttner et al., 2010; Liu et al., 2010; Liu et al., 2011; Song et al., 2014). Consistently, the GO term analysis showed a moderate enrichment for gene products involved in cytoskeleton organization (12.0% vs 1.9%, relative vs background frequency, $P=4.9\times10^{-6}$), which included genes such as *ACT1* (Fig. 3-3a & b). These genes are involved in cell polarization, endocytosis and other cytoskeleton-related functions. Also genes encoding for dynein motor components (*DYN1, DYN3,* and *PAC11*) and a microtubule plus-end binding protein (*PAC1*) were retrieved (Fig. 3-3a & b). Cytoplasmic dynein is responsible for transport of cargo along microtubules, organization of the microtubule network with respect to the cell cortex and positioning of microtubule organizing center (Moore et al., 2009). There is also a considerable enrichment of genes encoding for the dynactin complex (2.4% vs 0.1%, relative to the background frequency, P=0.013) including *LDB18, JNM1* and *NIP100* (Fig. 3-3a & b). Dynactin, a widely conserved multi-subunit complex, is necessary for the function of dynein in cytoplasm and takes part in a variety of microtubule-based transport and anchoring processes. It has also been found to interact with dynein, microtubules and various types of cargo (Schroer, 2004). Moreover, the movement and position of the mitotic spindle and nucleus are known to be impaired when dynactin is absent (Moore et al., 2008). In our screening, we found that prefoldin complex components (*GIM4, YKE2* and *PAC10*) as being required for proper Synphilin-1 inclusion formation in yeast cells. This result not only confirms previously reported data (Büttner et al., 2010; Swinnen et al., 2011), but it is especially interesting because the prefoldin complex is a chaperone that delivers unfolded proteins to cytosolic chaperonin (Vainberg et al., 1998), which has been implicated as a potent modulator of protein misfolding disease (Leroux and Hartl, 2000). Further understanding of the role of prefoldin complex and its co-player chaperonin in Synphilin-1 inclusion formation is likely to provide important insight into basic pathogenesis mechanisms of these proteins (Leroux and Hartl, 2000). Whether the

cytoskeletal components identified from our screening are involved in the formation of the inclusions or in their partitioning remains to be elucidated.

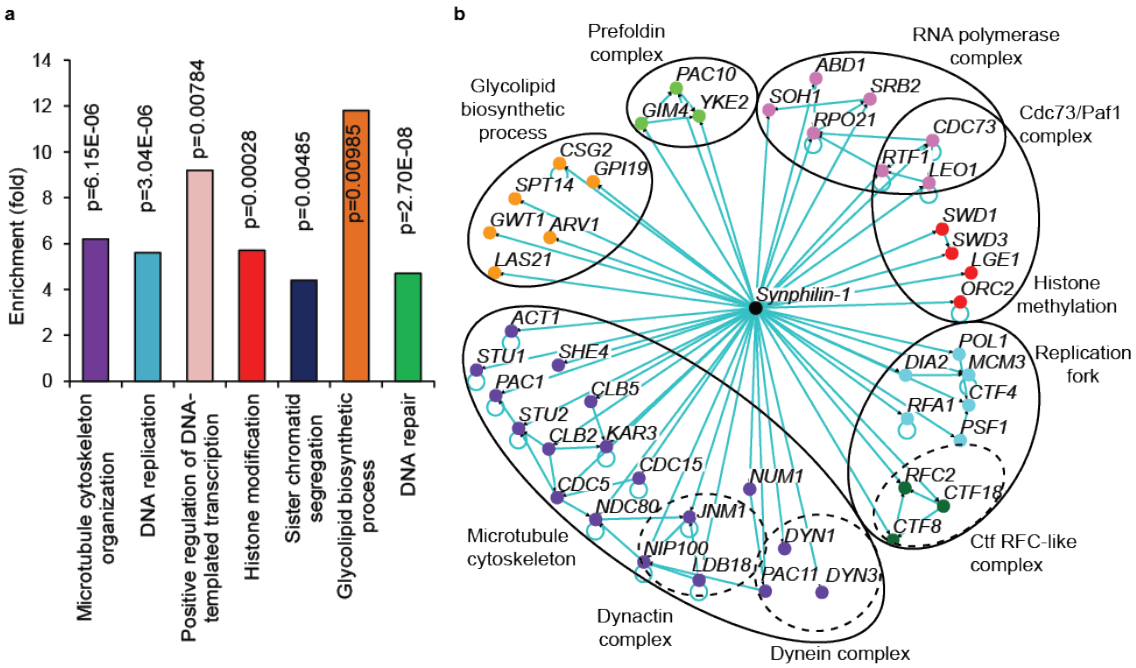

Figure 3-3. Functional enrichment and network analysis for the confirmed hits with decreased Synphilin-1 inclusion formation. a) Functional enrichment analysis of mutants with decreased Synphilin-1 inclusion formation. Confirmed mutants were analyzed for enrichment of GO functional categories. Enriched groups were scored by comparing to a background list of SGA-V2+ ts-V5 array using a cut-off of $p<0.05$. Functional groups are marked with different colors. **b**) Network analysis of mutants with decreased Synphilin-1 inclusion formation. Mutants showing fewer cells with Synphilin-1 inclusion were grouped into modules based on their known physical interactions and published information of the cellular components. The cellular components are shown in different colored nodes. The circles indicate subunits or protein complexes.

3.3.3. Genes involved in sister chromatid cohesion

Our screening results also show that the formation of Synphilin-1 inclusions is impinged in mutants involved in sister chromatid cohesion and spindle orientation function. GO term enrichment analysis showed that mitotic sister chromatid cohesion was about 5 fold enriched and this included genes encoding the Ctf18 RFC-like complex (*CTF18, CTF8, RFC2*) (Fig.

3-3a & b). The RFC complex is required for sister chromatid cohesion and chromosome transmission, and mutants carrying a *CTF8, CTF18,* or *DCC1* deletion display a severe sister chromatid cohesion defect (Mayer et al., 2001). It is possible that the establishment of sister chromatid cohesion plays a role in the formation of Synphilin-1 inclusions. Moreover, the Ctf18 protein co-localizes with the replication fork during DNA replication where it has an important role for sister chromatid cohesion (Lengronne et al., 2006). Related to this result, there was also a moderate enrichment for gene products involved in DNA replication initiation/Primase complex, such as *RFA1, PSF1, MCM3,* and *POL1* (Fig. 3-3a & b). However, for these mutants it is not clear whether the observed decrease in the inclusion formation phenotype of the corresponding mutants is functionally linked to the sister chromatid hits or whether it is simply due to a general reduction of DNA replication.

3.3.4. Genes involved in glycolipid biosynthetic process

The list of genes whose deletion is associated with decreased Synphilin-1 inclusion formation is also enriched in members of the glycolipid biosynthetic process (*CSG2, GPI19, LAS21, GWT1, ARV1 and SPT14*; 4.7% vs 0.4% in the background; $P=9.8\times10^{-3}$; Fig. 3-3a & b). Five of them (*GPI19, LAS21, GWT1, ARV1 and SPT14*) are especially involved in the glycosylphosphatidylinositol (GPI) anchor biosynthetic process. Among these, *GPI19* and *SPT14* belong to the glycosylphosphatidylinositol-N- acetylglucosaminyltransferase (GPI-GnT) complex, which mediates the first step in GPI biosynthesis.

Defects in the GPI-anchor synthesis has been linked with congenital diseases such as hyperphosphatasia with mental retardation syndrome (HPMRS), also known as Mabry syndrome (Thompson et al., 2010). Moreover, GPI anchors have been identified as factors that are required for the neurotoxic effect of scrapie prions (Chesebro et al., 2005). Here we show that the GPI anchor biosynthetic process components are required for Synphilin-1 inclusion formation, whether this indicates that there is a direct interaction between Synphilin-1 and GPI anchors needs to be tested. It is known that the Synphilin-1 associates with cell membrane structures such as lipid droplets and lipid rafts in mammalian and yeast

cells (Büttner et al., 2010; Takahashi et al., 2006). Further in-depth investigation on the interplay among Synphilin-1, GPI-anchor and cell membrane structures will provide novel clues on the pathological role of Synphilin-1.

3.3.5. Genes involved in Cdc73/Paf1 complex

We also found several mutants carrying deletions of genes belonging to the Cdc73/Paf1 complex that regulates transcription elongation from RNA polymerase (*rtf1Δ*, *cdc73Δ*, *leo1Δ*; 2.4% vs 0.1% in the background, $P=3.5\times10^{-3}$; Fig. 3-3a & b). This complex was initially identified as the RNA polymerase II-associated protein in yeast (Koch et al., 1999). The yeast Rtf1 protein is not only essential for Set1-mediated histone H3 methylation but also required for Dot-mediated methylation of histone H3 (Krogan et al., 2003). Moreover, there were also a few mutants with decreased Synphilin-1 inclusion formation that affect histone H3 methylation via the COMPASS (Complex Proteins Associated with Set1) complex, such as *swd1Δ*, *swd3Δ*, and *orc2Δ* (Fig. 3-3a & b). Whether this observation indicates that the Cdc73/Paf1 complex has a direct role in Synphilin-1 inclusion formation needs to be further investigated, since the decreased percentage of cells carrying Synphilin-1 inclusions may also be due to a general reduction of expression of the marker proteins.

3.3.6. Inclusion formation defective mutants showing increased Synphilin-1 cytotoxicity effect in yeast cells

It was previously demonstrated that Synphilin-1 inclusions are beneficial and have a positive effect on viability of human cell lines (Tanaka et al., 2004) and humanized yeast cells (Büttner et al., 2010). To test this further, we selected mutants of different cellular functional groups from the screening and analyzed their growth. For each of these mutants, the Synphilin-1 inclusion phenotype was manually checked (Fig. 3-4a) and this confirmed the decreased capacity to form inclusions (Fig. 3-4b). In addition, we further measured the expression of Synphilin-1 by Western blot, results showed no significant difference in the mutants as compared to the wild type ($p>0.05$, Student's *t*-test, Fig. 3-4c). Furthermore, we performed

complementation assays using Molecular Barcoded Yeast (MoBY) plasmids and this established that the reduced inclusion formation capacity is indeed solely due to the lack of function caused by the corresponding deletion in the mutants (Fig. 3-4d). Intriguingly, when assessing the growth rate all mutants showed a significantly prolonged generation time (Student's *t*-test, $p<0.05$), which is indicative for a synthetic sick effect when the expression of dsRed-Sy1 is combined with the deletion of these genes. No such effect was observed upon expression of solely dsRed, which served as control (Fig. 3-4e). This result strongly supports the hypothesis that the formation and maturation of inclusions is a cytoprotective process that helps to sequester soluble cytotoxic mis-conformers into inert deposits (Tan et al., 2009).

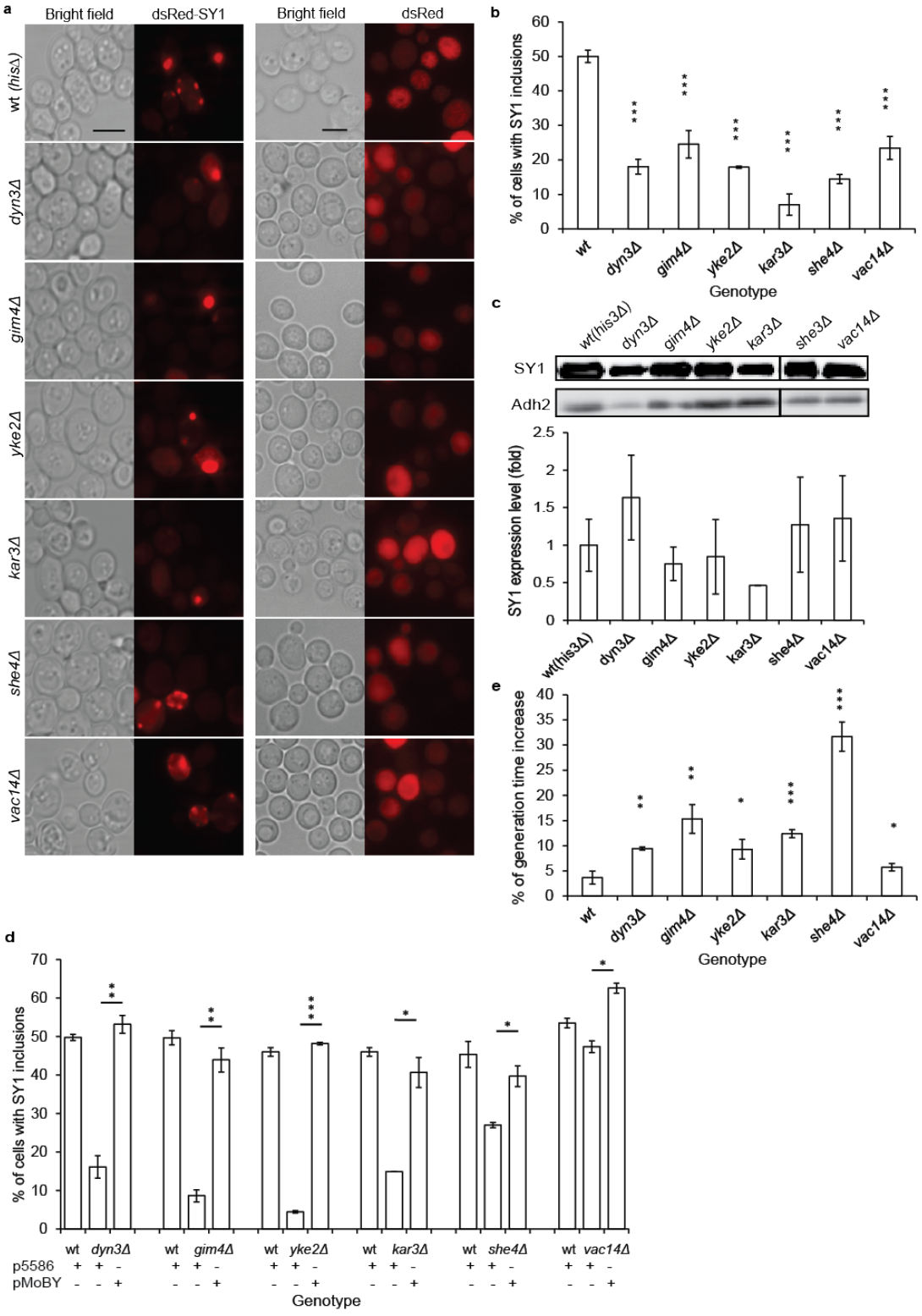

Figure 3-4. Complementation assays and growth analysis of mutants with decreased inclusion formation capacity. a) Images of selected mutants with a decreased number of cells showing Synphilin-1 (SY1) inclusions and the corresponding control mutant strains with only dsRed expression. Left panel, bright field; right panel, dsRed-Sy1 or dsRed. Scale bar, 5 μm. **b**) Quantification of the percentage of cells with Synphilin-1 inclusions in WT and mutants. A value of 0% means that there are no cells of that mutant with Synphilin-1 inclusions. Error bars represent standard deviation from triplicates each containing about

200 cells. **c**) Western blot analysis of the WT (*his3Δ*) strain and mutants expressing Synphilin-1. Immunodetection was performed using primary antibodies directed against Synphilin-1 or Adh2, which served as internal control protein. The quantification of Synphilin-1 expression levels is shown. Error bars represent standard deviation from triplicates samples. Asterisks denote significant differences between WT and mutants (Student's *t*-test): *P, 0.05; **P, 0.01; ***P, 0.001. **d**) Complementation assays further confirmed that the reduced inclusion formation capacity of the mutants is solely due to the lack of function caused by the corresponding deletion. The complementation assays were performed with MoBY plasmids and the empty vector control (p5586). Error bars represent standard deviation from triplicates containing about 200 cells. **e**) An increased Synphilin-1 cytotoxicity effect (prolonged generation time) was observed from the selected mutants. The generation times of mutants expressing dsRed-Sy1 and solely dsRed (control) were measured at 30°C. The differences of generation time increase between WT and mutants are shown. Data are represented as mean ± standard deviation SD. Asterisks denote significant differences between samples (Student's *t*-test): *P, 0.05; **P, 0.01; ***P, 0.001.

3.3.7. Mutants displaying an increased percentage of cells carrying Synphilin-1 inclusions

Our screening also identified 15 mutants that showed an increased percentage of cells with dsRed-Sy1 inclusions. In each case, the phenotype of the mutant was confirmed by manual analysis. Representative images of strong hits and their quantitative difference from wild-type cells are shown in Fig. 3-5a & b. Interestingly, when measuring the fluorescence signal intensity many mutants showed elevated levels as compared to the wild type strain, which suggests that the increased inclusion formation phenotype might be caused by an elevated level of Synphilin-1 expression (Supplementary Table 3-6). GO term analysis of these mutants revealed an enrichment for the transcription factor IID (TFIID) complex components (*TAF2*, *TAF4*, *TAF11* and *TAF12*; P=2.94E-06) (Fig. 3-5c & d and Supplementary Table 3-7). Hence, it will be informative to elucidate whether the increased inclusion formation phenotype is caused by a general transcription defect or whether it is the effect of dysregulation of specific downstream targets of the TFIID complex. For six mutants, i.e. *crm1-1, rtc1Δ, cdc24-3, arx1Δ rox1Δ* and *gdh1Δ,* their fluorescence intensities of the dsRed-Sy1 fusion were similar to that of the wild type strain. Here, the presence of *GDH1*, a NADP(+)-dependent glutamate dehydrogenase, is especially intriguing. Indeed, changes in the activity and regulation of human GDH have been reported in a number of conditions that

lead to neurodegeneration (McKenna, 2011).

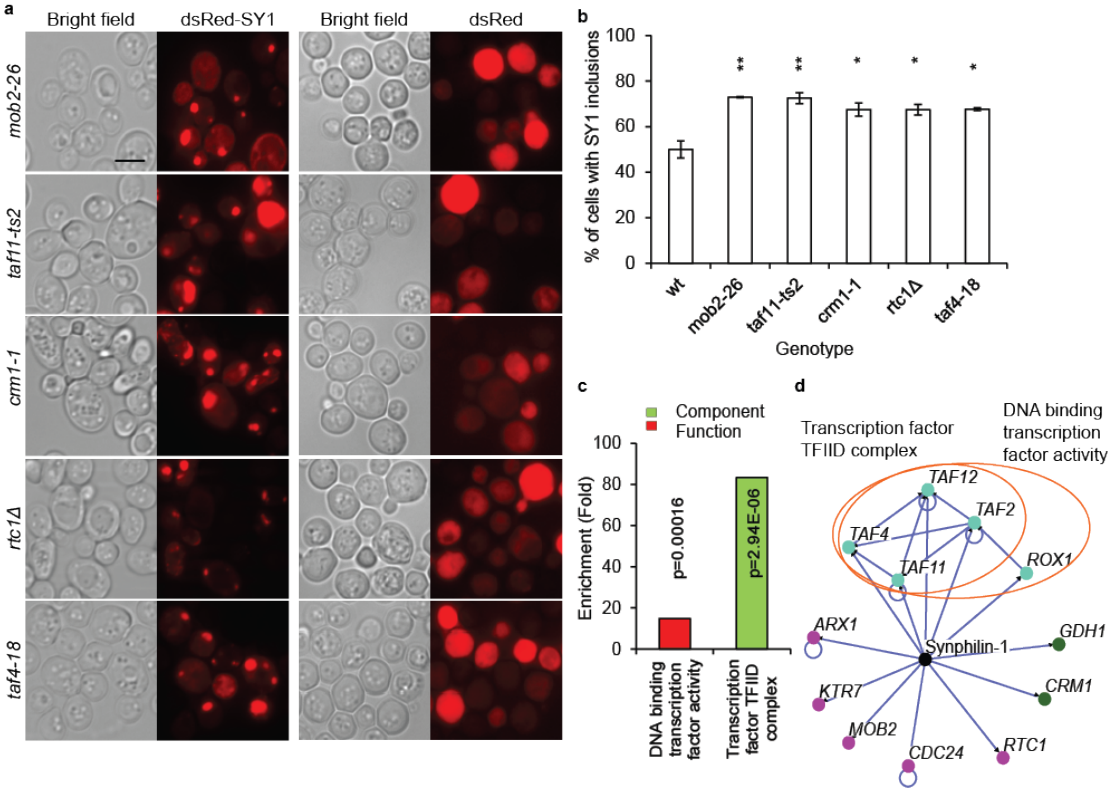

Figure 3-5. Mutants identified from the HCM screening with an increased percentage of cells carrying Synphilin-1 inclusions a) Representative images of strong hits from the imaging based screening showing cells with expression of dsRed-Sy1 or dsRed alone. Left panel, bright field; right panel, dsRed-Sy1 or dsRed. Scale bar, 5 μm. **b**) Quantification of percentage of cells with inclusions in WT and mutants. Error bars represent standard deviation from triplicates of about 200 cells each. Asterisks denote significant differences between WT and mutants (Student's *t*-test): *P, 0.05; **P, 0.01; ***P, 0.001. **c**) Functional enrichment analysis of mutants displaying increased Synphilin-1 inclusion formation. Confirmed mutants were analyzed for enrichment of GO functional categories. Enriched groups were scored by comparing to a background list of SGA-V2+ ts-V5 array. Functional groups are marked with different colors. **d**) Network analysis of mutants with an increased percentage of cells with Synphilin-1 inclusions. Mutants showing more cells with Synphilin-1 inclusions were grouped into modules based on their known physical interactions and published information of the cellular components. The cellular components are shown in different colored nodes. The circles indicate subunits or protein complexes.

In summary, we developed and validated a yeast HCM screening approach for the fluorescently tagged human Synphilin-1 protein. This genome-wide imaging screening enabled us to identify cellular components that regulate Synphilin-1 aggregation with unexpected functionalities. We found that dynein complex, dynactin, prefoldin complex, the

Ctf18 RFC-like complex, the RNA polymerase complex and the Cdc73/Paf1 complex are required for the formation of Synphilin-1 inclusions. These results gave an unbiased global view on the complexity of the machinery underlying inclusion formation by Synphilin-1 and provided further supports on the hypothesis that the Synphilin-1 inclusion formation has a cytoprotective effect to the cell. Synphilin-1 was found to be one of the constituents of Lewy bodies, a hallmark for PD (Wakabayashi et al., 2000). Our findings acquired from the yeast model, especially genes/pathways with homologues in human, provided valuable clues concerning the machinery controlling Synphilin-1 inclusion formation. Further investigation of these human homologue hits can provide novel insights for our understanding of the mechanisms of pathogenesis causing PD as well as other protein folding disorders.

3.4. Discussion

IBs formation is a hallmark of PD, overexpression of Synphilin-1 in yeast reproduces IBs formation, similar as in neuronal cells. Processes governing Synphilin-1 inclusion formation are rarely known, we provide a systematic analysis of factors required for Synphilin-1 inclusion formation. We developed and validated a yeast HCM screening approach for the fluorescently tagged human Synphilin-1 protein. This genome-wide imaging screening enabled us to identify cellular components that regulate Synphilin-1 aggregation with unexpected functionalities.

We found that dynein complex, dynactin and prefoldin complex are required for the formation of Synphilin-1 inclusions. Interestingly, a certain aggregated proteins deposit called aggresomes, is formed based on dynein-dependent retrograde transport along microtubules (Kopito, 2000; Tanaka et al., 2004). Moreover, cytoskeletal proteins are also reported involved in both formation and maintenance of yeast prions (Bailleul et al., 1999; Chernova et al., 2011; Ganusova et al., 2006). Thus it is very likely that cytoskeleton organization plays a crucial role in Synphilin-1 inclusion formation, the exact role of cytoskeletal components such as dynein, dynactin and prefoldin complex and their co-player chaperonin, remains to be further investigated. Thus, it is important to study the dynamic process of Synphilin-1 inclusion formation, leading edge techniques, such super-resolution live cell video

microscopy, will help us to obtain more details of cytoskeleton in the process of Synphilin-1 inclusion formation.

Even Synphilin-1 inclusions was considered to be the toxic species in some studies, due to the observation of Synphilin-1 inclusion associated with cerebellum (Nuber et al., 2010) and dopaminergic neurons (Krenz et al., 2009). However, increasing evidences show that inclusion formation of misfolded proteins is benefit for cells. For instance, a study reported that no signs of neurodegeneration were observed in the presence of insoluble Synphilin-1 deposits (Jin et al., 2008); spatial sequestration of mutant Htt decreases cytotoxicity of mutant Htt (Yang et al., 2016). Our study provides an unbiased global view on the complexity of the machinery underlying inclusion formation of Synphilin-1 and further provides supports on the hypothesis that the Synphilin-1 inclusion formation has a cytoprotective effect to the cell.

It is known that the Synphilin-1 associates with cell membrane structures such as lipid droplets and lipid rafts in mammalian and yeast cells (Büttner et al., 2010; Takahashi et al., 2006). Further in-depth investigation on the interplay among Synphilin-1, GPI-anchor and cell membrane structures will provide novel clues on the pathological role of Synphilin-1.

Our findings acquired from the yeast model, especially genes/pathways with homologues in human, provided valuable clues concerning the machinery controlling Synphilin-1 inclusion formation. Further investigation of these human homologue hits can provide novel insights for our understanding of the mechanisms of pathogenesis causing PD as well as other protein folding disorders.

Acknowledgements

The authors would like to thank C. Boone for providing the yeast mutant collections essential for this work. This work was supported by grants from the Swedish Natural Research Council (VR 2015-04984), Swedish Cancer Society (CAN 2015/406) and Carl Trygger Foundation (CTS 14: 295) to BL. The research leading to these results has received funding from the People Programme (Marie Curie Actions) of the European Union's Seventh Framework Programme (FP7/2007-2013) under REA grant agreement n°608743, the Knut and Alice

Wallenberg Foundation (Wallenberg Scholar), ERC (Advanced Grant; QualiAge) and the Swedish Natural Research Council to TN, a postdoctoral fellowship of the Flemish Research Fund FWO-Vlaanderen to VF and FWO grants (G.0694.13 and G.0A63.15) to VF and JW.

3.5. Supplementary information

SUPPLEMENTARY TABLES

Supplementary Table 3-1: Strains used in Chapter 3

Strain Name	Genotype and markers	Background/Source
BY4741 (WT)	*MATa his3Δ1 leu2Δ0 ura3Δ0 met15Δ0*	EUROSCARF; Wt control for strains constructed by PCR approach
Y7092-pSY285	*MATα can1Δ::STE2pr-Sp_his5 lyp1Δ ura3Δ0 leu2Δ0 his3Δ1 met15Δ0 LYS2+* pYX212-dsRed-SY1 (URA+)	This study, query strain
Y7092-pSY244	*MATα can1Δ::STE2pr-Sp_his5 lyp1Δ ura3Δ0 leu2Δ0 his3Δ1 met15Δ0 LYS2+* pYX212-dsRed (URA+)	This study, query strain, Control for strain expressing Synphilin-1
BY4741-pSY285	BY4741 with pYX212-dsRed-SY1 (URA+)	This study
BY4741-pSY244	BY4741 with pYX212-dsRed (URA+)	This study, Control for strain expressing Synphilin-1
BY4741-pSY285'	BY4741 with pYX212-dsRed-SY1 (Hyg+)	This study
BY4741-pSY244'	BY4741 with pYX212-dsRed (Hyg+)	This study, Control for strain expressing Synphilin-1
his3Δ-244	*MATa his3Δ::kanMX4 can1Δ::STE2pr-Sp_his5 lyp1Δ ura3Δ0 leu2Δ0 met15Δ0 LYS2+* pYX212-dsRed (URA+)	This study; Wt control for strains expressing Synphilin-1
his3Δ-285	*MATa his3Δ::kanMX4 can1Δ::STE2pr-Sp_his5 lyp1Δ ura3Δ0 leu2Δ0 met15Δ0 LYS2+* pYX212-dsRed-SY1 (URA+)	This study; Wt control for strains constructed by crossing
dyn3Δ-285	*MATa dyn3Δ::kanMX4 can1Δ::STE2pr-Sp_his5 lyp1Δ ura3Δ0 leu2Δ0 met15Δ0 LYS2+* pYX212-dsRed-SY1 (URA+)	This study
gim4Δ-285	*MATa gim4Δ::kanMX4 can1Δ::STE2pr-Sp_his5 lyp1Δ ura3Δ0 leu2Δ0 met15Δ0 LYS2+* pYX212-dsRed-SY1 (URA+)	This study
yke2Δ-285	*MATa yke2Δ::kanMX4 can1Δ::STE2pr-Sp_his5 lyp1Δ ura3Δ0 leu2Δ0 met15Δ0 LYS2+* pYX212-dsRed-SY1 (URA+)	This study
kar3Δ-285	*MATa kar3Δ::kanMX4 can1Δ::STE2pr-Sp_his5 lyp1Δ ura3Δ0 leu2Δ0 met15Δ0 LYS2+* pYX212-dsRed-SY1 (URA+)	This study

she4Δ-285	*MATa she4Δ::kanMX4 can1Δ::STE2pr-Sp_his5 lyp1Δ ura3Δ0 leu2Δ0 met15Δ0 LYS2+* pYX212-dsRed-SY1 (URA+)	This study
vac14Δ-285	*MATa vac14Δ::kanMX4 can1Δ::STE2pr-Sp_his5 lyp1Δ ura3Δ0 leu2Δ0 met15Δ0 LYS2+* pYX212-dsRed-SY1 (URA+)	This study
idh1Δ-285	*MATa idh1Δ::kanMX4 can1Δ::STE2pr-Sp_his5 lyp1Δ ura3Δ0 leu2Δ0 met15Δ0 LYS2+* pYX212-dsRed-SY1 (URA+)	This study
cbc2Δ-285	*MATa cbc2Δ::kanMX4 can1Δ::STE2pr-Sp_his5 lyp1Δ ura3Δ0 leu2Δ0 met15Δ0 LYS2+* pYX212-dsRed-SY1 (URA+)	This study
ctf18Δ-285	*MATa ctf18Δ::kanMX4 can1Δ::STE2pr-Sp_his5 lyp1Δ ura3Δ0 leu2Δ0 met15Δ0 LYS2+* pYX212-dsRed-SY1 (URA+)	This study
srb2Δ-285	*MATa srb2Δ::kanMX4 can1Δ::STE2pr-Sp_his5 lyp1Δ ura3Δ0 leu2Δ0 met15Δ0 LYS2+* pYX212-dsRed-SY1 (URA+)	This study
idh2Δ-285	*MATa idh2Δ::kanMX4 can1Δ::STE2pr-Sp_his5 lyp1Δ ura3Δ0 leu2Δ0 met15Δ0 LYS2+* pYX212-dsRed-SY1 (URA+)	This study
rtg3-285	MATa *rtg3Δ*::kanMX4 can1Δ::STE2pr-Sp_his5 lyp1Δ ura3Δ0 leu2Δ0 met15Δ0 LYS2+ pYX212-dsRed-SY1 (URA+)	This study
irc14-285	*MATa irc14Δ::kanMX4 can1Δ::STE2pr-Sp_his5 lyp1Δ ura3Δ0 leu2Δ0 met15Δ0 LYS2+* pYX212-dsRed-SY1 (URA+)	This study
tid3-1-285	*MATa tid3-1::kanMX4 can1Δ::STE2pr-Sp_his5 lyp1Δ ura3Δ0 leu2Δ0 met15Δ0 LYS2+* pYX212-dsRed-SY1 (URA+)	This study
cdc3-1-285	*MATa cdc3-1::kanMX4 can1Δ::STE2pr-Sp_his5 lyp1Δ ura3Δ0 leu2Δ0 met15Δ0 LYS2+* pYX212-dsRed-SY1 (URA+)	This study
his3Δ	BY4741 with *his3Δ::KanMX4*	SGA-V2 collection, Boone lab
dyn3Δ	BY4741 with *dyn3Δ::KanMX4*	SGA-V2 collection, Boone lab
gim4Δ	BY4741 with *gim4Δ::KanMX4*	SGA-V2 collection, Boone lab
yke2Δ	BY4741 with yke2*Δ::KanMX4*	SGA-V2 collection, Boone lab
kar3Δ	BY4741 with *kar3Δ::KanMX4*	SGA-V2 collection, Boone lab

she4Δ	BY4741 with *she4Δ::KanMX4*	SGA-V2 collection, Boone lab
vac14Δ	BY4741 with *vac14Δ::KanMX4*	SGA-V2 collection, Boone lab
dyn3Δ-SM	BY4741 with *dyn3Δ::KanMX4* (Hyg+) +pYX212-dsRed-SY1 +MoBY-DYN3(URA+)	This study
gim4Δ-SM	BY4741 with *gim4Δ::KanMX4* (Hyg+) +pYX212-dsRed-SY1 +MoBY-GIM4(URA+)	This study
yke2Δ-SM	BY4741 with *yke2Δ::KanMX4* (Hyg+) +pYX212-dsRed-SY1 +MoBY-YKE2(URA+)	This study
kar3Δ-SM	BY4741 with *kar3Δ::KanMX4* (Hyg+) +pYX212-dsRed-SY1 +MoBY-KAR3(URA+)	This study
she4Δ-SM	BY4741 with *she4Δ::KanMX4* (Hyg+) +pYX212-dsRed-SY1 +MoBY-SHE4(URA+)	This study
vac14Δ-SM	BY4741 with *vac14Δ::KanMX4* (Hyg+) +pYX212-dsRed-SY1 +MoBY-VAC14(URA+)	This study
his3Δ-SP	BY4741 with *his3Δ::KanMX4* +pYX212-dsRed-SY1 (Hyg+)+p5586(URA+)	This study
dyn3Δ-SP	BY4741 with *dyn3Δ::KanMX4* +pYX212-dsRed-SY1 (Hyg+)+p5586(URA+)	This study
gim4Δ-SP	BY4741 with *gim4Δ::KanMX4* +pYX212-dsRed-SY1 (Hyg+)+p5586(URA+)	This study
yke2Δ-SP	BY4741 with *yke2Δ::KanMX4* +pYX212-dsRed-SY1 (Hyg+)+p5586(URA+)	This study
kar3Δ-SP	BY4741 with *kar3Δ::KanMX4* +pYX212-dsRed-SY1 (Hyg+)+p5586(URA+)	This study
she4Δ-SP	BY4741 with *she4Δ::KanMX4* +pYX212-dsRed-SY1 (Hyg+)+p5586(URA+)	This study
vac14Δ-SP	BY4741 with *vac14Δ::KanMX4* +pYX212-dsRed-SY1 (Hyg+)+p5586(URA+)	This study
SGA-V2 collection	BY4741 with *xxxΔ::KanMX4* collection	Boone lab
Ts-V5 collection	BY4741 background, essential gene temperature sensitive allele collection	Boone lab
S2YDSY1 collection	SGA-V2 with pYX212-dsRed-Sy1	This study
S2YD collection	SGA-V2 with pYX212-dsRed (control for	This study

	S2YDSY1 collection	
Sts5YDSY1 collection	Ts-V5 with pYX212-dsRed-Sy1	This study
Sts5YD collection	Ts-V5 with pYX212-dsRed (control for Sts5YDSY1 collection)	This study

Supplementary Table 3-2: Plasmids used in Chapter 3

Plasmid Name	Genotype and markers	Background/Source
pYX285	pYX212-SY1-dsRed, (URA3+, AmpR)	BÜTTNER et al. 2010
pYX244	pYX212-dsRed, (URA3+, AmpR)	BÜTTNER et al. 2010
pYX285'	pYX212-SY1-dsRed, (Hygromycin B+, AmpR)	This study
pYX244'	pYX212-dsRed, (Hygromycin B+, AmpR)	This study
p5586	p5472+URA3+CEN+MAGIC (URA3+, tetracycline+, kanamycin+, chloramphenicol+)	MoBY-ORF library
pMoBY-DYN3	p5586-*DYN3* ORF (URA3+, Hygromycin B+, tetracycline+, kanamycin+, chloramphenicol+)	MoBY-ORF library
pMoBY-GIM4	p5586-*GIM4* ORF (URA3+, Hygromycin B+, tetracycline+, kanamycin+, chloramphenicol+)	MoBY-ORF library
pMoBY-YKE2	p5586-*YKE2* ORF (URA3+, Hygromycin B+, tetracycline+, kanamycin+, chloramphenicol+)	MoBY-ORF library
pMoBY-KAR3	p5586-*KAR3* ORF(URA3+, Hygromycin B+, tetracycline+, kanamycin+, chloramphenicol+)	MoBY-ORF library
pMoBY-SHE4	p5586-*SHE4* ORF (URA3+, Hygromycin B+, tetracycline+, kanamycin+, chloramphenicol+)	MoBY-ORF library
pMoBY-VAC14	p5586-*VAC14* ORF (URA3+, tetracycline+, kanamycin+, chloramphenicol+)	MoBY-ORF library
pSG32	(Hygromycin B+)	For hphMX4 amplify

Supplementary Table 3-3: Mutants with manually confirmed decreased Synphilin-1 inclusions phenotype

Number	Mutant	Percentage of cells with SY1 inclusions (%)	Relative intensity	Intensity *t*-test (P□value)
0	wt	50.00	100.00	
1	*cbc2Δ*	0.20	22.71	0.0702
2	*ctf18Δ*	1.37	61.44	0.2371
3	*tid3-1*	1.70	67.78	0.1161
4	*idh2Δ*	1.70	74.41	0.3265
5	*cdc3-1*	2.66	68.16	0.0531
6	*srb2Δ*	2.76	103.01	0.5860
7	*rtg3Δ*	2.91	42.39	0.0855
8	*irc14Δ*	3.24	62.78	0.0980
9	*idh1Δ*	3.41	68.76	0.0832
10	*cdc5-1*	4.22	70.19	0.0616
11	*cdc73Δ*	4.23	70.79	0.1479
12	*bre1Δ*	4.41	70.47	0.1634
13	*rad14Δ*	4.83	123.66	0.0013
14	*bap2Δ*	5.84	61.73	0.2459
15	*psf1-1*	5.90	98.45	0.6070
16	*abd1-5*	6.11	59.33	0.0731
17	*gpi19-2*	6.18	8□□48	0.2261
18	*act1-112*	6.23	62.15	0.1426
19	*cdc20-1*	6.38	58.30	0.1508
20	*jnm1Δ*	6.67	71.07	0.0656
21	*rfc2-1*	6.77	89.79	0.3747
22	*kar3Δ*	6.99	47.55	0.1204
23	*soh1Δ*	7.05	99.93	0.9894
24	*pac10Δ*	7.27	88.78	0.6408
25	*rpn12-1*	7.29	93.00	0.1913
2	*spt14-1-10c*	7.35	92.17	0.2130
27	*orc2-2*	7.45	97.09	0.6545
28	*cdc53-1*	7.67	60.00	0.0983
29	*act1-133*	7.87	62.94	0.0613
30	*rpn10Δ*	8.12	82.93	0.3363
31	*hur1Δ*	8.28	96.68	0.8663
32	*pmr1Δ*	8.38	80.18	0.2948
33	*ctf4Δ*	8.51	47.63	0.1020
34	*act1-105*	□□73	64.67	0.1957
35	*pol1-13*	8.93	88.12	0.3093
36	*spe3Δ*	8.99	86.02	0.1787

37	*smc1-2*	9.23	77.97	0.0543
38	*spt8Δ*	9.30	67.17	0.2603
39	*act1-3*	9.65	86.73	0.0884
40	*mcm3-1*	10.07	74.84	0.2017
41	*mms22Δ*	10.15	60.34	0.3571
42	*ira2Δ*	10.45	63.52	0.1043
43	*apc11-22*	10.47	72.38	0.1282
44	*gpr1Δ*	10.48	92.81	0.5443
45	*pds5-1*	10.92	58.63	0.1094
46	*isc1Δ*	10.99	93.85	0.9580
47	*rvs161Δ*	11.27	102.33	0.7764
48	*stu1-6*	11.38	90.15	0.2789
49	*est1Δ*	11.60	83.33	0.4955
50	*rfa1-m2*	11.92	90.36	0.1263
5	*rpo21-1*	11.99	62.24	0.0547
52	*stu2-10*	12.64	108.87	0.7958
53	*mms1Δ*	12.78	65.37	0.3096
54	*rcy1Δ*	13.11	64.18	0.1897
55	*act1-125*	13.28	66.49	0.1024
56	*ctf8Δ*	13.85	61.49	0.0987
57	*she4Δ*	14.42	65.36	0.2147
58	*asf1Δ*	14.42	78.89	0.2732
59	*cdc20-*	14.42	60.24	0.0866
60	*act1-129*	14.55	94.62	0.1015
61	*pib2Δ*	14.59	108.39	0.7504
62	*aro2Δ*	14.67	81.65	0.3638
63	*lat1Δ*	14.96	73.78	0.0602
64	*leo1Δ*	15.18	98.54	0.1710
65	*arg2Δ*	15.37	92.61	0.3546
66	*rad52Δ*	15.59	73.62	0.2094
67	*csg2Δ*	15.81	92.	0.7368
68	*lge1Δ*	15.85	76.55	0.4217
69	*aah1Δ*	16.17	76.85	0.3225
70	*rpe1Δ*	16.17	91.34	0.9704
71	*rad27Δ*	16.20	91.37	0.0791
72	*rtf1Δ*	16.37	75.43	0.0947
73	*cdc15-2*	16.61	86.59	0.1059
74	*clb5Δ*	16.71	81.56	0.9800
75	*pcf11-ts2*	16.81	75.80	0.1105
76	*pde2Δ*	16.91	91.56	0.3362
77	*nip100Δ*	17.01	67.94	0.5268
78	*dia2Δ*	17.34	150.63	0.0421
79	*sec66Δ*	17.44	89.21	0.1357

80	*yta7Δ*	17.54	97.63	0.6665
81	*sub1Δ*	17.64	79.22	0.6241
82	*yke2Δ*	17.85	89.72	0.6966
83	*gwt1-20*	17.97	107.70	0.9268
84	*dyn3Δ*	18.03	81.67	0.3326
85	*arv1Δ*	18.52	95.78	0.8862
86	*sla1Δ*	19.45	73.56	0.5605
87	*spf1Δ*	19.51	82.87	0.0528
88	*swd1Δ*	19.52	66.96	0.7769
89	*bts1Δ*	19.59	80.62	0.8082
90	*ubp15Δ*	19.85	64.47	0.0589
91	*dyn1Δ*	19.98	79.14	0.5109
92	*kem1Δ*	20.12	59.61	0.1279
93	*num1Δ*	20.14	81.76	0.0780
94	*swi6Δ*	20.27	62.52	0.0688
95	*chl1Δ*	20.96	78.81	0.4542
96	*gtr2Δ*	21.10	89.08	0.2366
97	*dep1Δ*	21.28	75.51	0.3573
98	*hex3Δ*	22.09	92.89	0.7206
99	*rtt109Δ*	22.17	103.60	0.1670
100	*ssk1Δ*	22.52	64.47	0.2329
101	*lrp1Δ*	22.63	107.11	0.2375
102	*ldb18Δ*	22.73	75.88	0.3947
103	*ade1Δ*	22.86	73.75	0.5854
104	*vac14Δ*	23.42	96.55	0.6339
105	*pac1Δ*	23.55	76.11	0.1951
106	*pdb1Δ*	23.98	60.15	0.1658
107	*ost4Δ*	24.17	93.49	0.3114
108	*swd3Δ*	24.30	79.39	0.7011
109	*spe2Δ*	24.32	80.62	0.5859
110	*gim4Δ*	24.53	88.24	0.2892
111	*thr4Δ*	24.54	73.25	0.1908
112	*las21Δ*	24.72	93.23	0.3713
113	*sac1Δ*	26.76	79.32	0.2403
114	*ded1-199*	27.03	67.87	0.0536
115	*stt3-7*	27.23	102.65	0.8626
116	*tps1Δ*	27.25	57.46	0.1786
117	*ecm8Δ*	2□.64	81.81	0.8692
118	*hoc1Δ*	27.84	77.74	0.4873
119	*pac11Δ*	28.55	87.05	0.1662
120	*mct1Δ*	28.70	74.61	0.1654
121	*nkp2Δ*	29.14	78.15	0.7418
122	*ecm33Δ*	30.06	75.96	0.9666

123	*nup133Δ*	30.21	88.16	0.7494
124	*gyp1Δ*	30.47	74.13	0.1783
125	*sic1Δ*	30.48	88.67	0.8745
126	*etr1Δ*	31.07	62.67	0.2541
127	*ald6Δ*	32.28	83.63	0.9568
128	*clb2Δ*	32.67	65.62	0.3195
129	*hom6Δ*	33.72	86.16	0.1411
130	*slm4Δ*	34.81	73.46	0.5164
131	*lip5Δ*	34.87	65.44	0.1015
132	*tip1Δ*	35.50	73.06	0.5078
133	*syg1Δ*	36.67	59.63	0.0813

* $p<0.05$ indicates significant signal intensity difference between wild-type and mutant

Supplementary Table 3-4: Functional enrichment analysis of confirmed hits with decrease of cells with Synphilin-1 inclusion

Terms	Gene(s) annotated to the term
Microtubule cytoskeleton organization	CDC15/STU1/NUM1/PAC11/ACT1/NDC80/DYN1/LDB18/STU2/CDC5/JNM1/NIP100/CLB2/CLB5/KAR3
DNA replication	DEP1/RFA1/ORC2/BRE1/PSF1/MCM3/HUR1/RFC2/RAD27/MMS22/CTF18/POL1/DIA2/LGE1/CLB5/CTF4/MMS1
Positive regulation of DNA-templated transcription, elongation	XRN1/RTF1/ASF1/YKE2/CDC73/SUB1/LEO1
Histone modification	DEP1/SWD1/ORC2/SWD3/BRE1/ACT1/RTF1/ASF1/RTT109/SPT8/CDC73/LEO1/LGE1
Sister chromatid segregation	SMC1/CDC20/SOH1/CTF8/RFC2/DYN1/MMS22/PDS5/CTF18/CHL1/CLB2/CTF4/KAR3
Glycolipid biosynthetic process	CSG2/GPI19/LAS21/GWT1/ARV1/SPT14
DNA repair	RFA1/BRE1/RPO21/PSF1/MCM3/SMC1/ACT1/SOH1/RTF1/RFC2/RAD27/NUP133/RTT109/MMS22/CDC73/RAD52/SUB1/PDS5/CTF18/RAD14/POL1/LEO1/CHL1/CTF4/MMS1

Supplementary Table 3-5: Human homologues of functional enriched yeast genes

Yeast Gene Name	Homologue Standard Name	Homologue Organism	Cross References Identifier	Homologue Diseases	Source
ACT1	ACTA1	H. sapiens	255310	MYOPATHY, CONGENITAL, WITH FIBER-TYPE DISPROPORTION; CFTD	Ensembl
ACT1	ACTA2	H. sapiens	614042	MOYAMOYA DISEASE 5; MYMY5	Ensembl
ACT1	ACTB	H. sapiens	243310	BARAITSER-WINTER SYNDROME 1; BRWS1	Ensembl
ACT1	ACTBL2	H. sapiens			Ensembl
ACT1	ACTC1	H. sapiens	613424	CARDIOMYOPATHY, DILATED, 1R; CMD1R LEFT VENTRICULAR NONCOMPACTION 4, INCLUDED; LVNC4, INCLUDED	Ensembl
ACT1	ACTG2	H. sapiens	155310	VISCERAL MYOPATHY; VSCM	Ensembl
ACT1	ACTR1A	H. sapiens			Ensembl
ACT1	ACTR1B	H. sapiens			Ensembl
ACT1	ACTRT1	H. sapiens			Ensembl
ACT1	ACTRT2	H. sapiens			Ensembl
ACT1	ACTRT3	H. sapiens			Ensembl
ASF1	ASF1A	H. sapiens			Ensembl
ASF1	ASF1B	H. sapiens			Ensembl
BRE1	RNF20	H. sapiens			Ensembl
BRE1	RNF40	H. sapiens			Ensembl
CDC15	MAP3K14	H. sapiens			Ensembl
CDC15	MAP3K15	H. sapiens			Ensembl
CDC15	MAP3K5	H. sapiens			Ensembl
CDC15	MAP3K6	H. sapiens			Ensembl
CDC15	MAP3K8	H. sapiens	211980	LUNG CANCER ALVEOLAR CELL CARCINOMA, INCLUDED	Ensembl
CDC5	PLK1	H. sapiens			Ensembl
CDC5	PLK2	H. sapiens			Ensembl
CDC5	PLK3	H. sapiens			Ensembl
CDC5	PLK4	H. sapiens	616171	MICROCEPHALY AND CHORIORETINOPATHY,	Ensembl

				AUTOSOMAL RECESSIVE, 2; MCCRP2	
CDC73	CDC73	H. sapiens	608266	PARATHYROID CARCINOMA	Ensembl
CDC73	CDC73	H. sapiens	145001	HYPERPARATHYROIDISM 2; HRPT2	Ensembl
CDC73	CDC73	H. sapiens	145000	HYPERPARATHYROIDISM 1; HRPT1	Ensembl
CHL1	BRIP1	H. sapiens	609054	FANCONI ANEMIA, COMPLEMENTATION GROUP J; FANCJ	Ensembl
CHL1	BRIP1	H. sapiens	114480	BREAST CANCER	Ensembl
CHL1	DDX11	H. sapiens	613398	WARSAW BREAKAGE SYNDROME; WABS	Ensembl
CHL1	RTEL1	H. sapiens	616373	PULMONARY FIBROSIS AND/OR BONE MARROW FAILURE, TELOMERE-RELATED, 3; PFBMFT3	Ensembl
CHL1	RTEL1	H. sapiens	615190	DYSKERATOSIS CONGENITA, AUTOSOMAL RECESSIVE 5; DKCB5 DYSKERATOSIS CONGENITA, AUTOSOMAL DOMINANT 4, INCLUDED; DKCA4, INCLUDED	Ensembl
CLB2	CCNA1	H. sapiens			Ensembl
CLB2	CCNA2	H. sapiens			Ensembl
CLB2	CCNB1	H. sapiens			Ensembl
CLB2	CCNB2	H. sapiens			Ensembl
CLB2	CCNB3	H. sapiens			Ensembl
CLB2	CCND1	H. sapiens	193300	VON HIPPEL-LINDAU SYNDROME; VHL VON HIPPEL-LINDAU SYNDROME, MODIFIERS OF, INCLUDED	Ensembl
CLB2	CCND1	H. sapiens	114500	COLORECTAL CANCER; CRC	Ensembl
CLB2	CCND1	H. sapiens	254500	MYELOMA, MULTIPLE AMYLOIDOSIS, SYSTEMIC, INCLUDED; AL, INCLUDED	Ensembl

CLB2	CCND2	H. sapiens	615938	MEGALENCEPHALY-POLYMICROGYRIA-POLYDACTYLY-HYDROCEPHALUS SYNDROME 3; MPPH3	Ensembl
CLB2	CCND3	H. sapiens			Ensembl
CLB2	CCNE1	H. sapiens			Ensembl
CLB2	CCNE2	H. sapiens			Ensembl
CLB2	CCNO	H. sapiens	615872	CILIARY DYSKINESIA, PRIMARY, 29; CILD29	Ensembl
CLB5	CCNA1	H. sapiens			Ensembl
CLB5	CCNA2	H. sapiens			Ensembl
CLB5	CCNB1	H. sapiens			Ensembl
CLB5	CCNB2	H. sapiens			Ensembl
CLB5	CCNB3	H. sapiens			Ensembl
CLB5	CCND1	H. sapiens	193300	VON HIPPEL-LINDAU SYNDROME; VHL VON HIPPEL-LINDAU SYNDROME, MODIFIERS OF, INCLUDED	Ensembl
CLB5	CCND1	H. sapiens	114500	COLORECTAL CANCER; CRC	Ensembl
CLB5	CCND1	H. sapiens	254500	MYELOMA, MULTIPLE AMYLOIDOSIS, SYSTEMIC, INCLUDED; AL, INCLUDED	Ensembl
CLB5	CCND2	H. sapiens	615938	MEGALENCEPHALY-POLYMICROGYRIA-POLYDACTYLY-HYDROCEPHALUS SYNDROME 3; MPPH3	Ensembl
CLB5	CCND3	H. sapiens			Ensembl
CLB5	CCNE1	H. sapiens			Ensembl
CLB5	CCNE2	H. sapiens			Ensembl
CLB5	CCNO	H. sapiens	615872	CILIARY DYSKINESIA, PRIMARY, 29; CILD29	Ensembl
CTF18	CHTF18	H. sapiens			Ensembl
CTF4	WDHD1	H. sapiens			Ensembl
GIM4	PFDN2	H. sapiens			Ensembl
GWT1	PIGW	H. sapiens	616025	HYPERPHOSPHATASIA WITH MENTAL RETARDATION SYNDROME 5; HPMRS5	Ensembl
KAR3	KIF25	H. sapiens			Ensembl
KAR3	KIFC1	H. sapiens			Ensembl
KAR3	KIFC3	H. sapiens			Ensembl

LEO1	LEO1	H. sapiens			Ensembl
MCM3	MCM3	H. sapiens			Ensembl
NDC80	NDC80	H. sapiens			Ensembl
NIP100	CLIP1	H. sapiens			Ensembl
NIP100	CLIP2	H. sapiens			Ensembl
NIP100	CLIP3	H. sapiens			Ensembl
PAC10	VBP1	H. sapiens			Ensembl
PDS5	PDS5A	H. sapiens			Ensembl
PDS5	PDS5B	H. sapiens			Ensembl
POL1	POLA1	H. sapiens	310465	N SYNDROME; NSX	Ensembl
PSF1	GINS1	H. sapiens			Ensembl
RFA1	RPA1	H. sapiens			Ensembl
RFC2	RFC4	H. sapiens			Ensembl
RTF1	RTF1	H. sapiens			Ensembl
SMC1	SMC1A	H. sapiens	300590	CORNELIA DE LANGE SYNDROME 2; CDLS2	Ensembl
SMC1	SMC1B	H. sapiens			Ensembl
SPT14	PIGA	H. sapiens	300868	MULTIPLE CONGENITAL ANOMALIES-HYPOTONIA-SEIZURES SYNDROME 2; MCAHS2	Ensembl
SPT14	PIGA	H. sapiens	300818	PAROXYSMAL NOCTURNAL HEMOGLOBINURIA 1; PNH1	Ensembl
STU2	CKAP5	H. sapiens			Ensembl
SUB1	SUB1	H. sapiens			Ensembl
SWD1	RBBP5	H. sapiens			Ensembl
XRN1	XRN1	H. sapiens			Ensembl
YKE2	PFDN6	H. sapiens			Ensembl

Supplementary Table 3-6: Mutants with manually confirmed increased Synphilin-1 inclusions phenotype

Number	Mutant	Percentage of cells with SY1 inclusions (%)	Relative intensity	Intensity *t*-test (P value)
0	wt	50.00	100.00	
1	*mob2-26*	73.01	141.41	0.0453
2	*taf11-ts2*	72.52	214.15	0.0165
3	*crm1-1*	68.70	110.51	0.5755
4	*rtc1Δ*	68.22	116.51	0.2105
5	*taf4-18*	67.69	141.59	0.0179
6	*cdc24-3*	67.21	113.76	0.6103
7	*taf12-W486*	65.61	163.97	0.0214
8	*arx1Δ*	63.23	124.13	0.5328
9	*ktr7Δ*	62.89	128.45	0.0253
10	*rox1Δ*	61.78	92.71	0.9362
11	*taf12-L464A*	58.07	266.95	0.0045
12	*taf12-9*	57.77	154.13	0.0385
13	*taf12-L446A*	57.71	193.79	0.0061
14	*taf2-1*	57.28	216.78	0.0040
15	*gdh1Δ*	54.82	102.01	0.0978

* $p<0.05$ indicates significant signal intensity difference between wild-type and mutant

Supplementary Table 3-7: Functional enrichment analysis of confirmed hits with increase of cells with Synphilin-1 inclusion

Terms	Gene(s) annotated to the term
DNA binding transcription factor activity	TAF2/TAF12/TAF11/TAF4/ROX1
Transcription factor TFIID complex	TAF2/TAF12/TAF11/TAF4

Supplementary Table 3-8: Mutants showed significant decrease in both the percentage of cells with Synphilin-1 inclusion and the fluorescence intensity

Number	Mutant	Percentage of cells with SY1 inclusions (%)	Relative intensity	Intensity *t*-test (P value)
0	wt	50.00	100.00	
1	*sem1Δ*	0.00	61.94	0.0002
2	*dbp5-2*	0.00	34.32	0.0030
3	*cdc10-5*	0.00	42.79	0.0162
4	*cdc40-ts*	0.29	47.33	0.0114
5	*bbp1-2*	0.42	23.54	0.0097
6	*dbp5-1*	0.46	25.95	0.0027
7	*hsl1Δ*	0.61	65.14	0.0442
8	*yhc1-7*	0.98	61.08	0.0135
9	*scd5-D338*	1.37	59.15	0.0303
10	*cks1-38*	1.52	39.71	0.0124
11	*nop2-10*	1.75	51.24	0.0481
12	*spt3Δ*	1.80	70.61	0.0299
13	*cdc28-td*	1.92	38.01	0.0259
14	*spc29-20*	2.04	59.88	0.0106
15	*nip7-1*	2.15	53.83	0.0098
16	*srm1-G282S*	2.21	60.57	0.0328
17	*cdc123-4*	2.28	35.70	0.0030
18	*pri2-1*	2.59	76.96	0.0201
19	*prp18-1202*	3.01	74.75	0.0490
20	*rtg2Δ*	3.09	53.06	0.0280
21	*med6-ts*	3.13	41.44	0.0092
22	*orc3-70*	3.14	67.46	0.0096
23	*cks1-35*	3.41	25.26	0.0200
24	*scd5-PP1D2*	3.47	42.85	0.0133
25	*mtr3-ts*	3.53	51.54	0.0110
26	*stu1-8*	3.56	50.81	0.0171
27	*apc11-13*	3.91	43.41	0.0072
28	*pol1-2*	4.06	67.81	0.0174

29	*orc2-1*	4.06	48.64	0.0205
30	*ded1-95*	4.20	52.68	0.0131
31	*las17-13*	4.83	49.88	0.0460
32	*act1-155*	4.95	52.21	0.0114
33	*act1-132*	5.31	61.03	0.0074
34	*dcc1Δ*	5.73	65.61	0.0094
35	*sup35-td*	6.02	45.82	0.0076
36	*bem2Δ*	6.05	50.21	0.0149
37	*spt6-14*	6.07	49.81	0.0281
38	*slu7-ts2*	6.09	65.87	0.0225
39	*cdc37-ts*	6.19	45.76	0.0036
40	*rmp1-ts*	6.75	54.20	0.0337
41	*cdc48-3*	6.97	58.69	0.0225
42	*rtg1Δ*	7.69	40.06	0.0359
43	*rna15-58*	7.77	71.03	0.0184
44	*cft2-1*	8.01	70.40	0.0286
45	*stu2-11*	8.26	73.30	0.0408
46	*lcb1-10*	8.35	58.60	0.0149
47	*lst8-6*	8.85	68.69	0.0329
48	*elm1Δ*	8.98	46.75	0.0176
49	*stu2-12*	8.99	55.24	0.0116
50	*cik1Δ*	9.02	57.19	0.0047
51	*mnn10Δ*	9.38	46.61	0.0081
52	*mps3-7*	9.40	43.24	0.0333
53	*arp1Δ*	9.44	81.88	0.0034
54	*stp1Δ*	9.83	80.72	0.0305
55	*orc2-4*	9.93	74.93	0.0468
56	*mud2Δ*	10.14	48.14	0.0037
57	*sub2-1*	10.45	35.45	0.0088
58	*ssd1Δ*	10.86	90.76	0.0497
59	*cdc28-4*	10.99	62.28	0.0200
60	*afg2-18*	11.16	57.09	0.0118
61	*spt5-194*	11.17	57.34	0.0382
62	*swi4Δ*	11.31	92.23	0.0495
63	*nup192-15*	11.32	65.10	0.0331
64	*cdc8-2*	12.30	88.38	0.0366
65	*cdc28-13*	12.30	56.84	0.0461
66	*xrs2Δ*	12.32	86.78	0.0159
67	*med8-51*	12.73	59.44	0.0191
68	*pfy1-4*	12.79	46.65	0.0294
69	*mre11Δ*	14.13	66.29	0.0471
70	*bim1Δ*	14.27	49.17	0.0270
71	*cdc33-E72G*	14.33	57.95	0.0094

72	*dam1-19*	14.59	46.89	0.0021
73	*pri1-M4*	15.66	79.81	0.0214
74	*sse1Δ*	15.96	53.16	0.0385
75	*gas1Δ*	17.47	77.04	0.0209
76	*mks1Δ*	20.12	46.09	0.0164
77	*cdc4-3*	20.20	67.39	0.0428
78	*rpo41Δ*	20.34	72.04	0.0171
79	*tfa2-45*	22.67	70.31	0.0223
80	*pol12-ts*	24.92	62.32	0.0186
81	*gcr2Δ*	26.82	41.63	0.0299
82	*enp1-1*	30.34	67.76	0.0337
83	*ume6Δ*	32.50	66.11	0.0210
84	*wbp1-1*	33.11	72.31	0.0313
85	*rio2-1*	35.75	65.69	0.0268
86	*pda1Δ*	36.10	79.11	0.0205

* $p<0.05$ indicates significant signal intensity difference between wild-type and mutant

SUPPLEMENTARY FIGURE

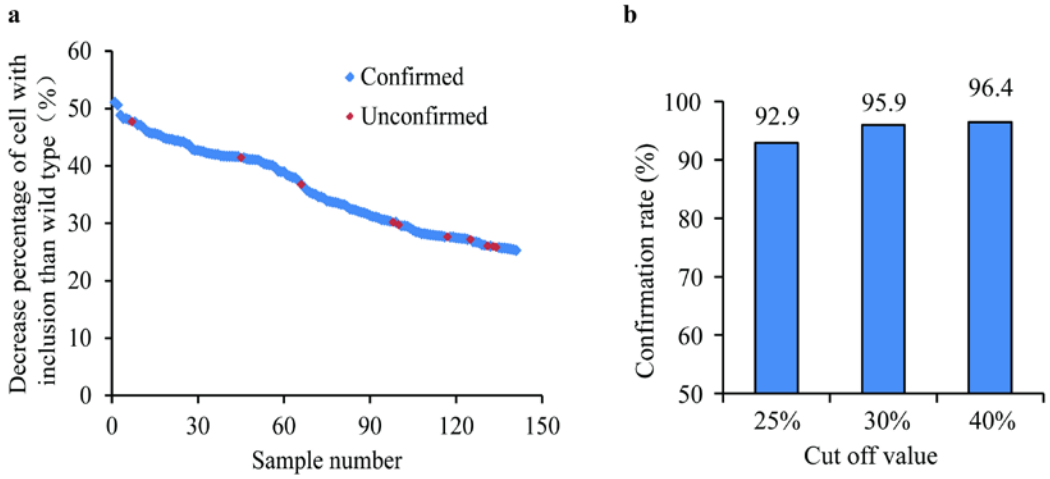

Supplementary Figure 3-1. Manual confirmation status of hits from HCM screening. a) The distribution of the confirmation status of decreased Synphilin-1 inclusion formation hits, sorted based on their difference (from high to low) from the WT strain. Blue dots represented confirmed hits, and red ones represented unconfirmed mutants. b) Confirmation rate of hits with decrease Synphilin-1 inclusion formation rate. Bars showed the confirmation rate by manual confirmation with different cut off values.

Chapter 4

Role of the ribosomal quality control machinery in nucleocytoplasmic translocation of polyQ-expanded huntingtin exon-1

This chapter is published as:

Zheng, J., Yang, J., Choe, Y., Hao, X., Cao, X., Zhao, Q., Zhang, Y., Franssens, V., Hartl, F. U., Nyström, T., Winderickx, J., Liu, B. (2017) Role of the ribosomal quality control machinery in nucleocytoplasmic translocation of polyQ-expanded huntingtin exon-1. *Biochemical and Biophysical Research Communications.*

Author Contributions:

B.L. conceived the project; B.L., J.W. and T.N. supervised J.Z., B.L. designed the experiments with input from J.Z.; J.Z. performed most of the experiments with assistance from J.Y., Y.C., X.H., X.C., Q.Z. and Y.Z.; B.L., J.Z., F.U.H., T.N. and J.W. analyzed the data, B.L. and J.Z. wrote the manuscript with contributions from J.W., F.U.H., T.N. and V.F..

Abstract

The subcellular localization of polyQ-expanded huntingtin exon-1 (Httex1) modulates polyQ toxicity in models of HD. Using genome-wide screens in a yeast model system, we report that the ribosome quality control (RQC) machinery, recently implicated in neurodegeneration, is a key determinant for the nucleocytoplasmic distribution of Httex1-103Q. Deletion of the RQC genes, *LTN1* or *RQC1*, caused the accumulation of Httex1-103Q in the nucleus through a process that required the CAT-tail tagging activity of Rqc2 and transport via the nuclear pore complex. We provide evidence that nuclear accumulation of Httex1-103Q enhances its cytotoxicity, suggesting that the RQC machinery plays an important role in protecting cells against the adverse effects of polyQ expansion proteins.

Keywords: polyQ protein; Huntington's disease; RQC; nucleocytoplasmic translocation

4.1. Introduction

HD is a neurodegenerative disorder caused by mutations expanding the CAG repeats in the exon-1 of Htt. These mutations result in expanded polyQ regions in the N-terminus of the mutant protein. The expanded polyQ region is responsible for polyQ aggregation and this is intimately linked with the Htt-mediated cytotoxicity that is typically associated with HD (Mangiarini et al., 1996). However, the exact mechanisms by which polyQ-expanded Httex1 causes cytotoxicity remain unclear. Although no conserved NLS have been identified in Htt, full-length and truncated N-terminal fragments of polyQ-expanded Htt have been reported to localize both in the cytoplasm and nucleus (Davies et al., 1997; DiFiglia et al., 1997; Saudou et al., 1998). These observations point towards a potential role of the nuclear localization of the polyQ protein in HD pathology. In a knock-in mouse polyQ toxicity model, expression of a polyQ construct that contains a NLS directed the majority of the polyQ proteins to the nucleus, which in turn was associated with enhanced toxicity and behavioral abnormalities (Schilling et al., 2004). Moreover, studies in a striatal cell model revealed that the nuclear

localization of polyQ-expanded Httex1 induced cell death by an apoptotic mechanism (Saudou et al., 1998). Later studies in yeast revealed that polyQ proteins interfered with protein quality control and clearance of misfolded proteins through sequestration of Sis1, an essential chaperone of the Hsp40 family (Park et al., 2013). However, the mechanisms involved in distribution of polyQ-expanded Httex1 between the cytoplasm and the nucleus remain to be elucidated.

The translation of truncated mRNAs or NS mRNAs results in ribosome stalling (Doma and Parker, 2006a; Inada and Aiba, 2005) and the dissociation of the stalled ribosomes into the 40S and 60S subunits (Brandman et al., 2012; Shao et al., 2013). The RQC complex, which comprises Ltn1/Rkr1, Rqc1, Rqc2/Tae2 and Cdc48 (Bengtson and Joazeiro, 2010; Brandman et al., 2012; Defenouillère et al., 2013), recognizes the 60S subunit and the aberrant nascent chain (NC). Rqc2 first binds to the 60S subunit, and recruits the RING domain E3 ubiquitin ligase Ltn1 (Defenouillère et al., 2013; Lyumkis et al., 2014; Shao et al., 2015) to ubiquitinate the aberrant NC to facilitate its degradation via the proteasome (Lyumkis et al., 2014; Shao et al., 2015; Shen et al., 2015). Meanwhile, Rqc2 adds carboxy-terminal Ala and Thr extensions (CAT-tails) to the stalled NC(Shen et al., 2015), and these CAT-tails have been shown to trigger aggregation of the NCs (Choe et al., 2016; Defenouillère et al., 2016; Yonashiro et al., 2016).

The yeast model has previously been used to study the toxicity of polyQ proteins (Gong et al., 2012; Meriin et al., 2002; Wang et al., 2009), and overexpression suppressor screens and screens based on the genome-wide deletion collection have been performed in order to elucidate the mechanisms and processes by which polyQ proteins induce cytotoxicity and to identify toxicity modifiers (Kayatekin et al., 2014; Mason et al., 2013; Willingham et al., 2003). Recently, Yang et al. established an image-based HCM system to identify the players involved in IB formation of a form of Httex1 with a 103Q repeat containing the proline-rich region of wild-type Htt (Supplementary Fig. 4-1A, right box). This revealed the involvement of the RQC-Hsf1 system to direct compartmentalization of polyQ-expanded Httex1 (Yang et al., 2016). Moreover, disruption of the RQC system by mutation of Listerin, the mammalian

homologue of *LTN1*, was shown to trigger neurodegeneration (Chu et al., 2009), while mutation of a central-nervous-system-specific tRNA was found to cause ribosome stalling and enhanced neurodegeneration (Ishimura et al., 2014).

In order to further investigate factors that alter the subcellular localization of polyQ-expanded Httex1, we performed a HCM screen in yeast using a toxic polyQ form of polyQ-expanded Httex1, Httex1-103Q, lacking the polyPro sequence (Supplementary Fig. 4-1A, left box) (Meriin et al., 2002). Surprisingly, we found that Httex1-103Q specifically accumulates in the nucleus in Ltn1-deficient cells. We also found that the RQC plays a key role in regulating the nuclear localization and toxicity of Httex1-103Q. In addition, we demonstrate that the nuclear pore complex (NPC) is required for nucleocytoplasmic transport of Httex1-103Q and that blocking nuclear import rescues the toxicity caused by this polyQ protein.

4.2. Materials and methods

4.2.1. *S. cerevisiae* strains

S. cerevisiae strains used in this study are listed in Supplementary Table 4-3. For the setup of the screens, the following starting query strains were constructed: Y7092 (see Supplementary Table 4-3 and reference (Tong and Boone, 2007) for more details) containing the pYES2-Httex1-103Q-GFP plasmid; *ltn1*Δ in the Y7092 background containing the pYES2-Httex1-103Q-GFP. The yeast single gene knock-out collection (SGA-V2)(Tong et al., 2001; Tong et al., 2004) and the essential gene temperature sensitive allele collection (ts-V5)(Li et al., 2011) were used as starting yeast collections for the query strain Y7092 pYES2-Httex1-103Q-GFP and *ltn1*Δ Y7092 pYES2-Httex1-103Q-GFP.

4.2.2. Growth conditions

SGA-V2 yeast cells were maintained and pre-cultured at 30°C. Temperature sensitive strains were kept at 22°C. The strains were grown on YPD or minimal selective medium supplemented with 2% glucose.

For the induction of Httex1-103Q expression, the yeast cells were diluted to OD_{600nm}=0.1 in minimal selective medium supplemented with 2% raffinose and grown at 30°C till an OD_{600nm} of 0.5. Subsequently 2% galactose was added to culture medium and the cells were grown at 30°C for 3 hours, unless otherwise indicated.

Raffinose and galactose were dissolved in dd H_2O, at a final concentration of 20% (w/v) and sterilized by filtration using filters with 0.2 μm pore size. Minimal selective medium were also filter sterilized.

4.2.3. Plasmids

All plasmids used in this study are listed in Supplementary Table 4-4. The polyQ construct used in this study consists of the N-terminal attached FLAG, exon-1 of *HTT* lacking the proline-rich region (PRR), and the C-terminal fusion GFP, under the control of GAL1 promoter (Supplementary Fig. 4-1a, left box)(Meriin et al., 2002). The constructs were subcloned into the pYES2 vector.

4.2.4. Strains and plasmids construction

The pYES2-Httex1-103Q-GFP plasmid was transformed into the query stains Y7092 and *ltn1*Δ Y7092. This generated respectively Y7092 pYES2-Httex1-103Q-GFP, *ltn1*Δ Y7092 pYES2-Httex1-103Q-GFP. The query strain Y7092 pYES2-Httex1-103Q-GFP was then used for the construction of the Httex1-103Q-GFP SGA collection, a yeast single gene knock-out collection containing the plasmid pYES2-Httex1-103Q-GFP, which was applied to the HCM-based screen. Similarly, the query strain *ltn1*Δ Y7092 pYES2-Httex1-103Q-GFP was used for the construction of the *ltn1*Δ Httex1-103Q-GFP SGA collection, a collection containing double gene knock-out strains and the plasmid pYES2-Httex1-103Q-GFP. The *ltn1*Δ Httex1-103Q-GFP SGA collection was used for identifying suppressors of toxicity caused by pYES2-Httex1-103Q-GFP in the *ltn1*Δ background. All the collections were constructed using the SGA methodology described as Tong et al.(Tong et al., 2001; Tong et al., 2004).

The plasmids pY2H-Httex1-103Q-GFP and pY2H-Httex1-103Q-mRFP were generated based on the plasmids pYES2-Httex1-103Q-GFP and pYES2-Httex1-103Q-mRFP, the coding sequence of *URA3* in pYES2-Httex1-103Q-GFP and pYES2-Httex1-103Q-mRFP was replaced by the *HphMX4* marker via PCR-mediated gene deletion, the HphMX4 cassette was amplified from the template plasmid pAG32.

The Molecular Barcoded Yeast (MoBY) plasmid, used in the complementation study, was made compatible with pYES2-Httex1-103Q-GFP in the double gene knock-out strains, by replacing the coding sequence of *URA3* in the MoBY plasmid with a *LEU2* cassette. The template used to amplify the *LEU2* cassette is the PRS415 plasmid.

4.2.5. DAPI staining

To visualize the nucleus, we used DAPI to stain the DNA. Yeast samples with different fluorescence labeled proteins were fixed using 3.7% formaldehyde at RT for 30 min, washed with 1X PBS for 3 times. Cells were then incubated in 0.1 μg/mL DAPI at RT for 30 min and finally washed 3 times with 1X PBS.

4.2.6. HCM-based screen system

All strains from the Httex1-103Q-GFP SGA collection were laid out on a Singer Plus Plate. The cells were then transferred to a 96-well plate with minimal selective liquid medium for pre-culture, using a SINGER ROTOR HDA Robot (Singer Instrument Co. Ltd). The cells were grown at 30°C for 2 days. The OD_{600nm} of the cells was measured in each well by a microplate reader (POLARstar Omega, BMG LABTECH). The cells were diluted to OD_{600nm}=0.1 in minimal selective medium with 2% raffinose, using liquid handling workstation (Hamilton). The OD_{600nm} of the cells was adjusted when necessary and the cells were kept shaking at 30°C until the OD_{600nm} reached 0.5. Next, 2% galactose was added to the culture medium, using the liquid handling workstation. Then the cells were incubated again at 30°C for 3 hours while shaking, to induce the expression of Httex1-103Q. After this, the cells were fixed in 3.7% of formaldehyde at room temperature for 30 min in 96-well plates, and

washed with 1XPSB for three times. Cells were stained by 0.1 μg/mL of DAPI for 30 min before visualization with a fluorescence microscope. A HCM system was applied for acquisition of the images. This system includes an automated high content microscope ImageXpress MICRO (MDC) and MetaXpress software which can be used to quantify cells with different characters. For each sample 15 images were obtained and analyzed and all samples were analyzed in double in a separate parallel experiment.

4.2.7. Conventional fluorescence microscopy

Cell samples with fluorescently labeled proteins, or stained by a fluorescent dye, were prepared as described in the section 4.2.2 *Growth conditions*, samples were visualized and imaged using the Zeiss Axiovert 200M inverted microscope, equipped with apotome and an AxioCam MR camera, using filtersets: 38 HE eGFP in green channel, and 49 DAPI in blue channel. An exposure time of 200 ms was set for GFP labeled 103Q protein, using the green channel. And an exposure time of 50 ms was set for DAPI signal, using the blue channel.

4.2.8. Super-resolution 3D-SIM

Sample preparation was performed similarly as described in the section 4.2.2 *Growth conditions*.

For super-resolution 3D-SIM, we used the same setting as previously described(Song et al., 2014). Excitation light wavelengths of 405nm (DAPI), and 488nm (GFP) were used respectively. Image acquisition, super-resolution processing and calculation were performed by ZEN black 2-1SP1 (Carl Zeiss, Jena, Germany).

4.2.9. Western blot analysis

Western blots were carried out as previous described (Yang et al., 2016).

4.2.10. Cell quantification and statistics

To specify the level of nuclear accumulation of Httex1-103Q, we quantified the “Class 1 cells

with 103Q nuclear accumulation (%)". These Class 1 cells are defined as cells that contain only one Httex1-103Q aggregate/inclusion, which shows an overlap with the DAPI signal. All cells were quantified using the Image J software. At least 500 cells were quantified in total and three replicates were analyzed for each condition.

To compare mean values between two samples, an unpaired two-tailed t-test was used, statistical significance was indicated as * $p<0.05$; ** $p<0.01$; *** $p<0.001$.

4.2.11. Generation time determinations

Yeast cells were grown to saturation in medium with glucose as the sole carbon source. Then the cells were diluted in medium with raffinose to OD_{600nm} =0.1 and incubated at 30°C while shaking until an OD_{600nm} of 0.5 was reached. Subsequently, the OD_{600nm} was adjusted to 0.01 in medium with galactose, which induces Httex1-103Q expression. Samples were applied to the Bioscreen C equipment, which enables the measurement of the cell's OD_{600nm} automatically. Generation time (doubling time) was determined by analyzing the OD_{600nm} of the cells at different time point, as described by Warringer and Blomberg (Warringer and Blomberg, 2003). The results were calculated from the mean of five repeats.

4.3. Results

4.3.1. A genome-wide HCM screen reveals a role for the RQC in nucleocytoplasmic translocation of Httex1-103Q.

Since neuronal intranuclear inclusions were described in HD mouse models (Davies et al., 1997; DiFiglia et al., 1997) and nuclear localization of mutant Htt was shown to be critical for HD pathology (Peters et al., 1999; Saudou et al., 1998), we sought to study the mechanisms involved in the intracellular distribution of polyQ-expanded Httex1 in more detail. To this end we opted to use the HCM approach and introduced the galactose-inducible Httex1-103Q-GFP construct (Supplementary Fig. 4-1A, left box) (Meriin et al., 2002) into the yeast genome-wide single deletion array (SGA-V2) with ~4700 yeast mutants (Tong et al., 2001) and the yeast temperature-sensitive (ts) conditional mutant array (ts-V5) with ~500 ts mutants (Li et al., 2011) (Fig. 4-1A, B). In the corresponding wild-type (WT) strains, Httex1-103Q-GFP formed multiple aggregate foci that are mainly distributed throughout the cytoplasm (Meriin et al., 2002), though a small proportion was observed to reside in the nucleus (Fig. 4-1C panel 1, D).

To identify factors affecting the intracellular distribution of Httex1-103Q-GFP, expression was induced by galactose for 3h, and then the cells were stained with DAPI to visualize the nucleus. Images were taken using a HCM in both the GFP and DAPI channels (Fig. 4-1B). Manual inspection of the images confirmed that the distribution of Httex1-103Q-GFP was indeed altered in some mutant strains. For further analysis, we focused on those mutant strains where a significant increase of Httex1-103Q-GFP in the nucleus was observed. We manually confirmed that deficiency of Ltn1, Rqc1, Rnq1 or Hsf1, caused the accumulation of Httex1-103Q-GFP in the nucleus, albeit to a different extent (Fig. 4-1C, D, Supplementary Table 4-1). In the *ltn1*Δ strain, approximately 20% of Httex1-103Q-GFP was exclusively localized in the nucleus (Class 1 cells with 103Q nuclear accumulation) (Fig. 4-1C panel 2, D and E). For the *rqc1*Δ, *rnq1*Δ and the ts-allele *hsf1*-848, this number was lower, ~2%, ~5% and ~5%, respectively, though this was still markedly higher than the ~0.5% obtained for the

WT strain.

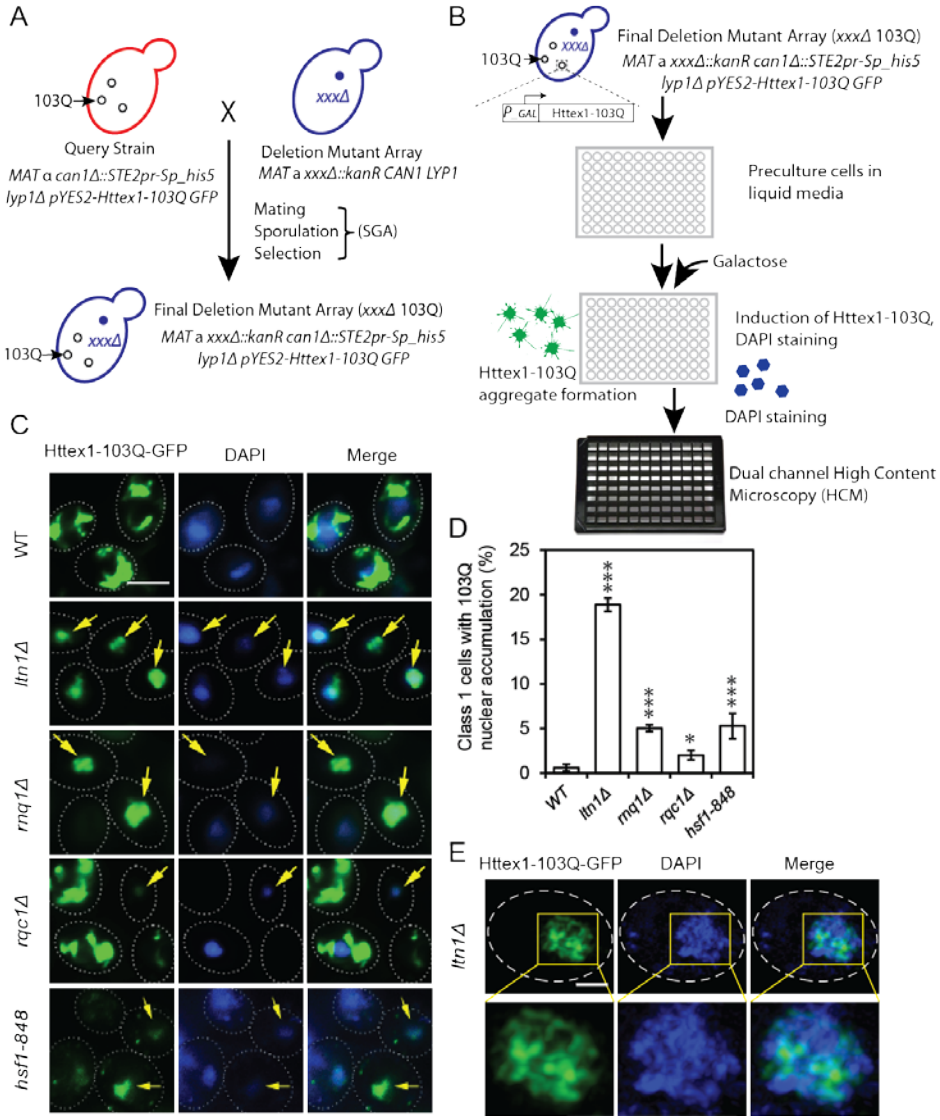

Figure 4-1. A genome-wide HCM screening identified loss-of-function genes that cause nuclear accumulation of Httex1-103Q. (**A**) Schematic representation of the yeast library construction used in this study. 103Q represents the plasmid pYES2-Httex1-103Q-GFP; *xxx* represents a gene that has been knocked out in a strain of the yeast knock-out collection; SGA, synthetic genetic array. (**B**) Main procedure followed for the HCM screen. Sample preparation is described in material and methods. Images were obtained in both GFP and DAPI channels. (**C**) Fluorescence images of mutants identified from the HCM screen that show nuclear accumulation of Httex1-103Q, nuclear Httex1-103Q was indicated by a yellow arrow. Scale represents 3 μm. (**D**) Quantification of cells which show nuclear accumulation of Httex1-103Q in class 1 cells in the indicated strains as described in **C**. Class 1 cell is defined as a cell that contains only one aggregate/inclusion. At least 500 cells were quantified in total and $N=3$, *$p<0.05$, **$p<0.01$, ***$p<0.001$. (**E**) Super-resolution microscopy revealed the morphology and localization of Httex1-103Q-GFP in *ltn1*Δ cells. The cells were stained with DAPI (blue). Scale represents 1 μm.

Since Ltn1 and Rqc1 are core components of the RQC complex (Brandman et al., 2012), our data suggest that the RQC machinery plays a crucial role in managing nuclear accumulation of polyQ-expanded Httex1. Rnq1 is a yeast prion that was previously shown to be required for aggregate formation by polyQ-expanded Httex1(Meriin et al., 2002), and indeed, overall aggregation of Httex1-103Q-GFP in the *RNQ1* mutant was low and Httex1-103Q-GFP accumulated in the nucleus in ~5% of cells. Hsf1 was previously reported to sense RQC-mediated translation-stress (Brandman et al., 2012), and thus the nuclear localization of Httex1-103Q-GFP in the *hsf1-848* mutant may be due to an altered chaperone pool.

4.3.2. Deficiency of the Ltn1 RING domain causes nuclear accumulation of Httex1-103Q

Ltn1 functions as a RING domain-dependent E3 ubiquitin ligase in quality control of NS proteins. To investigate whether the RING domain of Ltn1 is required for regulating the nuclear localization of the polyQ protein, we expressed Httex1-103Q-GFP in cells containing an Ltn1 mutant with a RING domain deletion (Ltn1-ΔRING). As shown in Supplementary Fig. 4-1B, C, the lack of this RING domain caused Httex1-103Q-GFP to accumulate in the nucleus as efficiently as in *ltn1*Δ cells. In addition, we mutated Trp-1542 in the RING domain of Ltn1 to either Ala or Glu. These changes were predicted to lower the E2 binding affinity of Ltn1 and to impair NS-protein degradation (Bengtson and Joazeiro, 2010). In both the W1542A and W1542E Ltn1 mutant strains, nuclear accumulation of Httex1-103Q-GFP was observed, although the effect was not as strong as in the *ltn1*Δ or Ltn1-ΔRING strains (Supplementary Fig. 4-1B, C). Thus, deficiency of the Ltn1 RING domain appears to be sufficient to trigger nuclear accumulation of Httex1-103Q.

Next, we asked whether nuclear accumulation of Httex1-103Q might be caused by a general failure in ubiquitin-mediated protein degradation. To test this possibility, we deleted the *RPN4* gene, a transcription factor that stimulates expression of proteasome genes. Since proteasomal degradation occurs to a large extent in the nucleus (McDonald and Byers, 1997), we expected Httex1-103Q-GFP to accumulate in the nucleus of *rpn4*Δ cells in case the protein is targeted

for degradation in this compartment. However, Httex1-103Q-GFP remained mainly cytoplasmic in *rpn4*Δ cells as well as in WT cells treated with the proteasome inhibitor MG132 (Supplementary Fig. 4-1E). In contrast, Httex1-103Q-GFP was clearly nuclear in *rqc1*Δ cells in which the Ltn1-mediated ubiquitination is still functional (Fig. 4-2A, B)(Brandman et al., 2012; Defenouillère et al., 2013; Yonashiro et al., 2016). This implies that the nuclear accumulation of Httex1-103Q is not simply due to deficient nuclear degradation of Httex1-103Q in the *ltn1*Δ cells, though it remains to be investigated how the Ltn1 RING domain functions in regulating nucleocytoplasmic translocation of Httex1-103Q.

4.3.3. Rqc2 is required for nuclear accumulation of Httex1-103Q

Within the RQC complex, Rqc2 is required for efficient recruitment of Ltn1 to translationally stalled proteins (Shao et al., 2015; Shen et al., 2015). Given this central role of Rqc2, we also investigated the requirement of Rqc2 for nuclear accumulation of Httex1-103Q. The distribution of Httex1-103Q-GFP in the single *rqc2*Δ deletion strain was similar to that observed in the WT strain with inclusions being located in the cytoplasm (Fig. 4-2A, B). Surprisingly, however, when the *RQC2* deletion was introduced in the *ltn1*Δ or *rqc1*Δ background it caused the complete suppression of the nuclear accumulation of Httex1-103Q-GFP (Fig. 4-2A, B). This suggests that Rqc2 has a crucial role in maintaining nuclear accumulation of Httex1-103Q in Ltn1 or Rqc1 mutant cells. As it was reported that Rqc2-dependent CAT-tails are present on NCs in *ltn1*Δ cells or *rqc1*Δ cells (Choe et al., 2016; Shen et al., 2015; Yonashiro et al., 2016), we wondered whether the CAT-tailing activity of Rqc2 would be necessary for nuclear accumulation of Httex1-103Q. To test this idea, we expressed in *ltn1*Δ*rqc2*Δ cells either WT Rqc2 or the so-called $Rqc2_{aaa}$ variant that fails to synthesize CAT-tails but is still able to recruit Ltn1 to the 60S ribosome (Choe et al., 2016; Shen et al., 2015). As expected, the expression of WT Rqc2 fully restored the nuclear accumulation of Httex1-103Q-GFP in the *ltn1*Δ*rqc2*Δ cells, while this was not the case upon $Rqc2_{aaa}$ expression (Fig. 4-2C, D). These results demonstrate that CAT-tailing activity of Rqc2 is required for the nuclear accumulation of Httex1-103Q in RQC-deficient cells.

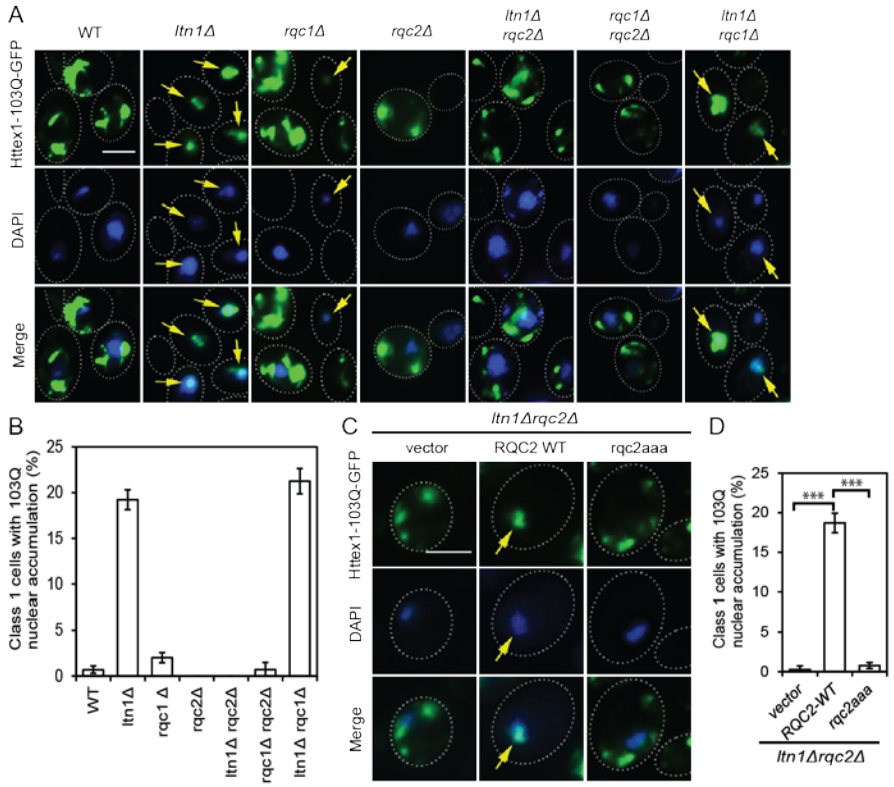

Figure 4-2. Role of RQC in regulating nuclear accumulation of Httex1-103Q. (**A**) Mutation of certain RQC genes alters the distribution of Httex1-103Q. Fluorescence images of WT or indicated RQC mutants overexpressing Httex1-103Q (green). Scale represents 3 µm. (**B**) Quantification of cells which show nuclear accumulation of Httex1-103Q in Class 1 cells in the indicated strains as described in **A**. (**C**) Representative fluorescence images showing the co-expression of empty vector (p413), RQC2 WT or variant $rqc2_{aaa}$ with Httex1-103Q in *ltn1*Δ*rqc2*Δ cells. Scale represents 3 µm. (**D**) Quantification of cells which show nuclear accumulation of Httex1-103Q in Class 1 cells in indicated strains as described in **C**. **p*<0.05, ***p*<0.01, ****p*<0.001.

4.3.4. Btn2 is involved in nucleocytoplasmic transport of Httex1-103Q

The protein-sorting factor Btn2 and the chaperone Hsp42 direct misfolded proteins to the intranuclear quality control compartment (INQ) and to CytoQ deposition sites in the cytosol, respectively (Miller et al., 2015). 3D-SIM analysis revealed that Httex1-103Q-GFP does not reside at such specific compartments but rather remains randomly distributed in the nucleus of *ltn1*Δ cells (Fig. 4-1E). However, mild overexpression of Btn2 is sufficient to block nuclear accumulation of Httex1-103Q in *ltn1*Δ cells, whereas the level of nuclear accumulation of Httex1-103Q increased in *ltn1*Δ*btn2*Δ cells as compared to WT cells and the single *ltn1*Δ deletion mutant (Fig. 4-3A, B). This result points to a role of Btn2 in the nucleocytoplasmic

translocation of Httex1-103Q. In line with this finding, Btn2 was previously shown to be sequestered in the aggregates of NS-proteins in *ltn1*Δ cells (Choe et al., 2016), which leads to the assumption that sequestration of Btn2 in endogenous NS-protein aggregates may cause the nuclear accumulation of Httex1-103Q in *ltn1*Δ cells. Notably, neither the single deletion of *BTN2* (Fig. 4-3A, B), nor the double deletion of *BTN2* and *CUR1* (homolog of *BTN2*) (Supplementary Fig. 4-2A, B), caused nuclear accumulation of Httex1-103Q, indicating that other factors also contribute to the process of Httex1-103Q nuclear accumulation.

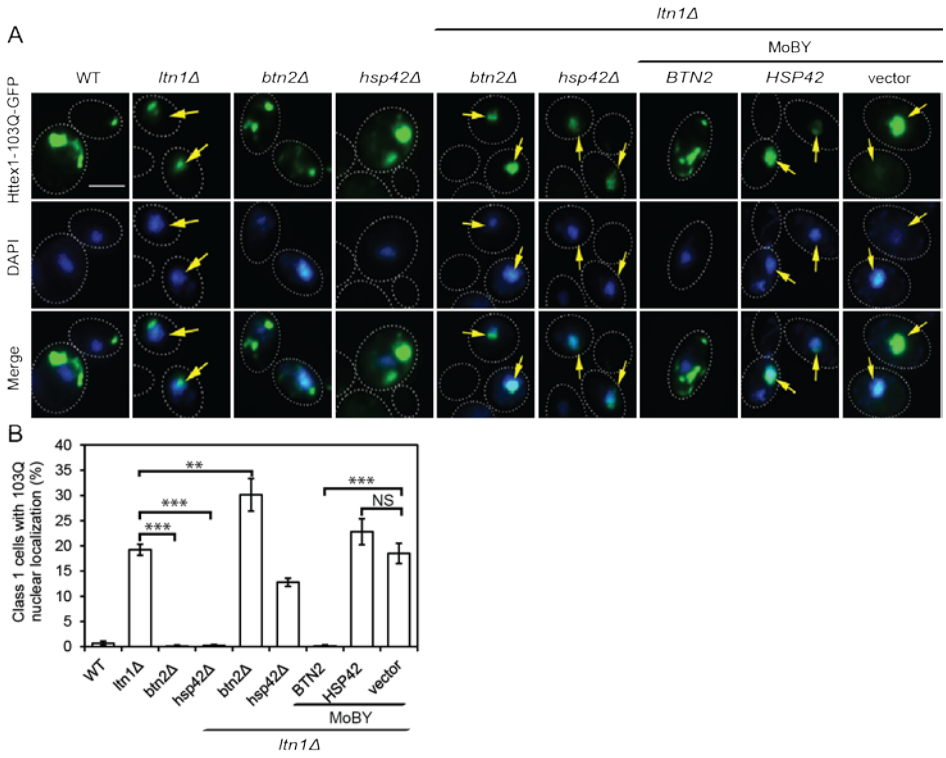

Figure 4-3. Btn2 counteracts the nuclear accumulation of Httex1-103Q in *ltn1*Δ cells. (**A**) Fluorescence images of Httex1-103Q (green) expression in the indicated strains. Samples were collected after three hours galactose induction. MoBY indicates molecular barcoded yeast, a low copy vector carrying the corresponding ORF or empty vector as control. The DNA was stained with DAPI (blue). Scale represents 3 μm. (**B**) Quantification of cells which shows nuclear accumulation of Httex1-103Q in Class 1 cells in the indicated strains as described in **A**. At least 500 cells were quantified in total and $N=3$, *$p<0.05$, **$p<0.01$, ***$p<0.001$, NS, not significant.

The small heat shock protein, Hsp42, is known to direct the cytosolic misfolded proteins into special deposition sites called CytoQ in the yeast cytosol (Miller et al., 2015). To test whether Hsp42 plays a role in regulating the localization of Httex1-103Q, we analyzed Httex1-103Q

aggregate localization in both Hsp42 mild overexpression and *HSP42* deletion strains. In contrast to Btn2, neither mild overexpression nor deletion of *HSP42* in *ltn1*Δ cells altered the nuclear accumulation of Httex1-103Q (Fig. 4-3A, B).

4.3.5. Nuclear accumulation of Httex1-103Q enhances its cytotoxicity

Genome-wide screens for suppressors of Httex1-103Q toxicity in yeast have been performed both in single gene deletion (Willingham et al., 2003) and gene overexpression collections (Kayatekin et al., 2014; Mason et al., 2013). As expression of Httex1-103Q produce significant toxicity in yeast (Meriin et al., 2002), and nuclear accumulation of Httex1-103Q enhances polyQ cytotoxicity in *ltn1*Δ background (Fig. 4-4C, D and E, panel 1 and 2), we set out to identify factors that contribute to Httex1-103Q-induced cytotoxicity in *ltn1*Δ cells. To this end, we constructed a yeast double deletion collection, in which each of the single deletion strains was combined with the additional deletion of *LTN1* and the expression of Httex1-103Q-GFP (Supplementary Fig. 4-3). We assessed Httex1-103Q cytotoxicity in different double deletion strains by scoring the size of the colonies (Wagih and Parts, 2014) and found that the additional loss of several NPC components (Nup60, Nup170, Nup188) and one karyopherin (Kap108) significantly suppressed the Httex1-103Q toxicity in the *ltn1*Δ background (Fig. 4-4D, E). Fluorescence microscopy demonstrated that Httex1-103Q-GFP no longer entered the nucleus in the *ltn1*Δ*nup60*Δ, *ltn1*Δ*nup170*Δ, *ltn1*Δ*nup188*Δ or *ltn1*Δ*kap108*Δ double deletion mutants (Fig. 4-4A, B). Hence, these results indicated that the core scaffold of the NPC, Nup170 and Nup188, as well as the nuclear import factor Kap108 (ortholog of vertebrate Importin 8) are essential for nuclear entry of Httex1-103Q in *ltn1*Δ cells.

Subsequent complementation assays further strengthened this conclusion. Indeed, mild overexpression of MoBY-*NUP60* in *ltn1*Δ*nup60*Δ cells or MoBY-*NUP170* in *ltn1*Δ*nup170*Δ cells was sufficient to restore the nuclear accumulation of Httex1-103Q-GFP (Supplementary Fig. 4-4A, B).

Next, we wondered if other NPCs or karyopherins could mediate nuclear localization and

cytotoxicity of Httex1-103Q. This was again performed by testing nuclear accumulation and cytotoxicity of Httex1-103Q-GFP in *ltn1*Δ cells in which non-essential NPC components and karyopherins were additionally deleted (Fig. 4-4C, D and E). Besides the core scaffold NPC subunits Nup170 and Nup188 and the karyopherin Kap108, Nup60, Mlp1 and Mlp2 were also found to be essential for nuclear accumulation and cytotoxicity of Httex1-103Q in the *ltn1*Δ background, while the Ran-GTP Gsp2, which mediates nuclear import of cargo, was not. The latter suggests that nucleocytoplasmic transport of mutant Htt could occur independently of Ran GTPase function, as previously observed (Cornett et al., 2005). However, it should be noted that yeast cells encode a Gsp2 paralogue, Gsp1, which may provide sufficient Ran-GTP activity to mediate nuclear import of Httex1-103Q in the absence of Gsp2.

Finally, we analyzed the correlation between Httex1-103Q nuclear accumulation and cytotoxicity. We found that the generation time of the cells increased as more Httex1-103Q accumulated in the nucleus (r=0.568, P=0.007, N=21) (Fig. 4-4F). This indicates that nuclear accumulation of Httex1-103Q might be critical for toxicity, in line with earlier studies performed in mammalian cells where nuclear targeting of polyQ-expanded Htt also enhanced its toxicity (Peters et al., 1999; Saudou et al., 1998; Schilling et al., 2004).

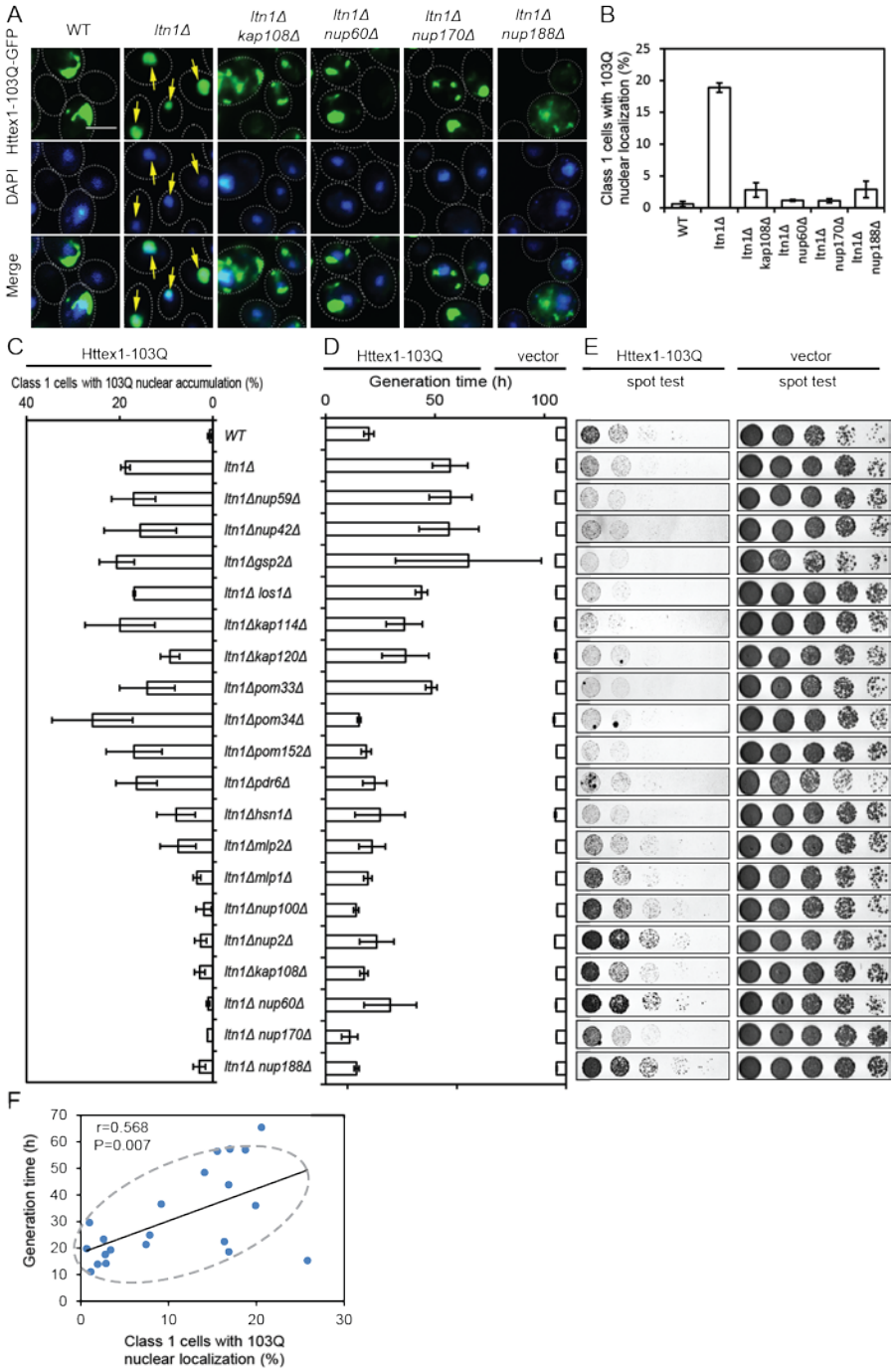

Figure 4-4. Nuclear Pore Complex (NPC) and karyopherins mediate nucleocytoplasmic transport and cytotoxicity of Httex1-103Q. (**A**) Representative fluorescence images of nuclear transport related mutants in *ltn1*Δ background expressing Httex1-103Q. Scale represents 3 μm. (**B**) Quantification of Class1 cells which shows nuclear accumulation of Httex1-103Q in the indicated strains as described in **A**. (**C**) Quantification of cells which shows nuclear accumulation of Httex1-103Q in Class 1 cells in the nuclear transport related mutants in *ltn1*Δ background. (**D**) Fitness of cells carrying the pYES2-Httex1-103Q-GFP plasmid compared to the pYES2-GFP control plasmid in mutants indicated in **C**. Generation time was calculated as described in the methods section, *N*=5. (**E**) Spot test to confirm the growth defect of strains as indicated in **C**. Five-fold serial dilutions of cells are shown, starting from OD_{600nm} =0.5. (**F**) Graph of dispersion reveals a positive relationship between the level of 103Q nuclear accumulation and generation

time. Correlation coefficient (r) and significance of the correlation coefficient P-value (P) were calculated based on the average of “Class 1 cells with 103Q nuclear accumulation (%)” and the average of “Generation time (h)” of each strain indicated in **C**, *N*=21.

4.4. Discussion

Previous studies have linked the nucleocytoplasmic trafficking of polyQ-expanded Htt to the pathology of HD. PolyQ-expanded Htt has indeed been reported to be distributed both in the cytoplasm and the nucleus (Davies et al., 1997; DiFiglia et al., 1997), and neuronal intranuclear inclusions were suggested to contribute to neurological dysfunction in a transgenic mouse model for HD (Davies et al., 1997).

Taking advantage of the novel HCM system, we identified the RQC machinery as a regulator of nucleocytoplasmic translocation of Httex1 polyQ proteins in yeast and confirmed that nuclear accumulation of polyQ proteins contributes to cytotoxicity in the yeast model. We found that the RQC complex component, Ltn1, plays a critical role in protecting yeast cells against nuclear accumulation and cytotoxicity of Httex1-103Q. This is in line with the observation that deficiency of Ltn1 causes neurodegeneration in mice (Chu et al., 2009), and that Ltn1 is involved in inclusion formation of Httex1 (Yang et al., 2016). Another component of the RQC complex, Rqc2, mediates the mRNA-independent elongation of NCs and marks the aberrant NS-proteins with CAT-tails for aggregation (Choe et al., 2016; Yonashiro et al., 2016). Our observation that the CAT-tailing activity of Rqc2 is required for the nuclear accumulation of Httex1-103Q, points to a link between the aggregation of endogenous NS-proteins and the import of Httex1-103Q into the nucleus. The RQC surveillance system works to clear endogenous NS-proteins which are generated during translation. As such, failure of the RQC surveillance system results in increased endogenous NS-inclusions. In turn, these NS-inclusions are known to sequester other proteins, such as Btn2 (Choe et al., 2016). We found that mild overexpression of *BTN2* is sufficient to block the nuclear accumulation of Httex1-103Q in *ltn1*Δ cells. This could be due to the imbalance of transport factors caused by the formation of the NS-protein aggregate in the *ltn1*Δ background (Fig. 4-5).

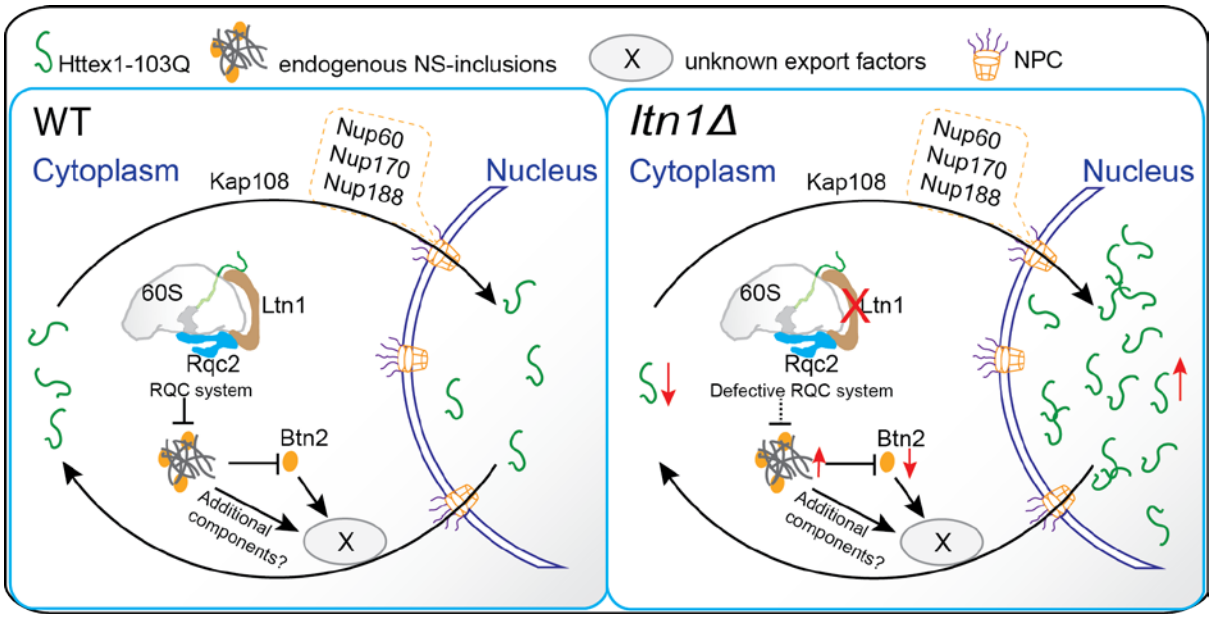

Figure 4-5. Schematic model for the RQC machinery in regulating nucleocytoplasmic translocation of Httex1-103Q. Httex1-103Q distributes both in the cytoplasm and the nucleus upon overexpression. Components of the NPC including Nup60, Nup170, Nup188, and karyopherin Kap108 mediate the import of Httex1-103Q. In WT cells, when the RQC system works efficiently, expression of Httex1-103Q largely aggregate in the cytoplasm. The RQC system regulates the transport/distribution of Httex1-103Q, by affecting the endogenous NS-inclusions formation, as NS-inclusions can sequester proteins (e.g. Btn2, Choe et al., 2016) that are involved in regulating the nucleocytoplasmic translocation of Httex1-103Q. Other factors that contribute to the RQC-dependent nucleocytoplasmic translocation of Httex1-103Q remain to be elucidated. In *ltn1*Δ cells, defective RQC surveillance results in increased endogenous NS-inclusions (Choe et al., 2016). Spatial sequestration of proteins by NS-inclusions, leads to limited factors that are required for the export of Httex1-103Q, which is responsible for the nuclear accumulation of Httex1-103Q.

It remains unclear whether the expression of Httex1-103Q affects the capacity of the RQC machinery or not. Expression of Httex1-103Q may instigate ribosomal stalling by sequestering the translation termination factor Sup35, in the Httex1-103Q aggregates (Serpionov et al., 2016), thereby enhancing translation read-though of stop codons (Gong et al., 2012) and increasing pressure on the RQC system. Hence, aberrant translation of polyQ protein at the ribosome may have an important role in the polyQ-induced toxicity in yeast.

Several studies have shown that the nuclear accumulation of Htt fragments is linked to HD-like phenotypes (Peters et al., 1999; Schilling et al., 2004) and the induction of neuronal apoptosis (Saudou et al., 1998). In line with this, our data produced in yeast indicate that the cytotoxicity of Httex1-103Q is significantly reduced when preventing its nuclear import by

deletion of the nucleocytoplasmic transport factors.

Nucleocytoplasmic translocation and the connection with cytotoxicity seem to be a general mechanism in disease pathogenesis. Recent studies in human embryonic kidney 293T cells demonstrated that cytoplasmic aggregates formed by artificial β-sheet proteins or by disease proteins like Htt96Q and TDP-43 fragments cause the sequestration and mislocalization of nuclear transport factors into the cytoplasm, which results in defects in nuclear protein import and mRNA export (Woerner et al., 2016). Likewise, screens performed in flies identified components of the NPC and different nuclear transport factors as modifiers of disease phenotypes and toxicity triggered by hexanucleotide repeat expansions in C9orf72, a gene associated to a mixed phenotype of frontotemporal dementia and amyotrophic lateral sclerosis (Zhang et al., 2015).We now report for the first time that the RQC system interferes with NPC-dependent nucleocytoplasmic translocation of Httex1-103Q so as to protect cells from polyQ protein cytotoxicity. Thus, enhancing the RQC capability or preventing nuclear import of polyQ proteins should be considered as possible strategies for the treatment of polyQ disorders.

Acknowledgements

We would like to thank Dr. C. Boone, M. Sherman, C. Joazeiro, T. Inada for providing essential regents, and S. Munck, N. Corthout for the support on 3D-SIM microscopy, the 3D-SIM microscope device was acquired through a CLME grant from Minister Lieten to the VIB BioImaging Core. This work was supported by grants from the Swedish Cancer Society (CAN 2012/601 and CAN 2015/406, to BL), the Swedish Natural Research Council (VR 2011-5923 and VR 2015-04984, to BL), the Carl Trygger Foundation (CTS 14: 295, to BL), the Fund for Scientific Research Flanders (FWO-Vlaanderen G0A6315 and G069413 to JW), an FWO postdoctoral fellowship (to VF) and a fellowship of the China Scholarship Council (to JZ). The research leading to these results has received funding from the People Programme (Marie Curie Actions) of the European Union's Seventh Framework Programme (FP7/2007-2013) under REA grant agreement n°608743. F.U.H. acknowledges funding by the Munich Cluster for Systems Neurology (SyNergy).

4.5. Supplementary information

SUPPLEMENTARY FIGURES

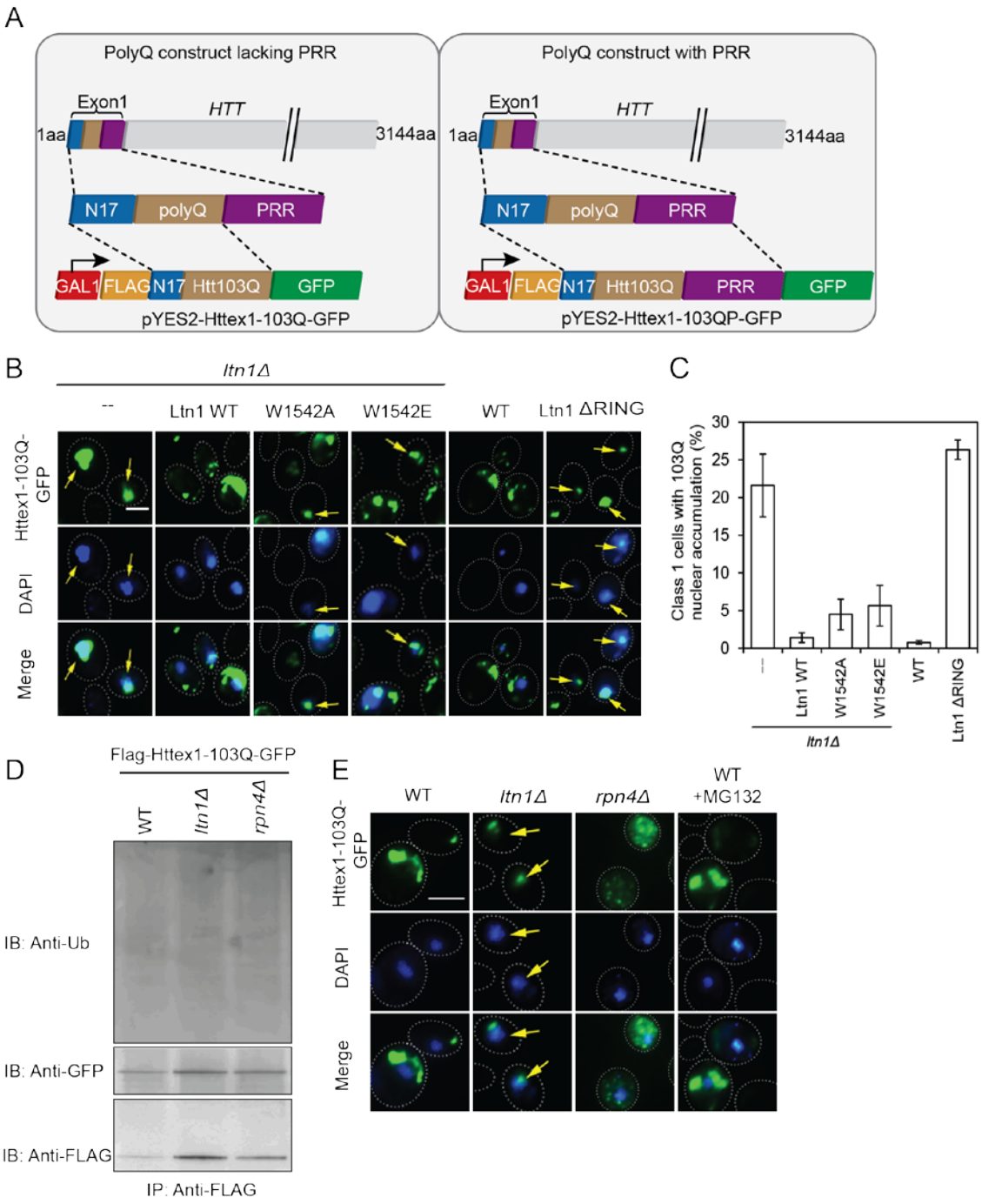

Supplementary Figure 4-1. Nuclear accumulation of Httex1-103Q is not simply caused by a defect in the ubiquitination proteasome system (UPS). (**A**) Schematic representation of the polyQ construct of Htt exon1 lacking the proline-rich region (PRR) (left box, used in this study) (Meriin et al., 2002) and the polyQ construct of Htt exon1 with PRR (right box)(Meriin et al., 2007). (**B**) Fluorescence images show the

co-expression of Httex1-103Q and Ltn1 WT/Trp 1542 mutants (Bengtson and Joazeiro, 2010) in *ltn1*Δ cells. (**C**) Quantification of cells which show nuclear accumulation of Httex1-103Q in Class 1 cells. (**D**) Western blot analysis to detect protein Httex1-103Q expression and ubiquitination of Httex1-103Q from WT, *ltn1*Δ or *rpn4*Δ cells. Flag-Httex1-103Q-GFP was immunoprecipitated (IP) from cell extracts of WT, *ltn1*Δ or *rpn4*Δ cells with a FLAG antibody, and followed by anti-FLAG, anti-GFP and anti-Ub immunoblotting (IB) respectively. (**E**) Fluorescence images of Httex1-103Q (green) expression in WT, *ltn1*Δ or *rpn4*Δ cells, as well as in WT cells treated with the proteasome inhibitor MG132. Disruption of the UPS did not cause significant nuclear accumulation of Httex1-103Q. Samples were collected after three hours galactose induction, and the DNA was stained by DAPI (blue). Scale represents 3 μm.

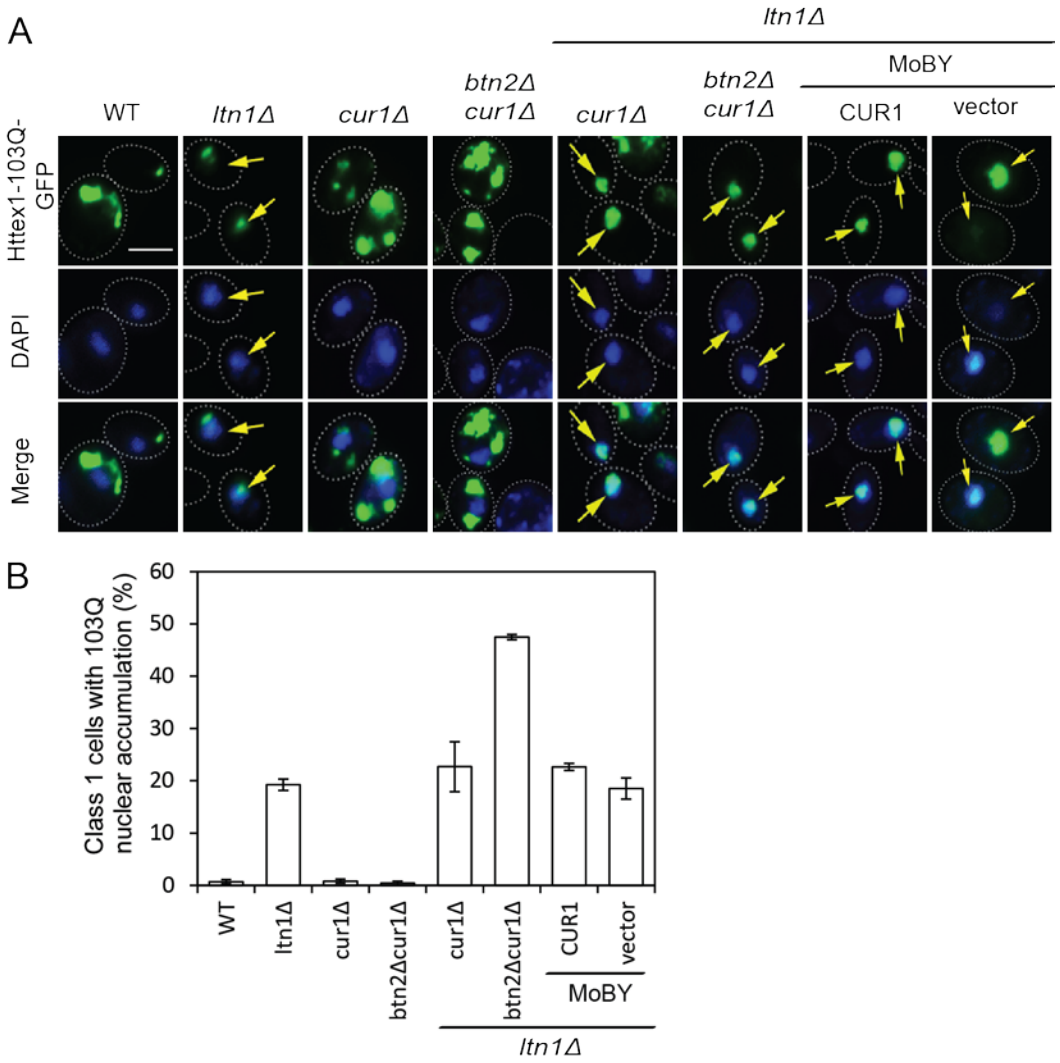

Supplementary Figure 4-2. The expression level of Cur1 does not affect nuclear accumulation of Httex1-103Q in *ltn1*Δ cells. (**A**) Fluorescence images of Httex1-103Q (green) expression in the indicated strains. Samples were collected after three hours galactose induction. The DNA was stained by DAPI (blue). Scale represents 3 μm. (**B**) Quantification of cells which shows nuclear accumulation of Httex1-103Q in Class 1 cells in the indicated strains as described in **A**.

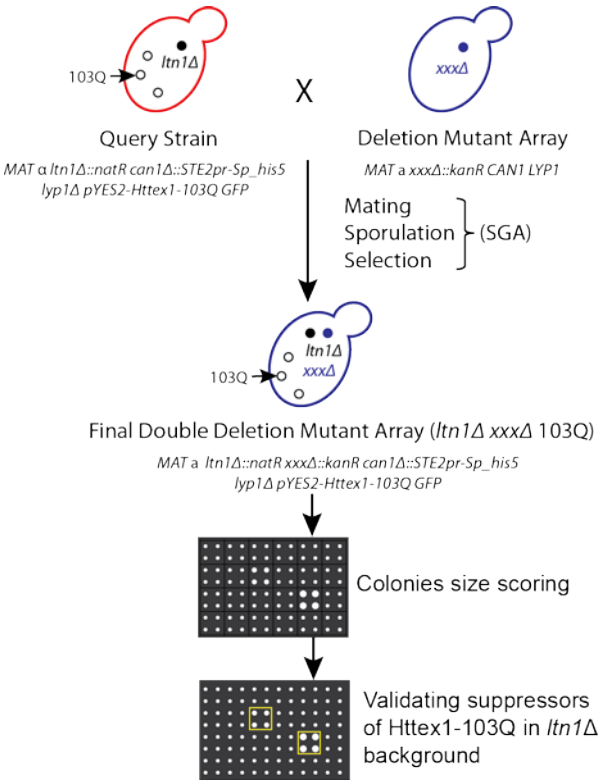

Supplementary Figure 4-3. Genome-wide screening to identify factors that suppress Httex1-103Q cytotoxicity in the *ltn1*Δ background. Schematic representation of the plasmid-carried double deletion yeast library construction and suppressor screen. 103Q represents plasmid pYES2-Httex1-103Q-GFP; *xxx* represents a gene that has been knocked out from the yeast knock-out collection; SGA, synthetic genetic array.

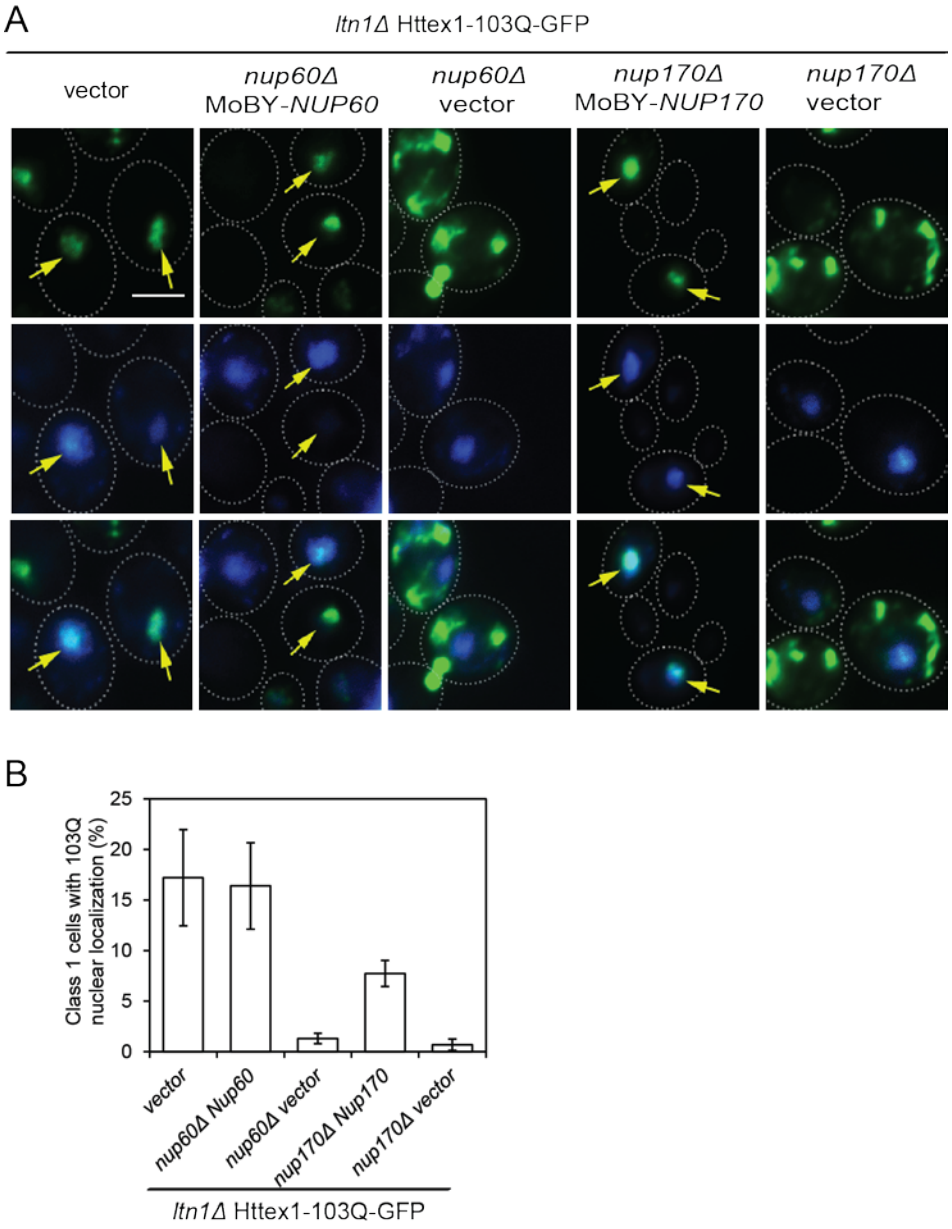

Supplementary Figure 4-4. Selected complementation assay to confirm the players that altered the nuclear accumulation of Httex1-103Q in the *ltn1*Δ background. (**A**) Fluorescence images of Httex1-103Q (green) expression in the selected NPC mutants *nup60*Δ/*nup170*Δ in the *ltn1*Δ background, while co-expressing with MoBY-*NUP60*/*NUP170* respectively, and the empty MoBY vector (p5586) serves as a control. Nuclear accumulation of Httex1-103Q can be restored by adding back a low copy MoBY vector containing its corresponding ORF. Scale represents 3 μm. (**B**) Quantification of cells which show nuclear accumulation of Httex1-103Q in Class 1 cells in the indicated strains as described in **A**.

SUPPLEMENTARY TABLES

Supplementary Table 4-1. Deficient genes that cause significant nuclear accumulation of Httex1-103Q. Related to Fig. 4-1

Systematic name	Standard name	Class 1 cells with 103Q nuclear accumulation(%)
YMR247C	*LTN1*	18.89
YGL073W	*HSF1*	5.29
YCL028W	*RNQ1*	5.03
YDR333C	*RQC1*	2.01

Supplementary Table 4-2. Loss-of-function suppressors of Httex1-103Q toxicity in the *ltn*Δ background. Related to Fig. 4 and S4. Hits with a score(Wagih and Parts, 2014) >0.8 were picked, and the growth effect by mutation of the hits confirmed by the Bioscreen C equipment (5 replicates for each sample) are listed in the table.

Systematic name	Standard name	SGA score
YFL023W	*BUD27*	2.652012
YBL079W	*NUP170*	1.857465
YPL009C	*RQC2*	1.712615
YCR063W	*BUD31*	1.648322
YDR002W	*yrb1-51*	1.262108
YOR083W	*WHI5*	1.254718
YPR176C	*bet2-1*	1.200333
YML103C	*NUP188*	1.121265
YHR003C	*YHR003C*	0.9933
YAR002W	*NUP60*	0.961654
YBR236C	*abd1-5*	0.943247
YOR061W	*CKA2*	0.927038
YLL026W	*HSP104*	0.909933
YLR335W	*NUP2*	0.899871
YIL112W	*HOS4*	0.878885
YGL019W	*CKB1*	0.84491
YBR082C	*UBC4*	0.83923

Supplementary Table 4-3. S. cerevisiae strains used in this study

NAME	BACKGROUND	GENOTYPE	SOURCE
BY4741	BY4741	MAT*a his3*Δ*1 leu2*Δ*0 met15*Δ*0 ura3*Δ*0*	EUROSCARF
Y7092	BY4742	MATα *can1*Δ::STE2pr-Sp_His3 *lyp1*Δ *his3*Δ*leu2*Δ *ura3*Δ *met15*Δ	Tong and Boone, 2001
Y7092 103Q	BY4742	MATα *can1*Δ::STE2pr-Sp_His3 *lyp1*Δ *his3*Δ*leu2*Δ *ura3*Δ *met15*Δ pYES2-Httex1-103Q-GFP	This study
Y7092 *ltn1*Δ 103Q	BY4742	MATα *ltn1*Δ::natMX4 *can1*Δ::STE2pr-Sp_His3 *lyp1*Δ *his3*Δ*leu2*Δ *ura3*Δ *met15*Δ pYES2-Httex1-103Q-GFP	This study
WT 103Q	SGA	MAT a *his3*Δ::kanMX4 *can1*Δ::STE2pr-Sp_his5 *lyp1*Δ *ura3*Δ0 *leu2*Δ0 *met15*Δ0 LYS2 pYES2-Httex1-103Q-GFP	Httex1-103Q-GFP SGA collection
*ltn1*Δ 103Q	SGA	MAT a *ltn1*Δ::kanMX4 can1Δ::STE2pr-Sp_his5 *lyp1*Δ *ura3*Δ0 *leu2*Δ0 *met15*Δ0 LYS2 pYES2-Httex1-103Q-GFP	Httex1-103Q-GFP SGA collection
*rnq1*Δ 103Q	SGA	MAT a *rnq1*Δ::kanMX4 *can1*Δ::STE2pr-Sp_his5 *lyp1*Δ *ura3*Δ0 *leu2*Δ0 *met15*Δ0 LYS2 pYES2-Httex1-103Q-GFP	Httex1-103Q-GFP SGA collection
*rqc1*Δ 103Q	SGA	MAT a *rqc1*Δ::kanMX4 *can1*Δ::STE2pr-Sp_his5 *lyp1*Δ *ura3*Δ0 *leu2*Δ0 *met15*Δ0 LYS2 pYES2-Httex1-103Q-GFP	Httex1-103Q-GFP SGA collection
hsf1-848 103Q	SGA	MAT a *hsf1-848*::kanMX4 *can1*Δ::STE2pr-Sp_his5 *lyp1*Δ *ura3*Δ0 *leu2*Δ0 *met15*Δ0 LYS2 pYES2-Httex1-103Q-GFP	Httex1-103Q-GFP TS collection
*ltn1*Δ 103Q pGAD-*LTN1*-HA	SGA	MAT a *ltn1*Δ::natMX4 *his3*Δ::kanMX4 *can1*Δ::STE2pr-Sp_his5 *lyp1*Δ *ura3*Δ0 *leu2*Δ0 met15Δ0 LYS2 pGAD-LTN1-HA pYES2-Httex1-103Q-GFP	This study
*ltn1*Δ 103Q pGAD-*LTN1*-W1542A-HA	SGA	MAT a *ltn1*Δ::natMX4 *his3*Δ::kanMX4 *can1*Δ::STE2pr-Sp_his5 *lyp1*Δ *ura3*Δ0 *leu2*Δ0 met15Δ0 LYS2 pGAD-LTN1-W1542A-HA pYES2-Httex1-103Q-GFP	This study
*ltn1*Δ 103Q pGAD-*LTN1*-W1542E-HA	SGA	MAT a *ltn1*Δ::natMX4 *his3*Δ::kanMX4 *can1*Δ::STE2pr-Sp_his5 *lyp1*Δ *ura3*Δ0 *leu2*Δ0 *met15*Δ0 LYS2 pGAD-LTN1-W1542E-HA pYES2-Httex1-103Q-GFP	This study
BY4741 Ltn1-FLAG 103Q	BY4741	MATa *his3*Δ1 *leu2*Δ0 *met15*Δ0 *ura3*Δ0 LTN1-5xFLAG::KANMX6 pYES2-Httex1-103Q-GFP	This study
BY4741 RINGΔLtn1-FLAG 103Q	BY4741	MATa *his3*Δ1 *leu2*Δ0 *met15*Δ0 *ura3*Δ0 *ltn1*Δ4452-5xFLAG::KANMX6 pYES2-Httex1-103Q-GFP	This study
*rqc2*Δ 103Q	SGA	MAT a *rqc2*Δ::kanMX4 *can1*Δ::STE2pr-Sp_his5 *lyp1*Δ	Httex1-103Q-G

		*ura3*Δ0 *leu2*Δ0 *met15*Δ0 LYS2 pYES2-Httex1-103Q-GFP-URA	FP SGA collection
*ltn1*Δ*rqc2*Δ 103Q	SGA	MAT a *ltn1*Δ::natMX4 *rqc2*Δ::kanMX4 *can1*Δ::STE2pr-Sp_his5 *lyp1*Δ *ura3*Δ0 *leu2*Δ0 *met15*Δ0 LYS2 pYES2-Httex1-103Q-GFP	*ltn1*Δ Httex1-103Q-G FP SGA collection
*rqc1*Δ*rqc2*Δ 103Q	SGA	MAT a *rqc1*Δ::kanMX4 *rqc2*Δ::natMX4 *can1*Δ::STE2pr-Sp_his5 *lyp1*Δ *ura3*Δ0 *leu2*Δ0 met15Δ0 LYS2+ pYES2-Httex1-103Q-GFP	*ltn1*Δ Httex1-103Q-G FP SGA collection
*ltn1*Δ*rqc1*Δ 103Q	SGA	MAT a *ltn1*Δ::natMX4 *rqc1*Δ::kanMX4 *can1*Δ::STE2pr-Sp_his5 *lyp1*Δ *ura3*Δ0 *leu2*Δ0 *met15*Δ0 LYS2 pYES2-Httex1-103Q-GFP	*ltn1Δ* Httex1-103Q-G FP SGA collection
*ltn1*Δ*rqc2*Δ p413 103Q	BY4741	BY4741 *ltn1*Δ::NatR *rqc2*Δ::KanR p413 pYES2-Htt103Q-GFP	This study
*ltn1*Δ*rqc2*Δ p413-RQC2 WT 103Q	BY4741	BY4741 *ltn1*Δ::NatR *rqc2*Δ::KanR p413-RQC2 WT pYES2-Htt103Q-GFP	This study
*ltn1*Δ*rqc2*Δ p413-rqc2$_{aaa}$ 103Q	BY4741	BY4741 *ltn1*Δ::NatR *rqc2*Δ::KanR p413-rqc2$_{aaa}$ pYES2-Htt103Q-GFP	This study
*btn2*Δ 103Q	SGA	MAT a *btn2*Δ::kanMX4 *can1*Δ::STE2pr-Sp_his5 *lyp1*Δ *ura3*Δ0 *leu2*Δ0 *met15*Δ0 LYS2 pYES2-Httex1-103Q-GFP	Httex1-103Q-G FP SGA collection
*hsp42*Δ 103Q	SGA	MAT a *hsp42*Δ::kanMX4 *can1*Δ::STE2pr-Sp_his5 *lyp1*Δ *ura3*Δ0 *leu2*Δ0 *met15*Δ0 LYS2 pYES2-Httex1-103Q-GFP	Httex1-103Q-G FP SGA collection
*ltn1*Δ*btn2*Δ 103Q	SGA	MAT a *ltn1*Δ::natMX4 *btn2*Δ::kanMX4 *can1*Δ::STE2pr-Sp_his5 *lyp1*Δ *ura3*Δ0 *leu2*Δ0 *met15*Δ0 LYS2 pYES2-Httex1-103Q-GFP	*ltn1Δ* Httex1-103Q-G FP SGA collection
*ltn1*Δ*hsp42*Δ 103Q	SGA	MAT a *ltn1*Δ::natMX4 *hsp42*Δ::kanMX4 *can1*Δ::STE2pr-Sp_his5 *lyp1*Δ *ura3*Δ0 *leu2*Δ0 *met15*Δ0 LYS2 pYES2-Httex1-103Q-GFP	*ltn1Δ* Httex1-103Q-G FP SGA collection
*ltn1*Δ pY2H-Httex1-103Q MoBY-*BTN2*	BY4741	BY4741 *ltn1*Δ::Kan pY2H-Httex1-103Q-GFP MoBY-*BTN2*	This study
*ltn1*Δ pY2H-Httex1-103Q MoBY-*HSP42*	BY4741	BY4741 *ltn1*Δ::Kan pY2H-Httex1-103Q-GFP MoBY-*HSP42*	This study
BTN2-GFP 103Q-mRFP	BY4741	BY4741 *BTN2::GFP-HIS3* pYES2-Httex1-103Q-mRFP	This study

*ltn1*Δ *BTN2*-GFP 103Q-mRFP	BY4741	BY4741 *ltn1Δ::Nat BTN2::GFP-HIS3* pYES2-Httex1-103Q-mRFP	this study
*ltn1*Δ 103Q	SGA	MAT a *ltn1*Δ::natMX4 *his3*Δ::kanMX4 *can1*Δ::STE2pr-Sp_his5 *lyp1*Δ *ura3*Δ0 *leu2*Δ0 *met15*Δ0 LYS2 pYES2-Httex1-103Q-GFP	*ltn1Δ* Httex1-103Q-GFP SGA collection
*ltn1*Δ*kap108*Δ 103Q	SGA	MAT a *ltn1*Δ::natMX4 *kap108*Δ::kanMX4 *can1*Δ::STE2pr-Sp_his5 *lyp1*Δ *ura3*Δ0 *leu2*Δ0 *met15*Δ0 LYS2 pYES2-Httex1-103Q-GFP	*ltn1Δ* Httex1-103Q-GFP SGA collection
*ltn1*Δ*nup60*Δ 103Q	SGA	MAT a *ltn1*Δ::natMX4 *nup60*Δ::kanMX4 *can1*Δ::STE2pr-Sp_his5 *lyp1*Δ *ura3*Δ0 *leu2*Δ0 *met15*Δ0 LYS2 pYES2-Httex1-103Q-GFP	*ltn1Δ* Httex1-103Q-GFP SGA collection
*ltn1*Δ*nup170*Δ 103Q	SGA	MAT a *ltn1*Δ::natMX4 *nup170*Δ::kanMX4 *can1*Δ::STE2pr-Sp_his5 *lyp1*Δ *ura3*Δ0 *leu2*Δ0 *met15*Δ0 LYS2 pYES2-Httex1-103Q-GFP	*ltn1Δ* Httex1-103Q-GFP SGA collection
*ltn1*Δ*nup188*Δ 103Q	SGA	MAT a *ltn1*Δ::natMX4 *nup188*Δ::kanMX4 *can1*Δ::STE2pr-Sp_his5 *lyp1*Δ *ura3*Δ0 *leu2*Δ0 *met15*Δ0 LYS2 pYES2-Httex1-103Q-GFP	*ltn1Δ* Httex1-103Q-GFP SGA collection
*ltn1*Δ*nup59*Δ 103Q	SGA	MAT a *ltn1*Δ::natMX4 *nup59*Δ::kanMX4 *can1*Δ::STE2pr-Sp_his5 *lyp1*Δ *ura3*Δ0 *leu2*Δ0 *met15*Δ0 LYS2 pYES2-Httex1-103Q-GFP	*ltn1Δ* Httex1-103Q-GFP SGA collection
*ltn1*Δ*nup42*Δ 103Q	SGA	MAT a *ltn1*Δ::natMX4 *nup42*Δ::kanMX4 *can1*Δ::STE2pr-Sp_his5 *lyp1*Δ *ura3*Δ0 *leu2*Δ0 *met15*Δ0 LYS2 pYES2-Httex1-103Q-GFP	*ltn1Δ* Httex1-103Q-GFP SGA collection
*ltn1*Δ*gsp2*Δ 103Q	SGA	MAT a *ltn1*Δ::natMX4 *gsp2*Δ::kanMX4 *can1*Δ::STE2pr-Sp_his5 *lyp1*Δ *ura3*Δ0 *leu2*Δ0 *met15*Δ0 LYS2 pYES2-Httex1-103Q-GFP	*ltn1Δ* Httex1-103Q-GFP SGA collection
*ltn1*Δ*los1*Δ 103Q	SGA	MAT a *ltn1*Δ::natMX4 *los1*Δ::kanMX4 *can1*Δ::STE2pr-Sp_his5 *lyp1*Δ *ura3*Δ0 *leu2*Δ0 *met15*Δ0 LYS2 pYES2-Httex1-103Q-GFP	*ltn1Δ* Httex1-103Q-GFP SGA collection
*ltn1*Δ*kap114*Δ 103Q	SGA	MAT a *ltn1*Δ::natMX4 *kap114*Δ::kanMX4 *can1*Δ::STE2pr-Sp_his5 *lyp1*Δ *ura3*Δ0 *leu2*Δ0 *met15*Δ0 LYS2 pYES2-Httex1-103Q-GFP	*ltn1Δ* Httex1-103Q-GFP SGA collection
*ltn1*Δ*kap120*Δ	SGA	MAT a *ltn1*Δ::natMX4 *kap120*Δ::kanMX4	*ltn1Δ*

103Q		*can1*Δ::STE2pr-Sp_his5 *lyp1*Δ *ura3*Δ0 *leu2*Δ0 *met15*Δ0 LYS2 pYES2-Httex1-103Q-GFP	Httex1-103Q-GFP SGA collection
*ltn1*Δ*pom33*Δ 103Q	SGA	MAT a *ltn1*Δ::natMX4 *pom33*Δ::kanMX4 *can1*Δ::STE2pr-Sp_his5 *lyp1*Δ *ura3*Δ0 *leu2*Δ0 *met15*Δ0 LYS2 pYES2-Httex1-103Q-GFP	*ltn1Δ* Httex1-103Q-GFP SGA collection
*ltn1*Δ*pom34*Δ 103Q	SGA	MAT a *ltn1*Δ::natMX4 *pom34*Δ::kanMX4 *can1*Δ::STE2pr-Sp_his5 *lyp1*Δ *ura3*Δ0 *leu2*Δ0 *met15*Δ0 LYS2 pYES2-Httex1-103Q-GFP	*ltn1Δ* Httex1-103Q-GFP SGA collection
*ltn1*Δ*pom152*Δ 103Q	SGA	MAT a *ltn1*Δ::natMX4 *pom152*Δ::kanMX4 *can1*Δ::STE2pr-Sp_his5 *lyp1*Δ *ura3*Δ0 *leu2*Δ0 *met15*Δ0 LYS2 pYES2-Httex1-103Q-GFP	*ltn1Δ* Httex1-103Q-GFP SGA collection
*ltn1*Δ*pdr6*Δ 103Q	SGA	MAT a *ltn1*Δ::natMX4 *pdr6*Δ::kanMX4 *can1*Δ::STE2pr-Sp_his5 *lyp1*Δ *ura3*Δ0 *leu2*Δ0 *met15*Δ0 LYS2 pYES2-Httex1-103Q-GFP	*ltn1Δ* Httex1-103Q-GFP SGA collection
*ltn1*Δ*hsn1*Δ 103Q	SGA	MAT a *ltn1*Δ::natMX4 *hsn1*Δ::kanMX4 *can1*Δ::STE2pr-Sp_his5 *lyp1*Δ *ura3*Δ0 *leu2*Δ0 *met15*Δ0 LYS2 pYES2-Httex1-103Q-GFP	*ltn1Δ* Httex1-103Q-GFP SGA collection
*ltn1*Δ*mlp2*Δ 103Q	SGA	MAT a *ltn1*Δ::natMX4 *mlp2*Δ::kanMX4 *can1*Δ::STE2pr-Sp_his5 *lyp1*Δ *ura3*Δ0 *leu2*Δ0 *met15*Δ0 LYS2 pYES2-Httex1-103Q-GFP	*ltn1Δ* Httex1-103Q-GFP SGA collection
*ltn1*Δ*mlp1*Δ 103Q	SGA	MAT a *ltn1*Δ::natMX4 *mlp1*Δ::kanMX4 *can1*Δ::STE2pr-Sp_his5 *lyp1*Δ *ura3*Δ0 *leu2*Δ0 *met15*Δ0 LYS2 pYES2-Httex1-103Q-GFP	*ltn1Δ* Httex1-103Q-GFP SGA collection
*ltn1*Δ*nup100*Δ 103Q	SGA	MAT a *ltn1*Δ::natMX4 *nup100*Δ::kanMX4 *can1*Δ::STE2pr-Sp_his5 *lyp1*Δ *ura3*Δ0 *leu2*Δ0 *met15*Δ0 LYS2 pYES2-Httex1-103Q-GFP	*ltn1Δ* Httex1-103Q-GFP SGA collection
*ltn1*Δ*nup2*Δ 103Q	SGA	MAT a *ltn1*Δ::natMX4 *nup2*Δ::kanMX4 *can1*Δ::STE2pr-Sp_his5 *lyp1*Δ *ura3*Δ0 *leu2*Δ0 *met15*Δ0 LYS2 pYES2-Httex1-103Q-GFP	*ltn1Δ* Httex1-103Q-GFP SGA collection
WT vector	SGA	MAT a *his3*Δ::kanMX4 *can1*Δ::STE2pr-Sp_his5 *lyp1*Δ *ura3*Δ0 *leu2*Δ0 *met15*Δ0 LYS2 pYES2-GFP	This study
*ltn1*Δ vector	SGA	MAT a *ltn1*Δ::natMX4 *his3*Δ::kanMX4 *can1*Δ::STE2pr-Sp_his5 *lyp1*Δ *ura3*Δ0 *leu2*Δ0 *met15*Δ0	This study

		LYS2 pYES2-GFP	
*ltn1*Δ*nup60*Δ	SGA	MAT a *ltn1*Δ::natMX4 *nup60*Δ::kanMX4	This study
vector		*can1*Δ::STE2pr-Sp_his5 *lyp1*Δ *ura3*Δ0 *leu2*Δ0 *met15*Δ0	
		LYS2 pYES2-GFP	
*ltn1*Δ*nup170*Δ	SGA	MAT a *ltn1*Δ::natMX4 *nup170*Δ::kanMX4	This study
vector		*can1*Δ::STE2pr-Sp_his5 *lyp1*Δ *ura3*Δ0 *leu2*Δ0 *met15*Δ0	
		LYS2 pYES2-GFP	
*ltn1*Δ*nup188*Δ	SGA	MAT a *tn1*Δ::natMX4 *nup188*Δ::kanMX4	This study
vector		*can1*Δ::STE2pr-Sp_his5 *lyp1*Δ *ura3*Δ0 *leu2*Δ0 *met15*Δ0	
		LYS2 pYES2-GFP	
*ltn1*Δ*nup59*Δ	SGA	MAT a *ltn1*Δ::natMX4 *nup59*Δ::kanMX4	This study
vector		*can1*Δ::STE2pr-Sp_his5 *lyp1*Δ *ura3*Δ0 *leu2*Δ0 *met15*Δ0	
		LYS2 pYES2-GFP	
*ltn1*Δ*nup42*Δ	SGA	MAT a *ltn1*Δ::natMX4 *nup42*Δ::kanMX4	This study
vector		*can1*Δ::STE2pr-Sp_his5 *lyp1*Δ *ura3*Δ0 *leu2*Δ0 *met15*Δ0	
		LYS2 pYES2-GFP	
*ltn1*Δ*gsp2*Δ vector	SGA	MAT a *ltn1*Δ::natMX4 *gsp2*Δ::kanMX4	This study
		*can1*Δ::STE2pr-Sp_his5 *lyp1*Δ *ura3*Δ0 *leu2*Δ0 *met15*Δ0	
		LYS2 pYES2-GFP	
*ltn1*Δ*los1*Δ vector	SGA	MAT a *ltn1*Δ::natMX4 *los1*Δ::kanMX4	This study
		*can1*Δ::STE2pr-Sp_his5 *lyp1*Δ *ura3*Δ0 *leu2*Δ0 *met15*Δ0	
		LYS2 pYES2-GFP	
*ltn1*Δ*kap114*Δ	SGA	MAT a *ltn1*Δ::natMX4 *kap114*Δ::kanMX4	This study
vector		*can1*Δ::STE2pr-Sp_his5 *lyp1*Δ *ura3*Δ0 *leu2*Δ0 *met15*Δ0	
		LYS2 pYES2-GFP	
*ltn1*Δ*kap120*Δ	SGA	MAT a *ltn1*Δ::natMX4 *kap120*Δ::kanMX4	This study
vector		*can1*Δ::STE2pr-Sp_his5 *lyp1*Δ *ura3*Δ0 *leu2*Δ0 *met15*Δ0	
		LYS2 pYES2-GFP	
*ltn1*Δ*pom33*Δ	SGA	MAT a *ltn1*Δ::natMX4 *pom33*Δ::kanMX4	This study
vector		*can1*Δ::STE2pr-Sp_his5 *lyp1*Δ *ura3*Δ0 *leu2*Δ0 *met15*Δ0	
		LYS2 pYES2-GFP	
*ltn1*Δ*pom34*Δ	SGA	MAT a *ltn1*Δ::natMX4 *pom34*Δ::kanMX4	This study
vector		*can1*Δ::STE2pr-Sp_his5 *lyp1*Δ *ura3*Δ0 *leu2*Δ0 *met15*Δ0	
		LYS2 pYES2-GFP	
*ltn1*Δ*pom152*Δ	SGA	MAT a *ltn1*Δ::natMX4 *pom152*Δ::kanMX4	This study
vector		*can1*Δ::STE2pr-Sp_his5 *lyp1*Δ *ura3*Δ0 *leu2*Δ0 *met15*Δ0	
		LYS2 pYES2-GFP	
*ltn1*Δ*pdr6*Δ vector	SGA	MAT a *ltn1*Δ::natMX4 *pdr6*Δ::kanMX4	This study
		*can1*Δ::STE2pr-Sp_his5 *lyp1*Δ *ura3*Δ0 *leu2*Δ0 *met15*Δ0	
		LYS2 pYES2-GFP	
*ltn1*Δ*hsn1*Δ vector	SGA	MAT a *ltn1*Δ::natMX4 *hsn1*Δ::kanMX4	This study
		*can1*Δ::STE2pr-Sp_his5 *lyp1*Δ *ura3*Δ0 *leu2*Δ0 *met15*Δ0	
		LYS2 pYES2-GFP	

*ltn1*Δ*mlp2*Δ vector	SGA	MAT a *ltn1*Δ::natMX4 *mlp2*Δ::kanMX4 *can1*Δ::STE2pr-Sp_his5 *lyp1*Δ *ura3*Δ0 *leu2*Δ0 *met15*Δ0 LYS2 pYES2-GFP	This study
*ltn1*Δ*mlp1*Δ vector	SGA	MAT a *ltn1*Δ::natMX4 *mlp1*Δ::kanMX4 *can1*Δ::STE2pr-Sp_his5 *lyp1*Δ *ura3*Δ0 *leu2*Δ0 *met15*Δ0 LYS2 pYES2-GFP	This study
*ltn1*Δ*nup100*Δ vector	SGA	MAT a *ltn1*Δ::natMX4 *nup100*Δ::kanMX4 *can1*Δ::STE2pr-Sp_his5 *lyp1*Δ *ura3*Δ0 *leu2*Δ0 *met15*Δ0 LYS2 pYES2-GFP	This study
*ltn1*Δ*nup2*Δ vector	SGA	MAT a *ltn1*Δ::natMX4 *nup2*Δ::kanMX4 *can1*Δ::STE2pr-Sp_his5 *lyp1*Δ *ura3*Δ0 *leu2*Δ0 *met15*Δ0 LYS2 pYES2-GFP	This study
*ltn1*Δ*kap108*Δ vector	SGA	MAT a *ltn1*Δ::natMX4 *kap108*Δ::kanMX4 *can1*Δ::STE2pr-Sp_his5 *lyp1*Δ *ura3*Δ0 *leu2*Δ0 *met15*Δ0 LYS2 pYES2-GFP	This study

Supplementary Table 4-4. Plasmids used in this study

NAME	SOURCE
pYES2-Httex1-103Q-GFP	Meriin et al., 2002
pY2H-Httex1-103Q-GFP	This study
pYES2-GFP	Preveral et al., 2006
pY2H-GFP	Lab stock
pGAD-*LTN1*	Bengtson et al., 2010
pGAD-*LTN1* W1542A	Bengtson et al., 2010
pGAD-*LTN1* W1542E	Bengtson et al., 2010
p413	Choe et al., 2016
p413*RQC2*- *RQC2* WT	Choe et al., 2016
p413*RQC2*-*rqc2*$_{aaa}$	Choe et al., 2016
p4339	Tong et al., 2001
p5586	MoBY collection (Ho et al., 2009)
MoBY-*HSP42*	MoBY collection (Ho et al., 2009)
MoBY-*BTN2*	MoBY collection (Ho et al., 2009)
MoBY-*NUP60*	MoBY collection (Ho et al., 2009)
MoBY-*NUP170*	MoBY collection (Ho et al., 2009)

Chapter 5

General discussion and future perspectives

Yeast is one of the best characterized eukaryotes with valuable features such as easy maintenance and culturing, rapid growth, as well as its well-characterized genome. Importantly, yeast and human share many aspects in cell biology and much of our fundamental biological knowledge comes from studies in yeast. In the past years, human disease-related proteins without a yeast ortholog have been successfully studied in yeast. These so-called humanized yeast models reproduce major features of the disease-related proteins similar as seen in mammalian model systems and, as such, the insights obtained from the studies in yeast have already contributed greatly to our understanding of the molecular mechanisms underlying the pathogenicity of these disease-related proteins (Braun et al., 2010; Fruhmann et al., 2017; Khurana and Lindquist, 2010; Winderickx et al., 2008).

In this thesis, we used yeast as a model to investigate the PD-related protein Synphilin-1 and the HD-related protein Htt. More specifically, in the first part we focused on how genetic alterations affect Synphilin-1 inclusion formation. In the second part, we investigated the influence of genetic alterations on the distribution and translocation of the polyQ proteins. So far, these processes are poorly understood. However, it is critical to obtain a more detailed insight in the basic molecular mechanisms of these processes to be able to develop effective diagnostic biomarkers as well as therapies for both neurodegenerative diseases. Using different genome-wide yeast screens we were able to identify key players in both processes. Here, we discuss the main findings of these studies and their role in the protein misfolding research, especially in PD and HD research.

5.1. Spatial sequestration of Synphilin-1 inclusion

The PQC system ensures that protein synthesis and folding occurs accurately, therefore aberrant products will be recognized and targeted for degradation. However, overwhelming aberrant products or defects in the PQC system will lead to sequestration of misfolded proteins in specific cellular compartments such as aggresomes, JUNQ/INQ, IPOD and CytoQ (Miller et al., 2015). Spatial sequestration of misfolded proteins is a common strategy of the cell’s defense against various types of stress, for example, overexpression of aberrant proteins

such as high temperature induced misfolded Ubc9^{ts} and unassembled VHL induce cellular compartment formation (Kaganovich et al., 2008; Miller et al., 2015); Heat-shock treatment also induces endogenous misfolded protein aggregation that associates with Hsp104 (Glover and Lindquist, 1998). Furthermore, microtubule-dependent aggresome formation was identified for several misfolded proteins (Kopito, 2000), including Synphilin-1 (Swinnen et al., 2011; Zaarur et al., 2008). Interestingly, it was also shown that Lewy bodies, which include Synphilin-1, share many similar properties with aggresomes. These findings combined with the identification of cytoskeleton components as important players in Synphilin-1 inclusion formation suggests that small Synphilin-1 inclusions present in most of the cells during exponential phase merge into large inclusions in stationary phase by traveling along the microtubules or actin cytoskeleton to a specific cellular compartment such as aggresomes. These inclusions might also share some similarities to the heat-shock induced Hsp104 associated aggregates, which are transported along actin cables to prevent aggregate accumulation in progeny (Liu et al., 2010; Swinnen et al., 2011). The exact mechanism of Synphilin-1 inclusion formation, however, is probably more complex, as Synphilin-1 inclusion formation not only depends on the actin cytoskeleton, but also on microtubules (Büttner et al., 2010; Zaarur et al., 2008; Zhao et al., 2016), while the formation of Hsp104 associated aggregates simply depends on actin cables (Liu et al., 2010). Future investigation needs to focus on the microtubule-dependent/independent mechanisms of Synphilin-1 inclusion formation, using leading edge techniques, such as super-resolution live cell video microscopy. This will enable researchers to obtain information about the dynamic interactions of the actin cytoskeleton and the microtubule network with the Synphilin-1 inclusions. Such studies will provide us more details of the role of the cytoskeleton in the process of Synphilin-1 inclusion formation, and will provide valuable insights in the nature of cellular aggregate/inclusion formation.

Previous studies also showed that Synphilin-1 associates with cell membrane structures such as lipid droplets and lipid rafts in mammalian and yeast cells (Büttner et al., 2010; Takahashi et al., 2006), which implies that lipid raft binding of Synphilin-1 might also be involved in spatial sequestration of Synphilin-1. Indeed, we found that a conserved glycolipid modified

complex, the GPI-anchor, is involved in Synphilin-1 inclusion formation. Defects in GPI-anchor biosynthetic players caused a decrease in the level of Synphilin-1 inclusions, thereby suggesting that the GPI-anchor integrity is essential for Synphilin-1 inclusion formation. Interestingly, an earlier study also reported that expression of a prion protein in mice lacking GPI anchors affected the amyloid structure formation of the prion protein (Chesebro et al., 2005). Together, these findings suggest that GPI anchors might be crucial for the aggregate/inclusion formation of different disease proteins. Further in-depth investigation of the interplay between Synphilin-1, GPI-anchor and cell membrane structures will provide novel clues about the pathological role of Synphilin-1.

Since Synphilin-1 inclusion formation was studied in a haploid background, which does not involve sister chromatid segregation, we were surprised to find out that components of the Ctf18 RFC-like complex affect Synphilin-1 inclusion formation. This implies that the Ctf18 RFC-like complex has multiple functions rather than playing simply a role in sister chromatid cohesion. In this respect it has also been reported that Ctf18-RFC has additional important functions in preserving genome stability (Gellon et al., 2011). Furthermore, the Ctf18 protein co-localizes with the replication fork during DNA replication where it plays an important role in sister chromatid cohesion (Lengronne et al., 2006). In line with this, we found that the DNA replication initiation/Primase complex also influences Synphilin-1 inclusion formation. However, much of the details still need to be further investigated.

Although inclusion formation is a hallmark of many neurodegenerative disorders, it is still controversial whether the inclusions are toxic or cytoprotective to the cells. Synphilin-1 inclusions was considered to be the toxic species in some studies, due to the observation that Synphilin-1 inclusions associated with the cerebellum (Nuber et al., 2010) and dopaminergic neurons (Krenz et al., 2009). Whereas increasing evidences supports the hypothesis that large inclusions are more likely to sequester malfunctioning misfolded proteins (Arrasate et al., 2004; Balchin et al., 2016; Choe et al., 2016; Yang et al., 2016). In our study, we observed a growth defect in mutants that fail to form large Synphilin-1 inclusions, supporting the hypothesis that Synphilin-1 inclusion formation has a cytoprotective effect to cells.

Overall, our study underlines the relevance of using yeast models to study protein misfolding diseases, and further investigation of disease proteins such as Synphilin-1 can provide novel insights for our understanding of the mechanisms of PD pathogenesis, as well as other protein folding disorders.

Although the use of this yeast model in a genome-wide screen was successful in identifying genes involved in Synphilin-1 inclusion formation, the exact role of these players in Synphilin-1 inclusion formation is still unclear. Thus, future studies need to

- confirm the findings in mammalian models, especially orthologs of candidates identified in this study that are involved in Synphilin-1 inclusion formation.
- investigate the exact role of actin cables and microtubule in managing Synphilin-1 inclusion formation, for example, using super-resolution live cell video microscopy, to analyze the dynamic interactions of the actin cytoskeleton and the microtubule network with Synphilin-1.
- investigate the biological processes that are required for the Synphilin-1 inclusion formation in detail (for example, test the role of lipid rafts in spatial distribution of Synphilin-1, and test if the involvement of lipid rafts is common in misfolded aggregate/inclusion formation).

5.2. The connection between the RQC machinery and the nucleocytoplasmic distribution of polyQ proteins

The non-pathological native Htt protein plays an important role in the early embryonic development (Cattaneo et al., 2005; Walker, 2007). This native Htt is mainly distributed in the cytoplasm (De Rooij et al., 1996; DiFiglia et al., 1995). In contrast, mutant Htt forms insoluble aggregates and distributes in the cytoplasm and the nucleus and thereby confers cytotoxicity in mice (Mangiarini et al., 1996) or yeast (Krobitsch and Lindquist, 2000). These findings suggest that mutations with polyQ-expanded Htt are the main cause of HD. Earlier studies have shown that the nuclear accumulation of mutant Htt is at least in part responsible for the HD pathogenesis (Davies et al., 1997; De Rooij et al., 1996; DiFiglia et al., 1997).

Recent studies identified the RQC as the machinery that ensures accurate translation at the ribosome, and recognizes aberrant translational products that are later targeted for degradation (Bengtson and Joazeiro, 2010; Brandman et al., 2012; Defenouillère et al., 2013). In our study, we found that deficiency of RQC components (e.g. Ltn1 or Rqc1) alters the subcellular distribution of the polyQ protein Httex1-103Q. However, it is not entirely clear how this machinery affects the subcellular distribution of Httex1-103Q.

At first sight it is expected that nuclear accumulation of Httex1-103Q in *ltn1*Δ cells might be the result of substrates that fail to become ubiquitinated by the E3 emzyme Ltn1, and consequently accumulate in the nucleus. Accordingly, deficiency of the Ltn1 RING domain causes nuclear accumulation of Httex1-103Q, as efficient as the deletion of *LTN1*. Thus, the ubiquitination-associated Ltn1 RING domain is responsible for changes in the subcellular distribution of Httex1-103Q. However, further investigation revealed that nuclear accumulation of Httex1-103Q is not simply due to deficient nuclear degradation of Httex1-103Q in *ltn1*Δ cells, since nuclear accumulation of Httex1-103Q was not observed when perturbing the UPS degradation alone.

Given that the RQC is machinery controls the nascent polypetides, it is unlikely that the RQC directly mediates nucleocytoplasmic translocation of Httex1-103Q. Defect of the RQC machinery, either by gene deletion, or by overwhelming stress from misfolded protein expression, has deteriorated consequence, which trigger NS-aggregate formation (Choe et al., 2016; Defenouillère et al., 2016; Yonashiro et al., 2016), and sequesters the chaperones Btn2 and Sis1 (Choe et al., 2016). We found that Btn2 regulates the nucleocytoplasmic transport of Httex1-103Q (Zheng et al., 2017), and that an imbalance of the transport factors (e.g. Btn2) caused by NS-aggregate formation further influence the nucleocytoplasmic distribution of Httex1-103Q. We hypothesize that the RQC system interferes with the subcellular distribution of polyQ proteins, possibly by affecting the endogenous NS-inclusions formation and the chaperone pool, in which Btn2 plays a critical role. However, other chaperones that have not yet been identified could play a role in this process as well. Future investigations to identify more transport factors or chaperones that participate in the nucleocytoplasmic transport of

Httex1-103Q will increase our understanding of Httex1-103Q nucleocytoplasmic translocation machinery.

It is still not clear whether overexpression of Httex1-103Q affects the capacity of the RQC machinery or not. Sequestration of Sup35, a translation termination factor, by Httex1-103Q (Fig. 2-10) (Serpionov et al., 2016), probably results in lower levels of available Sup35 that might increase the chance for ribosomal stalling, which in turn further elevates translational read-though of stop codons (Gong et al., 2012) and increases pressure on the RQC system. This may be one of the reasons that overexpression of Httex1-103Q introduces strong toxicity in wild type yeast (Meriin et al., 2002).

Another interesting question is what the exact role of Rqc2 and CAT-tails is in protein quality control. Addition of CAT-tails to substrates by Rqc2 triggers NS-aggregate formation (Choe et al., 2016; Yonashiro et al., 2016). Furthermore, a recent study reported that CAT-tails serve as a signal that provides a fail-safe mechanism that enables the degradation of RQC substrates, which were not recognized by Ltn1 (Kostova et al., 2017). This suggests that the short Ala- and Thr-rich CAT-tails are cellular signals that are involved in the protein quality control at the ribosome. Although we were able to show the CAT-tail tagging activity of Rqc2 is required for the nuclear distribution of Httex1-103Q, it is not clear whether aberrant Httex1-103Q is actually modified by CAT-tails or not (Zheng et al., 2017). Therefore it will be interesting to find out whether CAT-tails can serve as a NLS under certain circumstances. Future studies might provide answers to this question by mass spectrum analysis of Httex1-103Q and NS-proteins.

Next, the involvement of the Htt exon-1 PRR in the subcellular distribution of the polyQ protein needs to be further addressed. This PRR is critical for large inclusion formation and detoxification of polyQ proteins (Dehay and Bertolotti, 2006; Duennwald et al., 2006a). In parallel with our HCM screening in which we used the Httex1-103Q without the PRR, a similar HCM screening was performed using the polyQ protein reporter containing the PRR (Httex1-103QP) to identify factors that are required for inclusion formation of Httex1-103QP. This study revealed that RQC regulates compartmentalization of Httex1-103QP (Yang et al.,

2016). However, in our study using the reporter Httex1-103Q without the PRR, we found that RQC regulates the subcellular distribution of polyQ protein (Zheng et al., 2017), instead of compartmentalization. Thus, the PRR not only determines the inclusion formation of polyQ-expanded Htt exon-1, but also has an impact on the distribution of polyQ-expanded Htt exon-1. The distinct role of the RQC in the presence/absence of PRR, suggests that the RQC is closely connected to polyQ domain of Httex1 regardless of the presence of the PRR. Future studies that investigate the exact role of PRR and Ltn1 in protein aggregation, will provide valuable clues to elucidate the connections between RQC and PRR.

Finally, we demonstrated that deficiency of certain NPC components and transport factors suppresses the toxicity caused by Httex1-103Q in the *ltn1*Δ background, and blocks the nuclear accumulation of Httex1-103Q. In line with this it has been reported that nuclear accumulation of polyQ proteins promotes its cytotoxicity in neuronal cells (Saudou et al., 1998). In addition, several studies show that nucleocytoplasmic translocation is connected with disease pathogenesis in many aspects. In this respect, aberrant NPC was found to associate with neurofibrillary tangles in neurons from AD patients, which may contributes to the pathogenesis of AD (Sheffield et al., 2006). Furthermore, cytoplasmic aggregate formation of β-sheet proteins or the disease proteins Htt-96Q and TDP-43 fragments cause the sequestration and mislocalization of nuclear transport factors into the cytoplasm, which results in defects in nuclear protein import and mRNA export (Woerner et al., 2016). Furthermore, expression of hexanucleotide repeat expanded C9orf72 either in flies (Freibaum et al., 2015; Zhang et al., 2015) or yeast (Jovičić et al., 2015), identified NPC components and different nuclear transport factors as potential modifiers of disease phenotypes and toxicity.

5.3. Concluding remarks

Protein misfolding is a common feature of different neurodegenerative diseases. Several studies have shown that the state of protein aggregation, their formation and the subcellular localization of the aggregates are associated with cytotoxicity. Since the molecular basis of protein homeostasis and the toxic properties of proteins are conserved from simple organisms

such as yeast to human, studies in yeast models can provide valuable clues to understand the aggregation-management of disease proteins. In this thesis, we developed different high-content imaging-based screening methods based on yeast models and showed that aggregation of misfolded proteins is a complex system that involves multiple biological processes. Furthermore, we demonstrated that the subcellular distribution of the protein aggregates plays a crucial role in modulating the cytotoxicity.

First, the PD-related protein Synphilin-1 forms large inclusions upon expression in yeast. We investigated factors that are required for this Synphilin-1 inclusion formation and we established a high-content image-based screening approach that allowed us to analyze aggregate formation in a systematic manner. We observed that certain genetic alterations lead to failure of Synphilin-1 inclusion formation. These genetic alterations involve biological processes including cytoskeleton organization, histone modification, sister chromatid segregation, glycolipid biosynthetic process, DNA repair and replication. Although it is still elusive how these processes regulate the inclusion formation of Synphilin-1, further investigations will have to reveal how these processes may cooperate and, subsequently, confirmation of these findings in other PD models will be required. Importantly, we observed increased toxicity in the strains that failed to form larger Synphilin-1 inclusion, indicating that merging of smaller inclusions into larger deposits is indeed a cytoprotective cellular strategy. Our results provide an unbiased global view on the complexity of the machinery underlying the formation of these larger deposits and support the hypothesis that these deposits reflect inert entities sequestering the true toxic culprits.

Secondly, we explored the subcellular localization, translocation and toxicity of Htt polyQ proteins and found that that the nucleocytoplasmic distribution of Htt polyQ might be important for the polyQ-induced pathology in HD. By examining the subcellular localization of Httex1-103Q systematically with the HCM system, we identified factors that alter the subcellular distribution of Httex1-103Q, and validated that deficiency of RQC components significantly affects the distribution of Httex1-103Q. These observations led us to investigate the role of the RQC in managing the nucleocytoplasmic translocation of Httex1-103Q. Failure

of the RQC system causes NS-aggregate formation, which sequesters chaperones, including Btn2, a protein sorting factor that is essential for the nucleocytoplasmic transport of Httex1-103Q. In a later screen, which we developed to identify modifiers of Httex1-103Q toxicity involving the nucleocytoplasmic transport, we found that nucleocytoplasmic transport of Httex1-103Q is depended on the NPC, and confirmed that nuclear accumulation of Httex1 polyQ proteins in yeast enhanced Htt-cytotoxicity. Together, our findings led to the hypothesis that the RQC machinery regulates the nucleocytoplasmic distribution of Httex1 polyQ proteins by affecting the chaperone pool, which is critical in assisting nucleocytoplasmic transport of proteins. Thus, enhancing the RQC capability or preventing nuclear import of polyQ proteins should be considered as possible strategy for the treatment of polyQ disorders.

Earlier studies have shown that during ageing, cells gradually lose the ability to filter out damaged proteins and dysfunctional mitochondria (Higuchi et al., 2013; Liu et al., 2010; Nyström and Liu, 2014), which occurs together with an increased imbalance in the regulation of vacuolar acidity (Hill et al., 2016; Hughes and Gottschling, 2012; Wilms et al., 2017). As PD and HD are age-dependent neurodegenerative disorders, our findings on the spatial distribution and merging of Synphilin-1 inclusions as well as the role of the RQC machinery in protecting cells from misfolded polyQ proteins, suggests that these strategies play a role in anti-ageing and age-related diseases. Indeed, the reduced capability to handle misfolded and damaged proteins by sequestration and subsequent clearance via either the proteasome or via vacuolar degradation appears to be a common hallmark in different neurodegenerative disorders. Hence, future studies are necessary to investigate this capability in more detail during ageing and progress of age-related diseases. For instance, to investigate the inclusion formation of Synphilin-1 at different age-stages, this may be achieved by isolating young and old cells, quantifying the level of Synphilin-1 inclusion formation and correlating this to the number of offspring and survival. Mutants showing a lower ability to sequester misfolded Synphilin-1 in larger deposits potentially play a role in managing the ageing process. The monitoring of life-span of these mutants in yeast and other model systems might be useful to help us gain a better understanding of PD progression and ageing. To investigate the connection between RQC capability and ageing, studies may include the monitoring of

protein levels of RQC components (e.g. Ltn1 and Rqc2) in young cells and aged cells, or measuring the life-span, mitochondrial integrity and vacuolar acidity in cells with/without overexpression of RQC components. Based on findings of this thesis, it would be interesting to systematically evaluate the viability and aggregate morphology of different disease proteins (e.g. Synphilin-1, Htt, α-synuclein and Aβ42) in yeast in combination with additional RQC components (e.g. Ltn1 and Rqc2). These studies will provide valuable insights in whether enhanced RQC capability will alter the fitness and aggregate formation of certain disease protein or not. Eventually, these studies will provide clues about which molecular processes and pathways that are involved in altering phenotypes of these disease proteins in the presence of enhanced RQC capability.

Appendix

Medium protocol for the construction of the Synphilin-1 SGA collection

All components of the mediums used for the construction of the Synphilin-1 SGA collection are listed below, and all mediums described below are normalized to the final volume of 1L, the key steps and the corresponding medium protocol for the Synphilin-1 SGA collection construction are described in Fig. 2-2.

(1) Mating: YEPD + ADE

Reagent	Amount to add (per 1 L final volume)
Adenine	120mg
Yeast extract	10g
Peptone	20g
Agar	20g

a. Dissolve the compounds in the table (except agar) in 200mL DDH_2O and filter sterilze the sollution (0.2μm pore size, 500mL, Thermo Scientific).

b. Add 20g agar to 750mL DDH_2O in a 1-L flask and autoclave.

c. While stirring the autoclaved mixture and 200mL filter sterilzed sollution on a magnetic stir plate, add 50 mL of sterile 40% (w/v) glucose per liter of medium.

d. Cool down the medium to approximately 65°C, mix thoroughly and then pour the plates.

(2) Diploid: SD-Ura + G418

Reagent	Amount to add (per 1 L final volume)
Y.N.B. w/o amino acids and ammonium sulfate	1.7g
Monosodium gluatmic acid	1g
Dropout mix SD-Ura	0.77g
Agar	20g

a. Dissolve the compounds in the table (except agar) in 200mL DDH_2O and filter sterilze the sollution (0.2μm pore size, 500mL, Thermo Scientific).

b. Add 20g agar to 750mL DDH_2O in a 1-L flask and autoclave.

c. While stirring the autoclaved mixture and 200mL filter sterilzed sollution on a magnetic stir plate, add 50 mL of sterile 40% (w/v) glucose per liter of medium.

d. Cool down the medium to approximately 65°C, add 1ml 200mg/ml G418 (final concentration 200mg/L), mix thoroughly and then pour the plates.

(3) Sporulation: Spore medium –Ura

Reagent	Amount to add (per 1 L final volume)
Potassium acetate	10g
Yeast extract	1g
Glucose	0.5g
Amino-acids supplement powder mixture for sporulation (mix of 2g His, 2g Lys, 10g Leu)	0.1g
Agar	20g

a. Dissolve all compounds in the table in 1000mL DDH_2O in a 1-L flask and autoclave.

b. While stirring the autoclaved mixture on a magnetic stir plate. Cool down the medium to approximately 65°C, mix thoroughly and then pour the plates.

(4) Haploid: SD-His/Arg/Lys/Ura + canavanine & S-AEC

Reagent	Amount to add (per 1 L final volume)
Y.N.B. w/o amino acids and ammonium sulfate	1.7g
Monosodium gluatmic acid	1g
Drop-out mix (D.O. – His Arg Lys Ura)	2g
Agar	20g

a. Dissolve the compounds in the table (except agar) in 200mL DDH_2O and filter sterilze the sollution (0.2μm pore size, 500mL, Thermo Scientific).

b. Add 20g agar to 750mL DDH_2O in a 1-L flask and autoclave.

c. While stirring the autoclaved mixture and 200mL filter sterilzed sollution on a magnetic stir plate, add 50 mL of sterile 40% (w/v) glucose per liter of medium.

d. Cool down the medium to approximately 65°C, add 0.5 mL 100 mg/mL canavanine (final concentration 50mg/L) and 0.5 mL 100 mg/mL S-AEC (final concentration 50mg/L), mix thoroughly and then pour the plates.

(5) KanR Selection: SD-His/Arg/Lys/Ura + canavanine, S-AEC & G418

Reagent	Amount to add (per 1 L final volume)
Y.N.B. w/o amino acids and ammonium sulfate	1.7g
Monosodium gluatmic acid	1g
Drop-out mix (D.O. – His Arg Lys Ura)	2g
Agar	20g

a. Dissolve the compounds in the table (except agar) in 200mL DDH_2O and filter sterilze the sollution (0.2μm pore size, 500mL, Thermo Scientific).

b. Add 20g agar to 750mL DDH_2O in a 1-L flask and autoclave.

c. While stirring the autoclaved mixture and 200mL filter sterilzed sollution on a magnetic stir plate, add 50 mL of sterile 40% (w/v) glucose per liter of medium.

d. Cool down the medium to approximately 65°C, add 0.5 mL 100 mg/mL canavanine (final concentration 50mg/L), 0.5 mL 100 mg/mL S-AEC (final concentration 50mg/L) and 1ml 200mg/ml G418 (final concentration 200mg/L), mix thoroughly and then pour the plates.

Medium protocol for the construction of the Httex1-103Q SGA collection

The medium protocol is identical as the protocol described in the construction of the Synphilin-1 SGA collection as described above.

Medium protocol for the construction of the *ltn1*Δ Httex1-103Q SGA collection

All components of the mediums used for the construction of the *ltn1*Δ Httex1-103Q SGA collection are listed below, and all mediums described below are normalized to the final volume of 1L, the key steps and the corresponding medium protocol for the *ltn1*Δ Httex1-103Q SGA collection construction are described in Fig. 2-5.

(1) Mating: YEPD + ADE

Reagent	Amount to add (per 1 L final volume)
Adenine	120mg
Yeast extract	10g
Peptone	20g
Agar	20g

a. Dissolve the compounds in the table (except agar) in 200mL DDH_2O and filter sterilze the sollution (0.2μm pore size, 500mL, Thermo Scientific).

b. Add 20g agar to 750mL DDH_2O in a 1-L flask and autoclave.

c. While stirring the autoclaved mixture and 200mL filter sterilzed sollution on a magnetic stir

plate, add 50 mL of sterile 40% (w/v) glucose per liter of medium.

d. Cool down the medium to approximately 65°C, mix thoroughly and then pour the plates.

(2) Diploid: SD-Ura + G418

Reagent	Amount to add (per 1 L final volume)
Y.N.B. w/o amino acids and ammonium sulfate	1.7g
Monosodium gluatmic acid	1g
Dropout mix SD-Ura	0.77g
Agar	20g

a. Dissolve the compounds in the table (except agar) in 200mL DDH_2O and filter sterilze the sollution (0.2μm pore size, 500mL, Thermo Scientific).

b. Add 20g agar to 750mL DDH_2O in a 1-L flask and autoclave.

c. While stirring the autoclaved mixture and 200mL filter sterilzed sollution on a magnetic stir plate, add 50 mL of sterile 40% (w/v) glucose per liter of medium.

d. Cool down the medium to approximately 65°C, add 1ml 200mg/ml G418 (final concentration 200mg/L) and 1ml 100mg/ml clonNAT (final concentration 100mg/L), mix thoroughly and then pour the plates.

(3) Sporulation: Spore medium –Ura

Reagent	Amount to add (per 1 L final volume)
Potassium acetate	10g
Yeast extract	1g
Glucose	0.5g
Amino-acids supplement powder mixture for sporulation (mix of 2g His, 2g Lys, 10g Leu)	0.1g
Agar	20g

a. Dissolve all compounds in the table in 1000mL DDH_2O in a 1-L flask and autoclave.

b. While stirring the autoclaved mixture on a magnetic stir plate. Cool down the medium to approximately 65°C, mix thoroughly and then pour the plates.

(4) Haploid: SD-His/Arg/Lys/Ura + canavanine & S-AEC

Reagent	Amount to add (per 1 L final volume)
Y.N.B. w/o amino acids and ammonium sulfate	1.7g
Monosodium gluatmic acid	1g
Drop-out mix (D.O. – His Arg Lys Ura)	2g
Agar	20g

a. Dissolve the compounds in the table (except agar) in 200mL DDH_2O and filter sterilze the sollution (0.2μm pore size, 500mL, Thermo Scientific).

b. Add 20g agar to 750mL DDH_2O in a 1-L flask and autoclave.

c. While stirring the autoclaved mixture and 200mL filter sterilzed sollution on a magnetic stir plate, add 50 mL of sterile 40% (w/v) glucose per liter of medium.

d. Cool down the medium to approximately 65°C, add 0.5 mL 100 mg/mL canavanine (final concentration 50mg/L) and 0.5 mL 100 mg/mL S-AEC (final concentration 50mg/L), mix thoroughly and then pour the plates.

(5) KanR Selection: SD-His/Arg/Lys/Ura + canavanine, S-AEC & G418

Reagent	Amount to add (per 1 L final volume)
Y.N.B. w/o amino acids and ammonium sulfate	1.7g
Monosodium gluatmic acid	1g
Drop-out mix (D.O. – His Arg Lys Ura)	2g
Agar	20g

a. Dissolve the compounds in the table (except agar) in 200mL DDH_2O and filter sterilze the sollution (0.2μm pore size, 500mL, Thermo Scientific).

b. Add 20g agar to 750mL DDH_2O in a 1-L flask and autoclave.

c. While stirring the autoclaved mixture and 200mL filter sterilzed sollution on a magnetic stir plate, add 50 mL of sterile 40% (w/v) glucose per liter of medium.

d. Cool down the medium to approximately 65°C, add 0.5 mL 100 mg/mL canavanine (final concentration 50mg/L), 0.5 mL 100 mg/mL S-AEC (final concentration 50mg/L) and 1ml 200mg/ml G418 (final concentration 200mg/L), mix thoroughly and then pour the plates.

(6) NatR Selection: SD-His/Arg/Lys/Ura + canavanine, S-AEC, G418 & clonNAT

Reagent	Amount to add (per 1 L final volume)
Y.N.B. w/o amino acids and ammonium sulfate	1.7g
Monosodium gluatmic acid	1g
Drop-out mix (D.O. – His Arg Lys Ura)	2g
Agar	20g

a. Dissolve the compounds in the table (except agar) in 200mL DDH_2O and filter sterilze the sollution (0.2μm pore size, 500mL, Thermo Scientific).

b. Add 20g agar to 750mL DDH_2O in a 1-L flask and autoclave.

c. While stirring the autoclaved mixture and 200mL filter sterilzed sollution on a magnetic stir plate, add 50 mL of sterile 40% (w/v) glucose per liter of medium.

d. Cool down the medium to approximately 65°C, add 0.5 mL 100 mg/mL canavanine (final concentration 50mg/L), 0.5 mL 100 mg/mL S-AEC (final concentration 50mg/L), 1ml 200mg/ml G418 (final concentration 200mg/L) and 1ml 100mg/ml clonNAT (final concentration 100mg/L), mix thoroughly and then pour the plates.

Medium protocol for the construction of the Httex1-103Q-mRFP Yeast GFP Clone Collection

All components of the mediums used for the construction of the Httex1-103Q-mRFP Yeast GFP Clone Collection are listed below, and all mediums described below are normalized to the final volume of 1L, the key steps and the corresponding medium protocol for the Httex1-103Q-mRFP Yeast GFP Clone Collection construction are described in Fig. 2-6.

(1) Mating: YEPD + ADE

Reagent	Amount to add (per 1 L final volume)
Adenine	120mg
Yeast extract	10g
Peptone	20g
Agar	20g

a. Dissolve the compounds in the table (except agar) in 200mL DDH_2O and filter sterilze the sollution (0.2μm pore size, 500mL, Thermo Scientific).

b. Add 20g agar to 750mL DDH_2O in a 1-L flask and autoclave.

c. While stirring the autoclaved mixture and 200mL filter sterilzed sollution on a magnetic stir plate, add 50 mL of sterile 40% (w/v) glucose per liter of medium.

d. Cool down the medium to approximately 65°C, mix thoroughly and then pour the plates.

(2) Diploid: SD-Ura-His

Reagent	Amount to add (per 1 L final volume)
Y.N.B. w/o amino acids and ammonium sulfate	1.7g
Monosodium gluatmic acid	1g
Dropout mix SD-Ura-His	0.77g
Agar	20g

a. Dissolve the compounds in the table (except agar) in 200mL DDH_2O and filter sterilze the sollution (0.2μm pore size, 500mL, Thermo Scientific).

b. Add 20g agar to 750mL DDH_2O in a 1-L flask and autoclave.

c. While stirring the autoclaved mixture and 200mL filter sterilzed sollution on a magnetic stir plate, add 50 mL of sterile 40% (w/v) glucose per liter of medium.

d. Cool down the medium to approximately 65°C, mix thoroughly and then pour the plates.

(3) Sporulation: Spore medium –Ura

Reagent	Amount to add (per 1 L final volume)
Potassium acetate	10g
Yeast extract	1g
Glucose	0.5g
Amino-acids supplement powder mixture for sporulation (mix of 2g His, 2g Lys, 10g Leu)	0.1g
Agar	20g

a. Dissolve all compounds in the table in 1000mL DDH_2O in a 1-L flask and autoclave.

b. While stirring the autoclaved mixture on a magnetic stir plate. Cool down the medium to

approximately 65°C, mix thoroughly and then pour the plates.

(4) Haploid: SD-Leu/Arg/Lys/Ura + canavanine & S-AEC

Reagent	Amount to add (per 1 L final volume)
Y.N.B. w/o amino acids and ammonium sulfate	1.7g
Monosodium gluatmic acid	1g
Drop-out mix (D.O. –Leu Arg Lys Ura)	2g
Agar	20g

a. Dissolve the compounds in the table (except agar) in 200mL DDH_2O and filter sterilze the sollution (0.2μm pore size, 500mL, Thermo Scientific).

b. Add 20g agar to 750mL DDH_2O in a 1-L flask and autoclave.

c. While stirring the autoclaved mixture and 200mL filter sterilzed sollution on a magnetic stir plate, add 50 mL of sterile 40% (w/v) glucose per liter of medium.

d. Cool down the medium to approximately 65°C, add 0.5 mL 100 mg/mL canavanine (final concentration 50mg/L) and 0.5 mL 100 mg/mL S-AEC (final concentration 50mg/L), mix thoroughly and then pour the plates.

(5) SD-His Selection: SD-Leu/His/Arg/Lys/Ura + canavanine, S-AEC

Reagent	Amount to add (per 1 L final volume)
Y.N.B. w/o amino acids and ammonium sulfate	1.7g
Monosodium gluatmic acid	1g
Drop-out mix (D.O. – Leu His Arg Lys Ura)	2g
Agar	20g

a. Dissolve the compounds in the table (except agar) in 200mL DDH_2O and filter sterilze the

sollution (0.2μm pore size, 500mL, Thermo Scientific).

b. Add 20g agar to 750mL DDH_2O in a 1-L flask and autoclave.

c. While stirring the autoclaved mixture and 200mL filter sterilzed sollution on a magnetic stir plate, add 50 mL of sterile 40% (w/v) glucose per liter of medium.

d. Cool down the medium to approximately 65°C, add 0.5 mL 100 mg/mL canavanine (final concentration 50mg/L) and 0.5 mL 100 mg/mL S-AEC (final concentration 50mg/L), mix thoroughly and then pour the plates.

References

Aguilaniu, H., Gustafsson, L., Rigoulet, M., and Nyström, T. (2003). Asymmetric inheritance of oxidatively damaged proteins during cytokinesis. Science *299*, 1751-1753.

Anfinsen, C.B. (1973). Principles that govern the folding of protein chains. Science *181*, 223-230.

Arrasate, M., Mitra, S., Schweitzer, E.S., Segal, M.R., and Finkbeiner, S. (2004). Inclusion body formation reduces levels of mutant huntingtin and the risk of neuronal death. nature *431*, 805-810.

Baba, M., Nakajo, S., Tu, P.H., Tomita, T., Nakaya, K., Lee, V.M., Trojanowski, J.Q., and Iwatsubo, T. (1998). Aggregation of alpha-synuclein in Lewy bodies of sporadic Parkinson's disease and dementia with Lewy bodies. The American journal of pathology *152*, 879-884.

Bailleul, P.A., Newnam, G.P., Steenbergen, J.N., and Chernoff, Y.O. (1999). Genetic study of interactions between the cytoskeletal assembly protein sla1 and prion-forming domain of the release factor Sup35 (eRF3) in Saccharomyces cerevisiae. Genetics *153*, 81-94.

Balakrishnan, R., Park, J., Karra, K., Hitz, B.C., Binkley, G., Hong, E.L., Sullivan, J., Micklem, G., and Cherry, J.M. (2012). YeastMine--an integrated data warehouse for Saccharomyces cerevisiae data as a multipurpose tool-kit. Database : the journal of biological databases and curation *2012*, bar062.

Balchin, D., Hayer-Hartl, M., and Hartl, F.U. (2016). In vivo aspects of protein folding and quality control. Science *353*, aac4354.

Bao, Y.P., Cook, L.J., O'Donovan, D., Uyama, E., and Rubinsztein, D.C. (2002). Mammalian, yeast, bacterial, and chemical chaperones reduce aggregate formation and death in a cell model of oculopharyngeal muscular dystrophy. Journal of Biological Chemistry *277*, 12263-12269.

Bartlett, A.I., and Radford, S.E. (2009). An expanding arsenal of experimental methods yields an explosion of insights into protein folding mechanisms. Nature structural & molecular biology *16*, 582-588.

Baryshnikova, A., Costanzo, M., Dixon, S., Vizeacoumar, F.J., Myers, C.L., Andrews, B., and Boone, C. (2010). Synthetic genetic array (SGA) analysis in Saccharomyces cerevisiae and Schizosaccharomyces pombe. Methods in enzymology *470*, 145-179.

Baumeister, W., Walz, J., Zühl, F., and Seemüller, E. (1998). The proteasome: paradigm of a self-compartmentalizing protease. Cell *92*, 367-380.

Becker, T., Franckenberg, S., Wickles, S., Shoemaker, C.J., Anger, A.M., Armache, J.-P., Sieber, H., Ungewickell, C., Berninghausen, O., and Daberkow, I. (2012). Structural basis of highly conserved ribosome recycling in eukaryotes and archaea. nature *482*, 501-506.

Bengtson, M.H., and Joazeiro, C.A. (2010). Role of a ribosome-associated E3 ubiquitin ligase in protein quality control. nature *467*, 470-473.

Bostantjopoulou, S., Katsarou, Z., Karakasis, C., Peitsidou, E., Milioni, D., and Rossopoulos, N. (2013). Evaluation of non-motor symptoms in Parkinson’s Disease: An underestimated necessity. Hippokratia *17*, 214-219.

Boyle, E.I., Weng, S., Gollub, J., Jin, H., Botstein, D., Cherry, J.M., and Sherlock, G. (2004). GO::TermFinder--open source software for accessing Gene Ontology information and finding significantly enriched Gene Ontology terms associated with a list of genes. Bioinformatics *20*, 3710-3715.

Brandman, O., and Hegde, R.S. (2016). Ribosome-associated protein quality control. In Nature structural & molecular biology, pp. 7-15.

Brandman, O., Stewart-Ornstein, J., Wong, D., Larson, A., Williams, C.C., Li, G.-W., Zhou, S., King, D., Shen, P.S., and Weibezahn, J. (2012). A ribosome-bound quality control complex triggers degradation of

nascent peptides and signals translation stress. Cell *151*, 1042-1054.
Braun, R.J., Büttner, S., Ring, J., Kroemer, G., and Madeo, F. (2010). Nervous yeast: modeling neurotoxic cell death. Trends in biochemical sciences *35*, 135-144.
Breitkreutz, B.J., Stark, C., Reguly, T., Boucher, L., Breitkreutz, A., Livstone, M., Oughtred, R., Lackner, D.H., Bahler, J., Wood, V., *et al.* (2008). The BioGRID Interaction Database: 2008 update. Nucleic Acids Res *36*, D637-640.
Breitkreutz, B.J., Stark, C., and Tyers, M. (2003). Osprey: a network visualization system. Genome biology *4*, R22.
Brockwell, D.J., and Radford, S.E. (2007). Intermediates: ubiquitous species on folding energy landscapes? Current opinion in structural biology *17*, 30-37.
Büttner, S., Delay, C., Franssens, V., Bammens, T., Ruli, D., Zaunschirm, S., de Oliveira, R.M., Outeiro, T.F., Madeo, F., and Buée, L. (2010). Synphilin-1 enhances α-synuclein aggregation in yeast and contributes to cellular stress and cell death in a Sir2-dependent manner. PloS one *5*, e13700.
Carmichael, J., Chatellier, J., Woolfson, A., Milstein, C., Fersht, A.R., and Rubinsztein, D.C. (2000). Bacterial and yeast chaperones reduce both aggregate formation and cell death in mammalian cell models of Huntington's disease. Proceedings of the National Academy of Sciences *97*, 9701-9705.
Cattaneo, E., Rigamonti, D., Goffredo, D., Zuccato, C., Squitieri, F., and Sipione, S. (2001). Loss of normal huntingtin function: new developments in Huntington's disease research. Trends in neurosciences *24*, 182-188.
Cattaneo, E., Zuccato, C., and Tartari, M. (2005). Normal huntingtin function: an alternative approach to Huntington's disease. Nature Reviews Neuroscience *6*, 919-930.
Chartier-Harlin, M.-C., Dachsel, J.C., Vilariño-Güell, C., Lincoln, S.J., Leprêtre, F., Hulihan, M.M., Kachergus, J., Milnerwood, A.J., Tapia, L., and Song, M.-S. (2011). Translation initiator EIF4G1 mutations in familial Parkinson disease. The American Journal of Human Genetics *89*, 398-406.
Chen, B., Retzlaff, M., Roos, T., and Frydman, J. (2011). Cellular strategies of protein quality control. Cold Spring Harbor perspectives in biology *3*, a004374.
Chen, L., Muhlrad, D., Hauryliuk, V., Cheng, Z., Lim, M.K., Shyp, V., Parker, R., and Song, H. (2010). Structure of the Dom34-Hbs1 complex and implications for no-go decay. Nature structural & molecular biology *17*, 1233-1240.
Chen, Y., and Klionsky, D.J. (2011). The regulation of autophagy–unanswered questions. J Cell Sci *124*, 161-170.
Chernoff, Y.O., Lindquist, S.L., Ono, B.-i., Inge-Vechtomov, S.G., and Liebman, S.W. (1995). Role of the chaperone protein Hsp104 in propagation of the yeast prion-like factor [psi+]. Science *268*, 880-884.
Chernova, T.A., Romanyuk, A.V., Karpova, T.S., Shanks, J.R., Ali, M., Moffatt, N., Howie, R.L., O'Dell, A., McNally, J.G., Liebman, S.W., *et al.* (2011). Prion induction by the short-lived, stress-induced protein Lsb2 is regulated by ubiquitination and association with the actin cytoskeleton. Mol Cell *43*, 242-252.
Chesebro, B., Trifilo, M., Race, R., Meade-White, K., Teng, C., LaCasse, R., Raymond, L., Favara, C., Baron, G., Priola, S., *et al.* (2005). Anchorless prion protein results in infectious amyloid disease without clinical scrapie. science *308*, 1435-1439.
Chiabudini, M., Conz, C., Reckmann, F., and Rospert, S. (2012). Ribosome-associated complex and Ssb are required for translational repression induced by polylysine segments within nascent chains. Molecular and cellular biology *32*, 4769-4779.
Chiti, F., and Dobson, C.M. (2006). Protein misfolding, functional amyloid, and human disease. Annu Rev Biochem *75*, 333-366.

Choe, Y.-J., Park, S.-H., Hassemer, T., Körner, R., Vincenz-Donnelly, L., Hayer-Hartl, M., and Hartl, F.U. (2016). Failure of RQC machinery causes protein aggregation and proteotoxic stress. nature *531*, 191-195.
Choi, Y.-J., Kim, S.-I., Lee, J.-W., Kwon, Y.-S., Lee, H.J., Kim, S.-S., and Chun, W. (2012). Suppression of aggregate formation of mutant huntingtin potentiates CREB-binding protein sequestration and apoptotic cell death. Molecular and Cellular Neuroscience *49*, 127-137.
Chong, Y.T., Koh, J.L., Friesen, H., Duffy, K., Cox, M.J., Moses, A., Moffat, J., Boone, C., and Andrews, B.J. (2015). Yeast proteome dynamics from single cell imaging and automated analysis. Cell *161*, 1413-1424.
Chu, J., Hong, N.A., Masuda, C.A., Jenkins, B.V., Nelms, K.A., Goodnow, C.C., Glynne, R.J., Wu, H., Masliah, E., and Joazeiro, C.A. (2009). A mouse forward genetics screen identifies LISTERIN as an E3 ubiquitin ligase involved in neurodegeneration. Proceedings of the National Academy of Sciences *106*, 2097-2103.
Chung, K.K., Zhang, Y., Lim, K.L., Tanaka, Y., Huang, H., Gao, J., Ross, C.A., Dawson, V.L., and Dawson, T.M. (2001). Parkin ubiquitinates the alpha-synuclein-interacting protein, synphilin-1: implications for Lewy-body formation in Parkinson disease. Nature medicine *7*, 1144-1150.
Ciechanover, A., and Kwon, Y.T. (2015). Degradation of misfolded proteins in neurodegenerative diseases: therapeutic targets and strategies. Experimental & molecular medicine *47*, e147.
Cornett, J., Cao, F., Wang, C.-E., Ross, C.A., Bates, G.P., Li, S.-H., and Li, X.-J. (2005). Polyglutamine expansion of huntingtin impairs its nuclear export. Nature genetics *37*, 198-204.
Costanzo, M., Baryshnikova, A., Bellay, J., Kim, Y., Spear, E.D., Sevier, C.S., Ding, H., Koh, J.L., Toufighi, K., and Mostafavi, S. (2010). The genetic landscape of a cell. Science *327*, 425-431.
Cuéllar, J., Martín-Benito, J., Scheres, S.H., Sousa, R., Moro, F., López-Vinas, E., Gómez-Puertas, P., Muga, A., Carrascosa, J.L., and Valpuesta, J.M. (2008). The structure of CCT–Hsc70NBD suggests a mechanism for Hsp70 delivery of substrates to the chaperonin. Nature structural & molecular biology *15*, 858-864.
Cuervo, A.M., and Wong, E. (2014). Chaperone-mediated autophagy: roles in disease and aging. Cell research *24*, 92-104.
Davies, S.W., Turmaine, M., Cozens, B.A., DiFiglia, M., Sharp, A.H., Ross, C.A., Scherzinger, E., Wanker, E.E., Mangiarini, L., and Bates, G.P. (1997). Formation of neuronal intranuclear inclusions underlies the neurological dysfunction in mice transgenic for the HD mutation. Cell *90*, 537-548.
De Lau, L.M., and Breteler, M.M. (2006). Epidemiology of Parkinson's disease. The Lancet Neurology *5*, 525-535.
De Rooij, K.E., Dorsman, J.C., Smoor, M.A., Den Dunnen, J.T., and Van Ommen, G.-J.B. (1996). Subcellular localization of the Huntington's disease gene product in cell lines by immunofluorescence and biochemical subcellular fractionation. Human molecular genetics *5*, 1093-1099.
Defenouillère, Q., Yao, Y., Mouaikel, J., Namane, A., Galopier, A., Decourty, L., Doyen, A., Malabat, C., Saveanu, C., and Jacquier, A. (2013). Cdc48-associated complex bound to 60S particles is required for the clearance of aberrant translation products. Proceedings of the National Academy of Sciences *110*, 5046-5051.
Defenouillère, Q., Zhang, E., Namane, A., Mouaikel, J., Jacquier, A., and Fromont-Racine, M. (2016). Rqc1 and Ltn1 prevent C-terminal alanine-threonine tail (CAT-tail)-induced protein aggregation by efficient recruitment of Cdc48 on stalled 60S subunits. Journal of Biological Chemistry *291*, 12245-12253.
Dehay, B., and Bertolotti, A. (2006). Critical role of the proline-rich region in Huntingtin for aggregation and cytotoxicity in yeast. Journal of Biological Chemistry *281*, 35608-35615.

Derkatch, I.L., Bradley, M.E., Zhou, P., Chernoff, Y.O., and Liebman, S.W. (1997). Genetic and environmental factors affecting the de novo appearance of the [PSI+] prion in Saccharomyces cerevisiae. Genetics *147*, 507-519.

DiFiglia, M., Sapp, E., Chase, K., Schwarz, C., Meloni, A., Young, C., Martin, E., Vonsattel, J.-P., Carraway, R., and Reeves, S.A. (1995). Huntingtin is a cytoplasmic protein associated with vesicles in human and rat brain neurons. Neuron *14*, 1075-1081.

DiFiglia, M., Sapp, E., Chase, K.O., Davies, S.W., Bates, G.P., Vonsattel, J., and Aronin, N. (1997). Aggregation of huntingtin in neuronal intranuclear inclusions and dystrophic neurites in brain. Science *277*, 1990-1993.

Dimitrova, L.N., Kuroha, K., Tatematsu, T., and Inada, T. (2009). Nascent peptide-dependent translation arrest leads to Not4p-mediated protein degradation by the proteasome. Journal of Biological Chemistry *284*, 10343-10352.

Dinner, A.R., Šali, A., Smith, L.J., Dobson, C.M., and Karplus, M. (2000). Understanding protein folding via free-energy surfaces from theory and experiment. Trends in biochemical sciences *25*, 331-339.

Doma, M.K., and Parker, R. (2006a). Endonucleolytic cleavage of eukaryotic mRNAs with stalls in translation elongation. nature *440*, 561.

Doma, M.K., and Parker, R. (2006b). Endonucleolytic cleavage of eukaryotic mRNAs with stalls in translation elongation. nature *440*, 561-564.

Doyle, S.M., Genest, O., and Wickner, S. (2013). Protein rescue from aggregates by powerful molecular chaperone machines. Nature reviews Molecular cell biology *14*, 617-629.

Duennwald, M.L., Jagadish, S., Giorgini, F., Muchowski, P.J., and Lindquist, S. (2006a). A network of protein interactions determines polyglutamine toxicity. Proceedings of the National Academy of Sciences *103*, 11051-11056.

Duennwald, M.L., Jagadish, S., Muchowski, P.J., and Lindquist, S. (2006b). Flanking sequences profoundly alter polyglutamine toxicity in yeast. Proceedings of the National Academy of Sciences *103*, 11045-11050.

Duyao, M.P., Auerbach, A.B., Ryan, A., Persichetti, F., Barnes, G.T., McNeil, S.M., Ge, P., Vonsattel, J.-P., Gusella, J.F., and Joyner, A.L. (1995). Inactivation of the mouse Huntington's disease gene homolog Hdh. Science *269*, 407-410.

Engelender, S., Kaminsky, Z., Guo, X., Sharp, A.H., Amaravi, R.K., Kleiderlein, J.J., Margolis, R.L., Troncoso, J.C., Lanahan, A.A., and Worley, P.F. (1999). Synphilin-1 associates with α-synuclein and promotes the formation of cytosolic inclusions. Nature genetics *22*, 110-114.

Erjavec, N., Larsson, L., Grantham, J., and Nyström, T. (2007). Accelerated aging and failure to segregate damaged proteins in Sir2 mutants can be suppressed by overproducing the protein aggregation-remodeling factor Hsp104p. Genes & development *21*, 2410-2421.

Finley, D. (2009). Recognition and processing of ubiquitin-protein conjugates by the proteasome. Annual review of biochemistry *78*, 477-513.

Finley, D., Ulrich, H.D., Sommer, T., and Kaiser, P. (2012). The ubiquitin–proteasome system of Saccharomyces cerevisiae. Genetics *192*, 319-360.

Freibaum, B.D., Lu, Y., Lopez-Gonzalez, R., Kim, N.C., Almeida, S., Lee, K.-H., Badders, N., Valentine, M., Miller, B.L., and Wong, P.C. (2015). GGGGCC repeat expansion in C9orf72 compromises nucleocytoplasmic transport. nature.

Frischmeyer, P.A., van Hoof, A., O'Donnell, K., Guerrerio, A.L., Parker, R., and Dietz, H.C. (2002). An mRNA surveillance mechanism that eliminates transcripts lacking termination codons. Science *295*,

2258-2261.
Fruhmann, G., Seynnaeve, D., Zheng, J., Ven, K., Molenberghs, S., Wilms, T., Liu, B., Winderickx, J., and Franssens, V. (2016). Yeast buddies helping to unravel the complexity of neurodegenerative disorders. Mechanisms of ageing and development.
Fruhmann, G., Seynnaeve, D., Zheng, J., Ven, K., Molenberghs, S., Wilms, T., Liu, B., Winderickx, J., and Franssens, V. (2017). Yeast buddies helping to unravel the complexity of neurodegenerative disorders. Mechanisms of ageing and development *161*, 288-305.
Ganusova, E.E., Ozolins, L.N., Bhagat, S., Newnam, G.P., Wegrzyn, R.D., Sherman, M.Y., and Chernoff, Y.O. (2006). Modulation of prion formation, aggregation, and toxicity by the actin cytoskeleton in yeast. Mol Cell Biol *26*, 617-629.
Gellon, L., Razidlo, D.F., Gleeson, O., Verra, L., Schulz, D., Lahue, R.S., and Freudenreich, C.H. (2011). New functions of Ctf18-RFC in preserving genome stability outside its role in sister chromatid cohesion. PLoS genetics *7*, e1001298.
Giorgini, F., Guidetti, P., Nguyen, Q., Bennett, S.C., and Muchowski, P.J. (2005). A genomic screen in yeast implicates kynurenine 3-monooxygenase as a therapeutic target for Huntington disease. Nature genetics *37*, 526-531.
Glover, J.R., and Lindquist, S. (1998). Hsp104, Hsp70, and Hsp40: a novel chaperone system that rescues previously aggregated proteins. Cell *94*, 73-82.
Gokhale, K.C., Newnam, G.P., Sherman, M.Y., and Chernoff, Y.O. (2005). Modulation of prion-dependent polyglutamine aggregation and toxicity by chaperone proteins in the yeast model. Journal of Biological Chemistry *280*, 22809-22818.
Golovko, M.Y., Barceló-Coblijn, G., Castagnet, P.I., Austin, S., Combs, C.K., and Murphy, E.J. (2009). The role of α-synuclein in brain lipid metabolism: a downstream impact on brain inflammatory response. Molecular and cellular biochemistry *326*, 55-66.
Gong, H., Romanova, N.V., Allen, K.D., Chandramowlishwaran, P., Gokhale, K., Newnam, G.P., Mieczkowski, P., Sherman, M.Y., and Chernoff, Y.O. (2012). Polyglutamine toxicity is controlled by prion composition and gene dosage in yeast. PLoS Genet *8*, e1002634.
Grenson, M., Mousset, M., Wiame, J., and Bechet, J. (1966). Multiplicity of the amino acid permeases in Saccharomyces cerevisiae: I. Evidence for a specific arginine-transporting system. Biochimica et Biophysica Acta (BBA)-General Subjects *127*, 325-338.
Haas, A.L., Warms, J., Hershko, A., and Rose, I.A. (1982). Ubiquitin-activating enzyme. Mechanism and role in protein-ubiquitin conjugation. Journal of Biological Chemistry *257*, 2543-2548.
Haigis, M.C., and Yankner, B.A. (2010). The aging stress response. Molecular cell *40*, 333-344.
Hartl, F.U. (1996). Molecular chaperones in cellular protein folding. nature *381*, 571.
Hartl, F.U., and Hayer-Hartl, M. (2002). Molecular chaperones in the cytosol: from nascent chain to folded protein. Science *295*, 1852-1858.
Haslbeck, M., and Vierling, E. (2015). A first line of stress defense: small heat shock proteins and their function in protein homeostasis. Journal of molecular biology *427*, 1537-1548.
Higuchi, R., Vevea, J.D., Swayne, T.C., Chojnowski, R., Hill, V., Boldogh, I.R., and Pon, L.A. (2013). Actin dynamics affect mitochondrial quality control and aging in budding yeast. Current Biology *23*, 2417-2422.
Hill, S.M., Hao, X., Grönvall, J., Spikings-Nordby, S., Widlund, P.O., Amen, T., Jörhov, A., Josefson, R., Kaganovich, D., and Liu, B. (2016). Asymmetric inheritance of aggregated proteins and age reset in yeast are regulated by Vac17-dependent vacuolar functions. Cell reports *16*, 826-838.

Ho, C.H., Magtanong, L., Barker, S.L., Gresham, D., Nishimura, S., Natarajan, P., Koh, J.L., Porter, J., Gray, C.A., Andersen, R.J., *et al.* (2009). A molecular barcoded yeast ORF library enables mode-of-action analysis of bioactive compounds. Nat Biotechnol *27*, 369-377.

Hughes, A.L., and Gottschling, D.E. (2012). An early-age increase in vacuolar pH limits mitochondrial function and lifespan in yeast. nature *492*, 261.

Huh, W.-K., Falvo, J.V., Gerke, L.C., Carroll, A.S., Howson, R.W., Weissman, J.S., and O'Shea, E.K. (2003). Global analysis of protein localization in budding yeast. nature *425*, 686-691.

Inada, T., and Aiba, H. (2005). Translation of aberrant mRNAs lacking a termination codon or with a shortened 3′‐UTR is repressed after initiation in yeast. The EMBO journal *24*, 1584-1595.

Ishimura, R., Nagy, G., Dotu, I., Zhou, H., Yang, X.-L., Schimmel, P., Senju, S., Nishimura, Y., Chuang, J.H., and Ackerman, S.L. (2014). Ribosome stalling induced by mutation of a CNS-specific tRNA causes neurodegeneration. Science *345*, 455-459.

Ito-Harashima, S., Kuroha, K., Tatematsu, T., and Inada, T. (2007). Translation of the poly (A) tail plays crucial roles in nonstop mRNA surveillance via translation repression and protein destabilization by proteasome in yeast. Genes & development *21*, 519-524.

Ito, T., Niwa, J., Hishikawa, N., Ishigaki, S., Doyu, M., and Sobue, G. (2003). Dorfin localizes to Lewy bodies and ubiquitylates synphilin-1. The Journal of biological chemistry *278*, 29106-29114.

Iwata, A., Riley, B.E., Johnston, J.A., and Kopito, R.R. (2005). HDAC6 and microtubules are required for autophagic degradation of aggregated huntingtin. Journal of Biological Chemistry *280*, 40282-40292.

Jiang, H., Poirier, M.A., Liang, Y., Pei, Z., Weiskittel, C.E., Smith, W.W., DeFranco, D.B., and Ross, C.A. (2006). Depletion of CBP is directly linked with cellular toxicity caused by mutant huntingtin. Neurobiology of disease *23*, 543-551.

Jin, H.-G., Yamashita, H., Nakamura, T., Fukuba, H., Takahashi, T., Hiji, M., Kohriyama, T., and Matsumoto, M. (2008). Synphilin-1 transgenic mice exhibit mild motor impairments. Neuroscience letters *445*, 12-17.

Johnston, J.A., Ward, C.L., and Kopito, R.R. (1998). Aggresomes: a cellular response to misfolded proteins. J Cell Biol *143*, 1883-1898.

Jovičić, A., Mertens, J., Boeynaems, S., Bogaert, E., Chai, N., Yamada, S.B., Paul III, J.W., Sun, S., Herdy, J.R., and Bieri, G. (2015). Modifiers of C9orf72 dipeptide repeat toxicity connect nucleocytoplasmic transport defects to FTD/ALS. Nature neuroscience *18*, 1226-1229.

Kaganovich, D., Kopito, R., and Frydman, J. (2008). Misfolded proteins partition between two distinct quality control compartments. nature *454*, 1088-1095.

Kalinderi, K., Bostantjopoulou, S., and Fidani, L. (2016). The genetic background of Parkinson's disease: current progress and future prospects. Acta Neurologica Scandinavica.

Kayatekin, C., Matlack, K.E., Hesse, W.R., Guan, Y., Chakrabortee, S., Russ, J., Wanker, E.E., Shah, J.V., and Lindquist, S. (2014). Prion-like proteins sequester and suppress the toxicity of huntingtin exon 1. Proceedings of the National Academy of Sciences *111*, 12085-12090.

Kervestin, S., and Jacobson, A. (2012). NMD: a multifaceted response to premature translational termination. Nature reviews Molecular cell biology *13*, 700-712.

Khurana, V., and Lindquist, S. (2010). Modelling neurodegeneration in Saccharomyces cerevisiae: why cook with baker's yeast? Nature Reviews Neuroscience *11*, 436-449.

Kirschke, E., Goswami, D., Southworth, D., Griffin, P.R., and Agard, D.A. (2014). Glucocorticoid receptor function regulated by coordinated action of the Hsp90 and Hsp70 chaperone cycles. Cell *157*, 1685-1697.

Kirstein‐Miles, J., Scior, A., Deuerling, E., and Morimoto, R.I. (2013). The nascent polypeptide‐

associated complex is a key regulator of proteostasis. The EMBO journal *32*, 1451-1468.
Kobayashi, S. (2015). Choose delicately and reuse adequately: the newly revealed process of autophagy. Biological and Pharmaceutical Bulletin *38*, 1098-1103.
Koch, C., Wollmann, P., Dahl, M., and Lottspeich, F. (1999). A role for Ctr9p and Paf1p in the regulation G1 cyclin expression in yeast. Nucleic Acids Res *27*, 2126-2134.
Kopito, R.R. (2000). Aggresomes, inclusion bodies and protein aggregation. Trends in cell biology *10*, 524-530.
Kostova, K.K., Hickey, K.L., Osuna, B.A., Hussmann, J.A., Frost, A., Weinberg, D.E., and Weissman, J.S. (2017). CAT-tailing as a fail-safe mechanism for efficient degradation of stalled nascent polypeptides. Science *357*, 414-417.
Krenz, A., Falkenburger, B.H., Gerhardt, E., Drinkut, A., and Schulz, J.B. (2009). Aggregate formation and toxicity by wild‐type and R621C synphilin‐1 in the nigrostriatal system of mice using adenoviral vectors. Journal of neurochemistry *108*, 139-146.
Krobitsch, S., and Lindquist, S. (2000). Aggregation of huntingtin in yeast varies with the length of the polyglutamine expansion and the expression of chaperone proteins. Proceedings of the National Academy of Sciences *97*, 1589-1594.
Krogan, N.J., Dover, J., Wood, A., Schneider, J., Heidt, J., Boateng, M.A., Dean, K., Ryan, O.W., Golshani, A., Johnston, M., *et al.* (2003). The Paf1 complex is required for histone H3 methylation by COMPASS and Dot1p: linking transcriptional elongation to histone methylation. Mol Cell *11*, 721-729.
Krüger, R., Kuhn, W., Müller, T., Woitalla, D., Graeber, M., Kösel, S., Przuntek, H., Epplen, J.T., Schols, L., and Riess, O. (1998). AlaSOPro mutation in the gene encoding α-synuclein in Parkinson's disease. Nature genetics *18*, 106-108.
Kuroha, K., Akamatsu, M., Dimitrova, L., Ito, T., Kato, Y., Shirahige, K., and Inada, T. (2010). Receptor for activated C kinase 1 stimulates nascent polypeptide‐dependent translation arrest. EMBO reports *11*, 956-961.
Lakhani, V.V., Ding, F., and Dokholyan, N.V. (2010). Polyglutamine induced misfolding of huntingtin exon1 is modulated by the flanking sequences. PLoS computational biology *6*, e1000772.
Lee, J.W., Beebe, K., Nangle, L.A., Jang, J., Longo-Guess, C.M., Cook, S.A., Davisson, M.T., Sundberg, J.P., Schimmel, P., and Ackerman, S.L. (2006). Editing-defective tRNA synthetase causes protein misfolding and neurodegeneration. nature *443*, 50-55.
Lengronne, A., McIntyre, J., Katou, Y., Kanoh, Y., Hopfner, K.P., Shirahige, K., and Uhlmann, F. (2006). Establishment of sister chromatid cohesion at the S. cerevisiae replication fork. Mol Cell *23*, 787-799.
Leroux, M.R., and Hartl, F.U. (2000). Protein folding: versatility of the cytosolic chaperonin TRiC/CCT. Current biology : CB *10*, R260-264.
Lesage, S., Anheim, M., Letournel, F., Bousset, L., Honoré, A., Rozas, N., Pieri, L., Madiona, K., Dürr, A., and Melki, R. (2013). G51D α‐synuclein mutation causes a novel Parkinsonian–pyramidal syndrome. Annals of neurology *73*, 459-471.
Letzring, D.P., Dean, K.M., and Grayhack, E.J. (2010). Control of translation efficiency in yeast by codon–anticodon interactions. Rna *16*, 2516-2528.
Letzring, D.P., Wolf, A.S., Brule, C.E., and Grayhack, E.J. (2013). Translation of CGA codon repeats in yeast involves quality control components and ribosomal protein L1. Rna *19*, 1208-1217.
Li, Z., Vizeacoumar, F.J., Bahr, S., Li, J., Warringer, J., Vizeacoumar, F.S., Min, R., VanderSluis, B., Bellay, J., and DeVit, M. (2011). Systematic exploration of essential yeast gene function with temperature-sensitive mutants. Nature biotechnology *29*, 361-367.

Lindner, A.B., Madden, R., Demarez, A., Stewart, E.J., and Taddei, F. (2008). Asymmetric segregation of protein aggregates is associated with cellular aging and rejuvenation. Proceedings of the National Academy of Sciences *105*, 3076-3081.

Liu, B., Larsson, L., Caballero, A., Hao, X., Öling, D., Grantham, J., and Nyström, T. (2010). The polarisome is required for segregation and retrograde transport of protein aggregates. Cell *140*, 257-267.

Liu, B., Larsson, L., Franssens, V., Hao, X., Hill, S.M., Andersson, V., Höglund, D., Song, J., Yang, X., and Öling, D. (2011). Segregation of protein aggregates involves actin and the polarity machinery. Cell *147*, 959-961.

Liu, C.-W., Li, X., Thompson, D., Wooding, K., Chang, T.-l., Tang, Z., Yu, H., Thomas, P.J., and DeMartino, G.N. (2006). ATP binding and ATP hydrolysis play distinct roles in the function of 26S proteasome. Molecular cell *24*, 39-50.

Lopez, T., Dalton, K., and Frydman, J. (2015). The mechanism and function of group II chaperonins. Journal of molecular biology *427*, 2919-2930.

Losson, R., and Lacroute, F. (1979). Interference of nonsense mutations with eukaryotic messenger RNA stability. Proceedings of the National Academy of Sciences *76*, 5134-5137.

Lyumkis, D., dos Passos, D.O., Tahara, E.B., Webb, K., Bennett, E.J., Vinterbo, S., Potter, C.S., Carragher, B., and Joazeiro, C.A. (2014). Structural basis for translational surveillance by the large ribosomal subunit-associated protein quality control complex. Proceedings of the National Academy of Sciences *111*, 15981-15986.

MacDonald, M.E., Ambrose, C.M., Duyao, M.P., Myers, R.H., Lin, C., Srinidhi, L., Barnes, G., Taylor, S.A., James, M., and Groot, N. (1993). A novel gene containing a trinucleotide repeat that is expanded and unstable on Huntington's disease chromosomes. Cell *72*, 971-983.

Mangiarini, L., Sathasivam, K., Seller, M., Cozens, B., Harper, A., Hetherington, C., Lawton, M., Trottier, Y., Lehrach, H., and Davies, S.W. (1996). Exon 1 of the HD gene with an expanded CAG repeat is sufficient to cause a progressive neurological phenotype in transgenic mice. Cell *87*, 493-506.

Maquat, L.E., Kinniburgh, A.J., Rachmilewitz, E.A., and Ross, J. (1981). Unstable β-globin mRNA in mRNA-deficient β 0 thalassemia. Cell *27*, 543-553.

Mason, R.P., Casu, M., Butler, N., Breda, C., Campesan, S., Clapp, J., Green, E.W., Dhulkhed, D., Kyriacou, C.P., and Giorgini, F. (2013). Glutathione peroxidase activity is neuroprotective in models of Huntington's disease. Nature genetics *45*, 1249-1254.

Mason, R.P., and Giorgini, F. (2011). Modeling Huntington disease in yeast: perspectives and future directions. Prion *5*, 269-276.

Mayer, M.L., Gygi, S.P., Aebersold, R., and Hieter, P. (2001). Identification of RFC(Ctf18p, Ctf8p, Dcc1p): an alternative RFC complex required for sister chromatid cohesion in S. cerevisiae. Mol Cell *7*, 959-970.

McDonald, H.B., and Byers, B. (1997). A proteasome cap subunit required for spindle pole body duplication in yeast. The Journal of cell biology *137*, 539-553.

McKenna, M.C. (2011). Glutamate dehydrogenase in brain mitochondria: do lipid modifications and transient metabolon formation influence enzyme activity? Neurochemistry international *59*, 525-533.

Meriin, A.B., Mabuchi, K., Gabai, V.L., Yaglom, J.A., Kazantsev, A., and Sherman, M.Y. (2001). Intracellular aggregation of polypeptides with expanded polyglutamine domain is stimulated by stress-activated kinase MEKK1. The Journal of cell biology *153*, 851-864.

Meriin, A.B., Zhang, X., Alexandrov, I.M., Salnikova, A.B., Ter-Avanesian, M.D., Chernoff, Y.O., and Sherman, M.Y. (2007). Endocytosis machinery is involved in aggregation of proteins with expanded polyglutamine domains. The FASEB Journal *21*, 1915-1925.

Meriin, A.B., Zhang, X., He, X., Newnam, G.P., Chernoff, Y.O., and Sherman, M.Y. (2002). Huntingtin toxicity in yeast model depends on polyglutamine aggregation mediated by a prion-like protein Rnq1. The Journal of cell biology *157*, 997-1004.

Miller, S.B., Ho, C.T., Winkler, J., Khokhrina, M., Neuner, A., Mohamed, M.Y., Guilbride, D.L., Richter, K., Lisby, M., and Schiebel, E. (2015). Compartment‐specific aggregases direct distinct nuclear and cytoplasmic aggregate deposition. The EMBO journal, e201489524.

Mizushima, N., and Komatsu, M. (2011). Autophagy: renovation of cells and tissues. Cell *147*, 728-741.

Mizushima, N., Levine, B., Cuervo, A.M., and Klionsky, D.J. (2008). Autophagy fights disease through cellular self-digestion. nature *451*, 1069-1075.

Mizushima, N., Yoshimori, T., and Ohsumi, Y. (2011). The role of Atg proteins in autophagosome formation. Annual review of cell and developmental biology *27*, 107-132.

Moldavski, O., Amen, T., Levin-Zaidman, S., Eisenstein, M., Rogachev, I., Brandis, A., Kaganovich, D., and Schuldiner, M. (2015). Lipid Droplets Are Essential for Efficient Clearance of Cytosolic Inclusion Bodies. Developmental cell.

Moore, J.K., Li, J., and Cooper, J.A. (2008). Dynactin function in mitotic spindle positioning. Traffic *9*, 510-527.

Moore, J.K., Stuchell-Brereton, M.D., and Cooper, J.A. (2009). Function of dynein in budding yeast: mitotic spindle positioning in a polarized cell. Cell motility and the cytoskeleton *66*, 546-555.

Morton, A., Lagan, M., Skepper, J., and Dunnett, S. (2000). Progressive formation of inclusions in the striatum and hippocampus of mice transgenic for the human Huntington's disease mutation. Journal of neurocytology *29*, 679-702.

Nakatogawa, H., Suzuki, K., Kamada, Y., and Ohsumi, Y. (2009). Dynamics and diversity in autophagy mechanisms: lessons from yeast. Nature reviews Molecular cell biology *10*, 458-467.

Nasir, J., Floresco, S.B., O'Kusky, J.R., Diewert, V.M., Richman, J.M., Zeisler, J., Borowski, A., Marth, J.D., Phillips, A.G., and Hayden, M.R. (1995). Targeted disruption of the Huntington's disease gene results in embryonic lethality and behavioral and morphological changes in heterozygotes. Cell *81*, 811-823.

Nuber, S., Franck, T., Wolburg, H., Schumann, U., Casadei, N., Fischer, K., Calaminus, C., Pichler, B.J., Chanarat, S., and Teismann, P. (2010). Transgenic overexpression of the alpha-synuclein interacting protein synphilin-1 leads to behavioral and neuropathological alterations in mice. neurogenetics *11*, 107-120.

Nyström, T., and Liu, B. (2014). The mystery of aging and rejuvenation—a budding topic. Current opinion in microbiology *18*, 61-67.

Ogrodnik, M., Salmonowicz, H., Brown, R., Turkowska, J., Średniawa, W., Pattabiraman, S., Amen, T., Abraham, A.-c., Eichler, N., and Lyakhovetsky, R. (2014). Dynamic JUNQ inclusion bodies are asymmetrically inherited in mammalian cell lines through the asymmetric partitioning of vimentin. Proceedings of the National Academy of Sciences *111*, 8049-8054.

Park, S.-H., Kukushkin, Y., Gupta, R., Chen, T., Konagai, A., Hipp, M.S., Hayer-Hartl, M., and Hartl, F.U. (2013). PolyQ proteins interfere with nuclear degradation of cytosolic proteins by sequestering the Sis1p chaperone. Cell *154*, 134-145.

Park, Y.-N., Zhao, X., Yim, Y.-I., Todor, H., Ellerbrock, R., Reidy, M., Eisenberg, E., Masison, D.C., and Greene, L.E. (2014). Hsp104 overexpression cures Saccharomyces cerevisiae [PSI+] by causing dissolution of the prion seeds. Eukaryotic cell *13*, 635-647.

Parsell, D.A., Kowal, A.S., Singer, M.A., and Lindquist, S. (1994). Protein disaggregation mediated by heat-shock protein Hsp104. nature *372*, 475.

Pasanen, P., Myllykangas, L., Siitonen, M., Raunio, A., Kaakkola, S., Lyytinen, J., Tienari, P.J., Pöyhönen,

M., and Paetau, A. (2014). A novel α-synuclein mutation A53E associated with atypical multiple system atrophy and Parkinson's disease-type pathology. Neurobiology of aging *35*, 2180. e2181-2180. e2185.
Peters, J.-M., Franke, W.W., and Kleinschmidt, J.A. (1994). Distinct 19 S and 20 S subcomplexes of the 26 S proteasome and their distribution in the nucleus and the cytoplasm. Journal of Biological Chemistry *269*, 7709-7718.
Peters, M.F., Nucifora, F.C., Kushi, J., Seaman, H.C., Cooper, J.K., Herring, W.J., Dawson, V.L., Dawson, T.M., and Ross, C.A. (1999). Nuclear targeting of mutant Huntingtin increases toxicity. Molecular and Cellular Neuroscience *14*, 121-128.
Pisareva, V.P., Skabkin, M.A., Hellen, C.U., Pestova, T.V., and Pisarev, A.V. (2011). Dissociation by Pelota, Hbs1 and ABCE1 of mammalian vacant 80S ribosomes and stalled elongation complexes. The EMBO journal *30*, 1804-1817.
Polymeropoulos, M.H., Lavedan, C., Leroy, E., Ide, S.E., Dehejia, A., Dutra, A., Pike, B., Root, H., Rubenstein, J., and Boyer, R. (1997). Mutation in the α-synuclein gene identified in families with Parkinson's disease. Science *276*, 2045-2047.
Porcari, R., Proukakis, C., Waudby, C.A., Bolognesi, B., Mangione, P.P., Paton, J.F., Mullin, S., Cabrita, L.D., Penco, A., and Relini, A. (2015). The H50Q mutation induces a 10-fold decrease in the solubility of α-synuclein. Journal of Biological Chemistry *290*, 2395-2404.
Puschmann, A., Ross, O.A., Vilariño-Güell, C., Lincoln, S.J., Kachergus, J.M., Cobb, S.A., Lindquist, S.G., Nielsen, J.E., Wszolek, Z.K., and Farrer, M. (2009). A Swedish family with de novo α-synuclein A53T mutation: Evidence for early cortical dysfunction. Parkinsonism & related disorders *15*, 627-632.
Ribeiro, C.S., Carneiro, K., Ross, C.A., Menezes, J.R.L., and Engelender, S. (2002). Synphilin-1 is developmentally localized to synaptic terminals, and its association with synaptic vesicles is modulated by alpha-synuclein. Journal of Biological Chemistry *277*, 23927-23933.
Ripaud, L., Chumakova, V., Antonin, M., Hastie, A.R., Pinkert, S., Körner, R., Ruff, K.M., Pappu, R.V., Hornburg, D., and Mann, M. (2014). Overexpression of Q-rich prion-like proteins suppresses polyQ cytotoxicity and alters the polyQ interactome. Proceedings of the National Academy of Sciences *111*, 18219-18224.
Risseeuw, E.P., Daskalchuk, T.E., Banks, T.W., Liu, E., Cotelesage, J., Hellmann, H., Estelle, M., Somers, D.E., and Crosby, W.L. (2003). Protein interaction analysis of SCF ubiquitin E3 ligase subunits from Arabidopsis. The Plant Journal *34*, 753-767.
Rodrigo-Brenni, M.C., and Hegde, R.S. (2012). Design principles of protein biosynthesis-coupled quality control. Developmental cell *23*, 896-907.
Rubinsztein, D.C. (2006). The roles of intracellular protein-degradation pathways in neurodegeneration. nature *443*, 780-786.
Rubinsztein, D.C., DiFiglia, M., Heintz, N., Nixon, R.A., Qin, Z.-H., Ravikumar, B., Stefanis, L., and Tolkovsky, A. (2005). Autophagy and its possible roles in nervous system diseases, damage and repair. Autophagy *1*, 11-22.
Rujano, M.A., Bosveld, F., Salomons, F.A., Dijk, F., Van Waarde, M.A., Van Der Want, J.J., De Vos, R.A., Brunt, E.R., Sibon, O.C., and Kampinga, H.H. (2006). Polarised asymmetric inheritance of accumulated protein damage in higher eukaryotes. PLoS biology *4*, e417.
Saudou, F., Finkbeiner, S., Devys, D., and Greenberg, M.E. (1998). Huntingtin acts in the nucleus to induce apoptosis but death does not correlate with the formation of intranuclear inclusions. Cell *95*, 55-66.
Schaffar, G., Breuer, P., Boteva, R., Behrends, C., Tzvetkov, N., Strippel, N., Sakahira, H., Siegers, K., Hayer-Hartl, M., and Hartl, F.U. (2004). Cellular toxicity of polyglutamine expansion proteins: mechanism

of transcription factor deactivation. Molecular cell *15*, 95-105.
Schilling, G., Becher, M.W., Sharp, A.H., Jinnah, H.A., Duan, K., Kotzuk, J.A., Slunt, H.H., Ratovitski, T., Cooper, J.K., and Jenkins, N.A. (1999). Intranuclear inclusions and neuritic aggregates in transgenic mice expressing a mutant N-terminal fragment of huntingtin. Human molecular genetics *8*, 397-407.
Schilling, G., Savonenko, A.V., Klevytska, A., Morton, J.L., Tucker, S.M., Poirier, M., Gale, A., Chan, N., Gonzales, V., and Slunt, H.H. (2004). Nuclear-targeting of mutant huntingtin fragments produces Huntington's disease-like phenotypes in transgenic mice. Human molecular genetics *13*, 1599-1610.
Schilling, G., Sharp, A.H., Loev, S.J., Wagster, M.V., Li, S.-H., Stine, O.C., and Ross, C.A. (1995). Expression of the Huntington's disease (IT15) protein product in HD patients. Human molecular genetics *4*, 1365-1371.
Schneider, S.A., and Obeso, J.A. (2014). Clinical and pathological features of Parkinson's disease. In Behavioral Neurobiology of Huntington's Disease and Parkinson's Disease (Springer), pp. 205-220.
Schroer, T.A. (2004). Dynactin. Annu Rev Cell Dev Biol *20*, 759-779.
Serpionov, G.V., Alexandrov, A.I., and Ter-Avanesyan, M.D. (2016). Distinct mechanisms of mutant huntingtin toxicity in different yeast strains. FEMS yeast research, fow102.
Shao, S., Brown, A., Santhanam, B., and Hegde, R.S. (2015). Structure and assembly pathway of the ribosome quality control complex. Molecular cell *57*, 433-444.
Shao, S., von der Malsburg, K., and Hegde, R.S. (2013). Listerin-dependent nascent protein ubiquitination relies on ribosome subunit dissociation. Molecular cell *50*, 637-648.
Sheffield, L.G., Miskiewicz, H.B., Tannenbaum, L.B., and Mirra, S.S. (2006). Nuclear pore complex proteins in Alzheimer disease. Journal of Neuropathology & Experimental Neurology *65*, 45-54.
Shen, P.S., Park, J., Qin, Y., Li, X., Parsawar, K., Larson, M.H., Cox, J., Cheng, Y., Lambowitz, A.M., and Weissman, J.S. (2015). Rqc2p and 60S ribosomal subunits mediate mRNA-independent elongation of nascent chains. Science *347*, 75-78.
Shoemaker, C.J., Eyler, D.E., and Green, R. (2010). Dom34: Hbs1 promotes subunit dissociation and peptidyl-tRNA drop-off to initiate no-go decay. Science *330*, 369-372.
Shoemaker, C.J., and Green, R. (2011). Kinetic analysis reveals the ordered coupling of translation termination and ribosome recycling in yeast. Proceedings of the National Academy of Sciences *108*, E1392-E1398.
Singleton, A., Farrer, M., Johnson, J., Singleton, A., Hague, S., Kachergus, J., Hulihan, M., Peuralinna, T., Dutra, A., and Nussbaum, R. (2003). α-Synuclein locus triplication causes Parkinson's disease. Science *302*, 841-841.
Sitron, C.S., Park, J.H., and Brandman, O. (2017). Asc1, Hel2, and Slh1 couple translation arrest to nascent chain degradation. Rna *23*, 798-810.
Slow, E.J., Van Raamsdonk, J., Rogers, D., Coleman, S.H., Graham, R.K., Deng, Y., Oh, R., Bissada, N., Hossain, S.M., and Yang, Y.-Z. (2003). Selective striatal neuronal loss in a YAC128 mouse model of Huntington disease. Human molecular genetics *12*, 1555-1567.
Song, J., Yang, Q., Yang, J., Larsson, L., Hao, X., Zhu, X., Malmgren-Hill, S., Cvijovic, M., Fernandez-Rodriguez, J., and Grantham, J. (2014). Essential Genetic Interactors of SIR2 Required for Spatial Sequestration and Asymmetrical Inheritance of Protein Aggregates. PLoS genetics *10*, e1004539.
Specht, S., Miller, S.B., Mogk, A., and Bukau, B. (2011). Hsp42 is required for sequestration of protein aggregates into deposition sites in Saccharomyces cerevisiae. J Cell Biol *195*, 617-629.
Spiess, C., Meyer, A.S., Reissmann, S., and Frydman, J. (2004). Mechanism of the eukaryotic chaperonin: protein folding in the chamber of secrets. Trends in cell biology *14*, 598-604.

Spillantini, M.G., Schmidt, M.L., Lee, V.M.-Y., Trojanowski, J.Q., Jakes, R., and Goedert, M. (1997). α-Synuclein in Lewy bodies. nature *388*, 839-840.
Spokoini, R., Moldavski, O., Nahmias, Y., England, J.L., Schuldiner, M., and Kaganovich, D. (2012). Confinement to organelle-associated inclusion structures mediates asymmetric inheritance of aggregated protein in budding yeast. Cell reports *2*, 738-747.
Swinnen, E., Buttner, S., Outeiro, T.F., Galas, M.-C., Madeo, F., Winderickx, J., and Franssens, V. (2011). Aggresome formation and segregation of inclusions influence toxicity of alpha-synuclein and synphilin-1 in yeast. Biochem Soc Trans *39*, 1476-1481.
Szargel, R., Rott, R., Eyal, A., Haskin, J., Shani, V., Balan, L., Wolosker, H., and Engelender, S. (2009). Synphilin-1A inhibits seven in absentia homolog (SIAH) and modulates α-synuclein monoubiquitylation and inclusion formation. Journal of Biological Chemistry *284*, 11706-11716.
Takahashi, T., Yamashita, H., Nagano, Y., Nakamura, T., Kohriyama, T., and Matsumoto, M. (2006). Interactions of Synphilin‐1 with phospholipids and lipid membranes. FEBS letters *580*, 4479-4484.
Tan, J.M., Wong, E.S., and Lim, K.L. (2009). Protein misfolding and aggregation in Parkinson's disease. Antioxidants & redox signaling *11*, 2119-2134.
Tanaka, M., Kim, Y.M., Lee, G., Junn, E., Iwatsubo, T., and Mouradian, M.M. (2004). Aggresomes formed by α-synuclein and synphilin-1 are cytoprotective. Journal of Biological Chemistry *279*, 4625-4631.
Thompson, M.D., Nezarati, M.M., Gillessen-Kaesbach, G., Meinecke, P., Mendoza-Londono, R., Mornet, E., Brun-Heath, I., Squarcioni, C.P., Legeai-Mallet, L., Munnich, A., *et al.* (2010). Hyperphosphatasia with seizures, neurologic deficit, and characteristic facial features: Five new patients with Mabry syndrome. American journal of medical genetics Part A *152A*, 1661-1669.
Thrower, J.S., Hoffman, L., Rechsteiner, M., and Pickart, C.M. (2000). Recognition of the polyubiquitin proteolytic signal. The EMBO journal *19*, 94-102.
Tofaris, G., and Spillantini, M. (2007). Physiological and pathological properties of α-synuclein. Cellular and Molecular Life Sciences *64*, 2194-2201.
Tolosa, E., Wenning, G., and Poewe, W. (2006). The diagnosis of Parkinson's disease. The Lancet Neurology *5*, 75-86.
Tong, A.H.Y., and Boone, C. (2007). 16 High-Throughput Strain Construction and Systematic Synthetic Lethal Screening in. Methods in Microbiology *36*, 369-707.
Tong, A.H.Y., Evangelista, M., Parsons, A.B., Xu, H., Bader, G.D., Page, N., Robinson, M., Raghibizadeh, S., Hogue, C.W., and Bussey, H. (2001). Systematic genetic analysis with ordered arrays of yeast deletion mutants. Science *294*, 2364-2368.
Tong, A.H.Y., Lesage, G., Bader, G.D., Ding, H., Xu, H., Xin, X., Young, J., Berriz, G.F., Brost, R.L., and Chang, M. (2004). Global mapping of the yeast genetic interaction network. Science *303*, 808-813.
Truant, R., Atwal, R.S., and Burtnik, A. (2007). Nucleocytoplasmic trafficking and transcription effects of huntingtin in Huntington's disease. Progress in neurobiology *83*, 211-227.
Tsuboi, T., Kuroha, K., Kudo, K., Makino, S., Inoue, E., Kashima, I., and Inada, T. (2012). Dom34: hbs1 plays a general role in quality-control systems by dissociation of a stalled ribosome at the 3′ end of aberrant mRNA. Molecular cell *46*, 518-529.
Vacher, C., Garcia-Oroz, L., and Rubinsztein, D.C. (2005). Overexpression of yeast hsp104 reduces polyglutamine aggregation and prolongs survival of a transgenic mouse model of Huntington's disease. Human molecular genetics *14*, 3425-3433.
Vainberg, I.E., Lewis, S.A., Rommelaere, H., Ampe, C., Vandekerckhove, J., Klein, H.L., and Cowan, N.J. (1998). Prefoldin, a chaperone that delivers unfolded proteins to cytosolic chaperonin. Cell *93*, 863-873.

van den Elzen, A.M., Henri, J., Lazar, N., Gas, M.E., Durand, D., Lacroute, F., Nicaise, M., van Tilbeurgh, H., Séraphin, B., and Graille, M. (2010). Dissection of Dom34–Hbs1 reveals independent functions in two RNA quality control pathways. Nature structural & molecular biology *17*, 1446-1452.
van Hoof, A., Frischmeyer, P.A., Dietz, H.C., and Parker, R. (2002). Exosome-mediated recognition and degradation of mRNAs lacking a termination codon. Science *295*, 2262-2264.
Van Raamsdonk, J.M., Pearson, J., Slow, E.J., Hossain, S.M., Leavitt, B.R., and Hayden, M.R. (2005). Cognitive dysfunction precedes neuropathology and motor abnormalities in the YAC128 mouse model of Huntington's disease. The Journal of Neuroscience *25*, 4169-4180.
Verma, R., Oania, R.S., Kolawa, N.J., and Deshaies, R.J. (2013). Cdc48/p97 promotes degradation of aberrant nascent polypeptides bound to the ribosome. eLife *2*, e00308.
Vizeacoumar, F.J., van Dyk, N., Vizeacoumar, F.S., Cheung, V., Li, J., Sydorskyy, Y., Case, N., Li, Z., Datti, A., and Nislow, C. (2010). Integrating high-throughput genetic interaction mapping and high-content screening to explore yeast spindle morphogenesis. The Journal of cell biology *188*, 69-81.
Wagih, O., and Parts, L. (2014). Gitter: a robust and accurate method for quantification of colony sizes from plate images. G3: Genes| Genomes| Genetics *4*, 547-552.
Wakabayashi, K., Engelender, S., Yoshimoto, M., Tsuji, S., Ross, C.A., and Takahashi, H. (2000). Synphilin‐1 is present in Lewy bodies in Parkinson's disease. Annals of neurology *47*, 521-523.
Walker, F.O. (2007). Huntington's disease. The Lancet *369*, 218-228.
Walter, G.M., Raveh, A., Mok, S.A., McQuade, T.J., Arevang, C.J., Schultz, P.J., Smith, M.C., Asare, S., Cruz, P.G., and Wisen, S. (2014). High‐Throughput Screen of Natural Product Extracts in A Yeast Model of Polyglutamine Proteotoxicity. Chemical biology & drug design *83*, 440-449.
Wang, Y., Meriin, A.B., Costello, C.E., and Sherman, M.Y. (2007). Characterization of proteins associated with polyglutamine aggregates: a novel approach towards isolation of aggregates from protein conformation disorders. Prion *1*, 128-135.
Wang, Y., Meriin, A.B., Zaarur, N., Romanova, N.V., Chernoff, Y.O., Costello, C.E., and Sherman, M.Y. (2009). Abnormal proteins can form aggresome in yeast: aggresome-targeting signals and components of the machinery. The FASEB Journal *23*, 451-463.
Warringer, J., and Blomberg, A. (2003). Automated screening in environmental arrays allows analysis of quantitative phenotypic profiles in Saccharomyces cerevisiae. Yeast *20*, 53-67.
Wendler, P., Shorter, J., Plisson, C., Cashikar, A.G., Lindquist, S., and Saibil, H.R. (2007). Atypical AAA+ subunit packing creates an expanded cavity for disaggregation by the protein-remodeling factor Hsp104. Cell *131*, 1366-1377.
Willingham, S., Outeiro, T.F., DeVit, M.J., Lindquist, S.L., and Muchowski, P.J. (2003). Yeast genes that enhance the toxicity of a mutant huntingtin fragment or α-synuclein. Science *302*, 1769-1772.
Wilms, T., Swinnen, E., Eskes, E., Dolz-Edo, L., Uwineza, A., Van Essche, R., Rosseels, J., Zabrocki, P., Cameroni, E., and Franssens, V. (2017). The yeast protein kinase Sch9 adjusts V-ATPase assembly/disassembly to control pH homeostasis and longevity in response to glucose availability. PLoS genetics *13*, e1006835.
Winderickx, J., Delay, C., De Vos, A., Klinger, H., Pellens, K., Vanhelmont, T., Van Leuven, F., and Zabrocki, P. (2008). Protein folding diseases and neurodegeneration: lessons learned from yeast. Biochimica et Biophysica Acta (BBA)-Molecular Cell Research *1783*, 1381-1395.
Woerner, A.C., Frottin, F., Hornburg, D., Feng, L.R., Meissner, F., Patra, M., Tatzelt, J., Mann, M., Winklhofer, K.F., and Hartl, F.U. (2016). Cytoplasmic protein aggregates interfere with nucleocytoplasmic transport of protein and RNA. Science *351*, 173-176.

Wolfe, K.J., and Cyr, D.M. (2011). Amyloid in neurodegenerative diseases: friend or foe? Paper presented at: Seminars in cell & developmental biology (Elsevier).
Wolfe, K.J., Ren, H.Y., Trepte, P., and Cyr, D.M. (2014). Polyglutamine-rich suppressors of huntingtin toxicity act upstream of Hsp70 and Sti1 in spatial quality control of amyloid-like proteins.
Wolff, S., Weissman, J.S., and Dillin, A. (2014). Differential scales of protein quality control. Cell *157*, 52-64.
Xie, Z., and Klionsky, D.J. (2007). Autophagosome formation: core machinery and adaptations. Nature cell biology *9*, 1102-1109.
Yan Tong, A.H., and Boone, C. (2006). Synthetic genetic array analysis in Saccharomyces cerevisiae. Yeast Protocol, 171-191.
Yang, J., Hao, X., Cao, X., Liu, B., and Nyström, T. (2016). Spatial sequestration and detoxification of Huntingtin by the ribosome quality control complex. eLife *5*, e11792.
Yang, X., Shen, Y., Garre, E., Hao, X., Krumlinde, D., Cvijović, M., Arens, C., Nyström, T., Liu, B., and Sunnerhagen, P. (2014). Stress Granule-Defective Mutants Deregulate Stress Responsive Transcripts.
Yonashiro, R., Tahara, E.B., Bengtson, M.H., Khokhrina, M., Lorenz, H., Chen, K.-C., Kigoshi-Tansho, Y., Savas, J.N., Yates III, J.R., and Kay, S.A. (2016). The Rqc2/Tae2 subunit of the ribosome-associated quality control (RQC) complex marks ribosome-stalled nascent polypeptide chains for aggregation. eLife *5*, e11794.
Zaarur, N., Meriin, A.B., Gabai, V.L., and Sherman, M.Y. (2008). Triggering Aggresome Formation DISSECTING AGGRESOME-TARGETING AND AGGREGATION SIGNALS IN SYNPHILIN 1. Journal of Biological Chemistry *283*, 27575-27584.
Zarranz, J.J., Alegre, J., Gómez‐Esteban, J.C., Lezcano, E., Ros, R., Ampuero, I., Vidal, L., Hoenicka, J., Rodriguez, O., and Atarés, B. (2004). The new mutation, E46K, of α‐synuclein causes parkinson and Lewy body dementia. Annals of neurology *55*, 164-173.
Zhang, K., Donnelly, C.J., Haeusler, A.R., Grima, J.C., Machamer, J.B., Steinwald, P., Daley, E.L., Miller, S.J., Cunningham, K.M., and Vidensky, S. (2015). The C9orf72 repeat expansion disrupts nucleocytoplasmic transport. nature *525*, 56-61.
Zhang, X., Smith, D.L., Meriin, A.B., Engemann, S., Russel, D.E., Roark, M., Washington, S.L., Maxwell, M.M., Marsh, J.L., and Thompson, L.M. (2005). A potent small molecule inhibits polyglutamine aggregation in Huntington's disease neurons and suppresses neurodegeneration in vivo. Proceedings of the National Academy of Sciences of the United States of America *102*, 892-897.
Zhang, Y., Ma, C., Yuan, Y., Zhu, J., Li, N., Chen, C., Wu, S., Yu, L., Lei, J., and Gao, N. (2014). Structural basis for interaction of a cotranslational chaperone with the eukaryotic ribosome. Nature structural & molecular biology *21*, 1042-1046.
Zhao, L., Yang, Q., Zheng, J., Zhu, X., Hao, X., Song, J., Lebacq, T., Franssens, V., Winderickx, J., Nystrom, T., *et al.* (2016). A genome-wide imaging-based screening to identify genes involved in synphilin-1 inclusion formation in Saccharomyces cerevisiae. Scientific Reports *6*.
Zheng, J., Yang, J., Choe, Y.-J., Hao, X., Cao, X., Zhao, Q., Zhang, Y., Franssens, V., Hartl, F.U., and Nyström, T. (2017). Role of the ribosomal quality control machinery in nucleocytoplasmic translocation of polyQ-expanded huntingtin exon-1. Biochemical and biophysical research communications.
ZWOLSHEN, J.H., and Bhattacharjee, J. (1981). Genetic and biochemical properties of thialysine-resistant mutants of Saccharomyces cerevisiae. Microbiology *122*, 281-287.

List of publications

Zheng, J., Yang, J., Choe, Y., Hao, X., Cao, X., Zhao, Q., Zhang, Y., Franssens, V., Hartl, F. U., Nyström, T., Winderickx, J., Liu, B. (2017) Role of the ribosomal quality control machinery in nucleocytoplasmic translocation of polyQ-expanded huntingtin exon-1. *Biochemical and Biophysical Research Communications*.

Zhao, L., Yang, Q., **Zheng, J.**, Zhu, X., Hao, X., Song, J., Lebacq, T., Franssens, V., Winderickx, J., Nystrom, T., and Liu, B. (2016) A genome-wide imaging-based screening to identify genes involved in Synphilin-1 inclusion formation in *Saccharomyces cerevisiae*. Scientific Reports 6.

Fruhmann G., Seynnaeve D., **Zheng J**., Ven K., Molenberghs S., Wilms T., Liu B., Winderickx J., Franssens V. (2017) Yeast buddies helping to unravel the complexity of neurodegenerative disorders. *Mechanisms of Ageing and Development*, 161, 288-305